Université du Québec
à Rimouski

CARACTÉRISATION ET DEVENIR DE LA MATIÈRE ORGANIQUE DISSOUTE ISSUE DU DÉGEL DU PERGÉLISOL CÔTIER (MER DE BEAUFORT, TNO, CANADA)

Mémoire présenté

dans le cadre du programme de maîtrise en océanographie

en vue de l'obtention du grade de maître ès sciences

PAR

© AUDE FLAMAND

Avril 2023

Composition du jury :

Simon Bélanger, président du jury, UQAR (Université du Québec à Rimouski)

Gwénaëlle Chaillou, directrice de recherche, UQAR-ISMER

Jean-François Lapierre, codirecteur de recherche, Université de Montréal

Céline Guéguen, examinatrice externe, Université de Sherbrooke

Dépôt initial le 19 décembre 2022 Dépôt final le 06 avril 2023

REMERCIEMENTS

Tout au long de ma maîtrise j'ai eu la chance d'être accompagnée et soutenue par un grand nombre de personnes, que ce soit ma famille, mon copain, mes ami.e.s, ou bien encore mes professeur.e.s. Je tiens à remercier toutes les personnes qui ont été directement ou indirectement impliquées dans mon cheminement académique.

Merci à Gwénaëlle, ma directrice de maîtrise. Merci de m'avoir toujours appuyée, encouragée et conseillée dans tout ce que j'entreprenais. Merci de m'avoir appris à avoir confiance en mes décisions et de m'avoir permis d'accomplir tous ces différents projets. Merci à Jean-François, mon codirecteur, d'avoir toujours était très présent et pour ses très bons conseils. Merci à vous deux de m'avoir inclus au sein de vos laboratoires et équipes respectives, et de m'avoir aussi bien accompagnée tout au long de mon parcours.

Merci à ma maman et mon papa de m'avoir toujours encouragée et de toujours avoir su m'aider à aller jusqu'au bout de mes projets. Je les remercie aussi de m'avoir fait découvrir, dès mon plus jeune âge, la grandeur et la beauté de l'océan à travers leur amour pour la voile. Merci de votre soutien et vos conseils qui m'ont été très précieux tout au long de ce parcours. Je tiens aussi à remercier mes frères et sœurs, Louis, Eugénie et Hortense, qui ont toujours été une source de bons conseils, de soutien et d'inspiration.

Merci à Édouard, qui m'a toujours soutenu dans mes décisions et qui a toujours su m'écouter et me conseiller lors des périodes plus difficiles de cette maîtrise. Merci d'avoir était aussi présent malgré la distance. Merci de toujours me pousser à accomplir ce qui me passionne. Merci à mes super copines de Rimouski, Charlotte et Jeanne. Merci de toujours avoir eu les bons mots et d'avoir été d'aussi bons conseils. Plusieurs des différents projets que j'ai entrepris lors de ma maîtrise ont porté fruit grâce à votre soutien et votre implication. La maîtrise m'aura apporté des expériences incroyables, mais aussi des amies en or.

Je tiens aussi à remercier tous ceux qui ont fait de ma maîtrise une expérience incroyable et inoubliable, merci de votre aide et de votre soutien : Bryan, Hugo, Gwendoline, Jordan, Olivier, Éléonore, Antoine et Ludo. Finalement, je tiens à remercier Kanelsa, Shania, Bruce, Michele et Betty pour avoir rendu mes étés à Tuktoyaktuk absolument magiques, et de m'avoir si bien accueillie. Merci de m'avoir appris autant de choses et, sans qui, mon expérience de maîtrise n'aurait jamais été la même.

RÉSUMÉ

L'augmentation du taux d'érosion côtière et de dégel du pergélisol le long de la côte Arctique représente une source majeure de matière organique dissoute (DOM), vers l'océan côtier. Cette matière, issue du pergélisol, a la capacité d'influencer grandement les écosystèmes côtiers marins, la chimie de l'océan ou encore les chaînes trophiques. Le fer, qui interagit avec la matière organique, aurait la capacité de contrôler la mobilité et l'export de la DOM issue du pergélisol. L'objectif de ce projet de maîtrise était de caractériser l'origine et le devenir de la MO issue du pergélisol dans la zone côtière de la mer de Beaufort, afin de mieux comprendre le rôle des marges continentales arctiques dans le transfert de matière du continent à l'océan. Plus spécifiquement, il vise à 1) caractériser et tracer la signature optique de la DOM nouvellement mobilisée des falaises côtières de pergélisol à la zone infralittorale et 2) évaluer expérimentalement l'affinité de la DOM issue du pergélisol côtier avec les hydroxydes de fer, en caractérisant et quantifiant la portion piégée. Au cours des étés 2019 et 2021, des échantillons d'eau de fonte de pergélisol, d'eau souterraine de plage et d'eau de mer ont été prélevés sur plusieurs transects, des falaises côtières jusqu'à 1 - 2 km de la ligne de rivage. Les concentrations de carbone organique dissous (DOC) et de matière organique dissoute chromophorique (CDOM) diminuent rapidement dans le gradient de salinité, dès que la matière est mobilisée dans la phase dissoute. Une analyse de la fraction fluorescente de la DOM (FDOM) par une méthode multifactorielle (PARAFAC) a permis de caractériser la FDOM issue de l'eau de fonte comme étant à haut poids moléculaire, humique et terrigène et la FDOM issue d'échantillons collectés au large de la côte, comme étant protéinique, à faible poids moléculaire et d'origine microbienne. La signature optique de l'eau de fonte de pergélisol s'estompe rapidement dans le gradient continent-océan. Des expérimentations ont révélé que cette perte de signal pourrait être causée par l'interaction de la DOM avec des hydroxydes de fer réactifs qui pourraient alors agir comme un piège, permanent ou temporaire, à l'export de cette matière vers les eaux côtières arctiques. L'export de molécules de plus petits poids moléculaires non stabilisées par le fer serait alors favorisé. Globalement, cette étude a permis de montrer que des processus de régulation prennent place dès la mobilisation de la MO issue du dégel du pergélisol contrôlant ainsi les flux de carbone terrigène vers les eaux côtières arctiques.

Mots clés : pergélisol, arctique, matière organique dissoute, carbone organique dissous, océan côtier, hydroxyde de fer réactif

.

ABSTRACT

Increasing rates of coastal erosion and permafrost thaw along the Arctic coast represent a major source of dissolved organic matter (DOM) to the coastal environment. This material, originating from thawing permafrost, can greatly influence marine coastal ecosystems, ocean chemistry and food web dynamics. Iron, an element that interacts with organic matter, could have the ability to control the mobility and export of this permafrost-derived DOM. The objective of this master's project was to characterize the origin and fate of permafrost-derived OM in the coastal Beaufort Sea, to better understand the role of Arctic continental margins in the transfer of material from the continent to the ocean. Specifically, it aimed at 1) Characterizing and trace the optical signature of newly mobilized DOM from coastal permafrost cliffs to the subtidal zone and 2) experimentally assess the affinity of DOM from coastal permafrost with iron hydroxides, characterizing and quantifying the trapped portion. During the summers of 2019 and 2021, permafrost meltwater, beach groundwater, and seawater samples were collected from several coastal bluffs transects up to 1–2 km from the shoreline. Dissolved organic carbon (DOC) and chromophoric dissolved organic matter (CDOM) concentrations decreased rapidly across the salinity gradient once the material was into the dissolved phase. A PARAFAC analysis of fluorescent DOM indicated that permafrost-derived DOM had a high molecular weight, humic, and was from terrigenous origin, while coastal ocean-derived FDOM was protein-rich with low molecular weight, and from microbial (autochthonous) origin. The optical signature of meltwater faded along the continent-ocean continuum. Experiments revealed that this loss of signal could be caused by the interaction of DOM with reactive iron hydroxides which could act as a permanent or temporary trap, during its export to Arctic coastal waters. The export of smaller molecules, which are not stabilized by iron, would be favored. Overall, this study has shown that regulatory processes take place from the mobilization of permafrost-derived OM, controlling the flow of terrigenous carbon into Arctic coastal waters.

Keywords: permafrost, Arctic, dissolved organic matter, dissolved organic carbon, coastal ocean, reactive iron hydroxide.

TABLES DES MATIÈRES

LISTE DES TABLEAUX

LISTE DES FIGURES

LISTE DES ABRÉVIATIONS, DES SIGLES ET DES ACRONYMES

MO	Matière organique (ou OM pour *Organic Matter*)
Abs	Absorbance
BIX	Indice biologique (ou *Biological Index*)
CDOM	Matière organique dissoute colorée (CDOM pour *Chromophoric Dissolved Organic Matter*)
DIC	Carbone inorganique dissous (DIC pour *Dissolved inorganic Carbon*)
DOC	Carbone organique dissous (DOC pour *Dissolved Organique Carbon)*
DOM	Matière organique dissoute (DOM pour *Dissolved Organique Matter)*
EEM	Matrice d'émission et d'excitation (EEM pour *Emission and Excitation Matrice)*
F.I.	Intensité de fluorescence (ou *Fluorescence Intensity*)
FDOM	Matière organique dissoute fluorescente (FDOM pour *Fluorescent Dissolved Organic Matter*)
FI	Indice de fluorescence (FI pour *Fluorescence Index*)
GC-MS	Chromatographie en phase gazeuse couplée à un spectromètre de masse (GC-MS pour *Gas chromatography-mass spectrometry)*
HCA	Analyse de regroupement hiérarchique (HCA pour *Hierarchical Clustering Analysis*)
HIX	Indice d'humification (ou *Humification Index*)
HMW	Haut poids moléculaire (HMW pour *High Molecular Weight*)
HPLC	Chromatographie liquide à hautes pressions (HPLC pour *High Performance Liquid Chromatography)*
LMW	Faible poids moléculaire (LMW pour *Low Molecular Weight*)
OC	Carbone organique (OC pour *Organic Carbon)*
PARAFAC	Analyse factorielle parallèle (PARAFAC pour *Parallel Factor Analysis)*

POC	Carbone organique particulaire (POC pour *Particulate Organic Carbon)*
R.U.	Unité Raman
S_R	Rapport de pente (ou *Slope Ratio*)
$SUVA_{254}$	Absorbance UV spécifique à 254 nm
TNO/NWT	Territoire du Nord-Ouest (NWT pour *Northwest Territories*)
TOC	Carbone organique total (TOC pour *Total Organic Carbon*)

INTRODUCTION GÉNÉRALE

L'océan joue un rôle clé dans le maintien de la composition de l'atmosphère, en agissant comme le puit de carbone le plus important sur Terre (Ridgwell & Arndt, 2015). Il est estimé que, dans l'océan, les stocks de carbone organique particulaire (POC) et dissous (DOC) sont de ~30 et 662 PgC (1 Pg = 1 015 g), respectivement, et que l'océan absorberait ~2 Pg de CO_2 par année causant graduellement son acidification (Carlson et al., 2015; Eppley et al., 1987; Hansell et al., 2009).

Le pergélisol est un réservoir important de carbone avec 1 460 – 1 700 PgC (Schuur et al., 2013) réparti sur 15 % du sol mondial (Schuur et al., 2015) et représente, en raison de sa fonte bien amorcée, une nouvelle source de carbone à l'océan qui perturbe les écosystèmes côtiers et la chimie des océans (Guo et al., 2007; Stedmon et al., 2011a). En effet, les perturbations des conditions environnementales (forçages atmosphérique et marin), influencées par les changements climatiques, induisent une augmentation sans précédent des taux d'érosion côtière (augmentation de plus de 80 % dans la zone côtière la mer de Beaufort dans les deux dernières décennies) (Jones et al., 2020) et de dégel du pergélisol (Turetsky et al., 2020) le long de la côte Arctique. Il a été estimé que le dégel abrupt du pergélisol serait responsable du déversement dans l'océan Arctique de 41 à 288 PgC d'ici 2100 et de 616 PgC d'ici 2300 (Schuur et al., 2013; Zimov et al., 2006). De plus, selon des prédictions climatologiques, ~40 % du pergélisol mondial pourrait disparaître d'ici la fin du siècle (Chadburn et al., 2017). En dépit de l'importance de ces nouveaux apports latéraux de carbone, on en sait encore très peu sur la composition et le devenir de la matière nouvellement mobilisée par l'érosion et le dégel du pergélisol s'écoulant vers les milieux côtiers. Dans un contexte de changements climatiques et de mobilisation massive de carbone par le pergélisol, il est primordial de mieux comprendre les processus biogéochimiques impliqués dans la régulation de cette importante source de carbone pour l'océan côtier.

LA MATIERE ORGANIQUE

La matière organique (MO) est un mélange hétérogène de composés produits par les organismes vivants, qu'ils soient animaux ou végétaux. Dans le milieu aquatique, elle se compose de matière organique particulaire (POM) et de matière organique dissoute (DOM) (Repeta, 2015). Ces différentes fractions se différencient par filtration : la fraction particulaire est retenue par un filtre alors que la fraction dissoute passe à travers, la taille des pores du filtre variant selon l'analyste (mais souvent entre 0,2 et 0,7 µm) (Benner, 2002; He et al., 2016; Repeta, 2015).

La MO se compose principalement d'atome de carbone, d'azote, de phosphore et d'hydrogène qui sont arrangés pour former différentes classes de molécules, des plus simples (acides aminés, sucres simples, vitamines et acides gras) aux plus complexes (protéines, polysaccharides et lignines) (Repeta, 2015). Elle se compose aussi de substances humiques (SH). Les SH marines se composent d'acides humiques et d'acides fulviques (Harvey et al., 1983; Lipczynska-Kochany, 2018). L'origine de la MO détermine les caractéristiques chimiques de celle-ci, elle peut alors être définie comme étant autochtone ou allochtone. En milieu marin, on parle cependant couramment de MO autochtone marine et de MO allochtone terrigène.

PUITS ET SOURCES DE DOM

La DOM en milieu aquatique permet de stocker différents nutriments. Elle les rend ainsi moins biodisponibles et prolonge leur temps de résidence dans la colonne d'eau (Carlson et al., 2015). De la même manière, elle affecte la biodisponibilité des métaux traces essentiels et séquestre une grande quantité de carbone. Par ses propriétés optiques, elle atténue le rayonnement de courtes longueurs d'ondes émis par le soleil dans la zone euphotique (Carlson et al., 2015; Mustaffa et al., 2020; Schindler et al., 1997)

La DOM marine est produite et reminéralisée par différents processus biotiques et abiotiques. La majorité de la production de la MO dans l'océan ouvert est opérée dans la zone euphotique et dépend majoritairement des producteurs primaires marins (Buchan et al., 2014; Carlson, 2002). La DOM marine est aussi produite par la libération extracellulaire du phytoplancton, la libération et l'excrétion des brouteurs (zooplancton), la lyse cellulaire (virale et bactérienne), la solubilisation des particules détritiques et sédimentaires et par les procaryotes. Une majorité des déchets organiques produits par ces processus est utilisée par les procaryotes hétérotrophes, oxydée par différents processus photochimiques ou alors séquestrée dans le sédiment (Fig. 1) (Buchan et al., 2014; Carlson et al., 2015). La MO terrigène, quant à elle, provient de la dégradation d'organismes morts, d'excréments d'organismes vivants et de la biomasse continentale et est acheminée à l'environnement aquatique par l'intermédiaire de différentes sources, comme l'atmosphère (pluie et poussière) (Simoneit, 2005), les rivières (Simoneit, 2005), les ruissellements (Eckard et al., 2017), les eaux souterraines (Connolly et al., 2020) ou encore par l'érosion côtière (Kipp et al., 2018). Dans le milieu aquatique, la MO terrigène et la MO d'origine marine sont consommées par les mêmes processus (Fig. 1) (Hedges et al., 1997; Lønborg et al., 2020; Stedmon et al., 2003). La MO marine et la MO terrigène se distinguent par leur poids moléculaire relatif, la MO marine ayant un poids moléculaire plus faible elle serait alors plus réactive (Hedges et al., 1997).

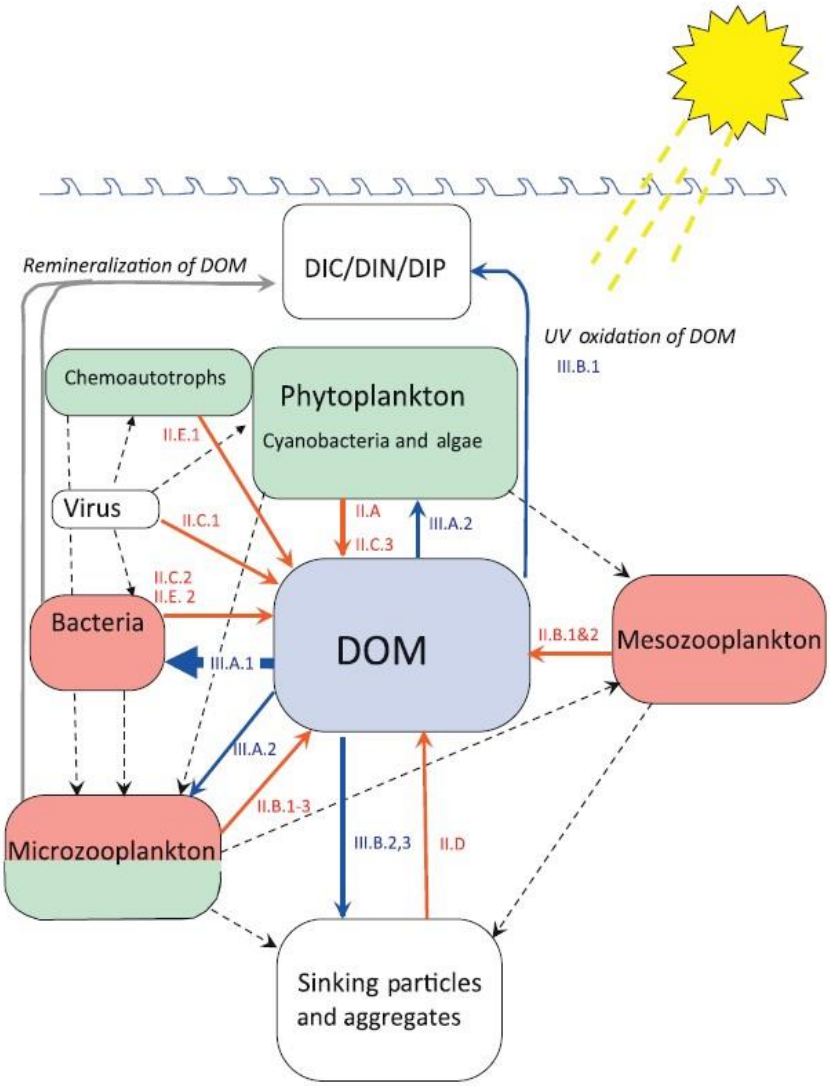

Figure 1. Processus de production et de consommation de la DOM marine. Les flèches noires pointillées représentent l'interaction entre les chaînes trophiques, les flèches rouges représentent la production, et les bleues la consommation de la DOM (Carlson et al., 2015; Helms et al., 2008)

SOURCE DE DOC ET DE DOM A L'OCEAN ARCTIQUE

L'océan Arctique représente seulement 1 % du volume océanique mondial, mais joue un rôle clé dans la circulation océanique globale, en participant à la formation, à la ventilation ainsi qu'à l'acheminement de DOC des masses d'eau profonde de l'Hémisphère Nord

(Anderson et al., 2015; Menard et al., 1966). L'océan Arctique exporte ~27 × 10^{12} gC an^{-1} de DOC au nord de l'Atlantique, tandis que l'océan Pacifique et les grands fleuves Arctique, Ob, Yenisey, Lena, Kolyma, Mackenzie et Yukon (Fig. 2) y importent ~18 × 10^{12} gC an^{-1} et 25 et 36 ×10^{12} gC an^{-1}, respectivement (Burn et al., 2009). Les six grands fleuves Arctique possèdent un bassin versant total de ~17 × 10^{6} km^2 et contribuent de plus de 65 % à la décharge annuelle totale (Holmes et al., 2012), acheminant de grandes quantités de DOC d'origine terrigène (tDOC) à l'océan Arctique (Amon et al., 2012). Les masses d'eau en provenance de l'océan Atlantique et Pacifique ont une concentration moyenne de DOC de 60 et 70 µM, respectivement, pour une décharge moyenne de ~8 Sv an^{-1} (1Sv = 1 million m^3 s^{-1}). Tandis que les fleuves sibériens ont une concentration moyenne de DOC comprise entre 600 à 990 µM et le fleuve Mackenzie de ~350 µM, pour une décharge moyenne de 0,12 Sv an^{-1} ; une concentration en DOC beaucoup plus élevée pour une décharge beaucoup plus faible (Amon et al., 2012; Raymond et al., 2007; Stedmon et al., 2011a). La glace marine représente aussi une source de DOC avec une concentration moyenne totale de ~100 µM de DOC et une décharge moyenne de ~0,45 Sv an^{-1} (Thomas et al., 1995). Il est important de noter que ces apports sont saisonniers (Amon et al., 2012).

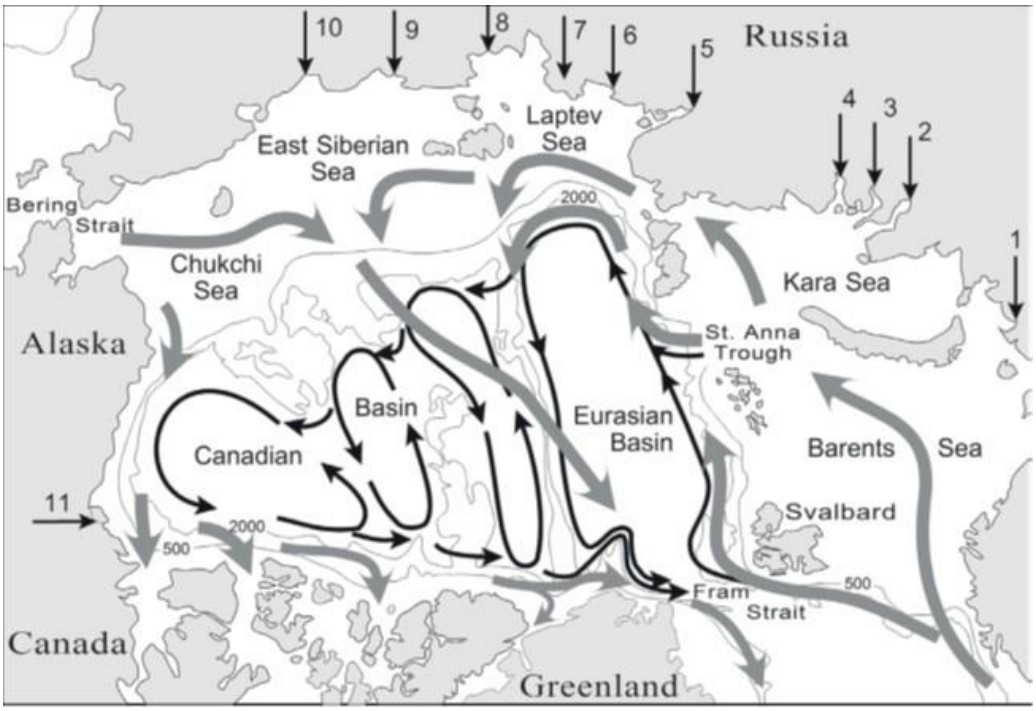

Figure 2. Circulation de la couche de surface (0 - 100 m) (flèches grises) et intermédiaire (500 - 2000 m) (flèches noires) de l'océan Arctique et ses fleuves principaux (flèches numérotées montre l'embouchure des fleuves). 1. Pechora, 2. Ob, 3. Pyr, 4. Yenisey, 5. Katanga, 6. Olenek, 7. Lena, 8. Yana, 9. Indigirka, 10. Kolyma, 11. Mackenzie. Le fleuve du Yukon se déverse dans la mer de Bering (en dehors de la carte) et pénètre dans l'océan Arctique par le détroit de Bering (Anderson et al., 2015)

Lors des crues printanières, les grands fleuves véhiculent une quantité importante de tDOC à l'océan, sur une courte période, influençant la composition de la MO, la chimie de l'eau et les écosystèmes récepteurs (Amon et al., 2012). Dans la zone côtière de la mer de Kara, Köhler et al. (2003) ont montré qu'une fraction importante du DOC acheminée par les fleuves Ob et Yenisei, pendant les périodes de crues, serait réfractaire à la minéralisation et à la floculation, expliquant la pérennité du signal terrigène jusqu'au centre de l'océan Arctique (Amon, 2004; Letscher et al., 2011; Mathis et al., 2014; Opsahl et al., 1999). Selon l'étude, cette fraction de DOC aurait un comportement conservatif lors de son mélange aux masses d'eaux salées de l'océan Arctique, et la fraction restante (~30 %) serait plus labile et dégradée après seulement quelques jours ou quelques semaines (Holmes et al., 2008; Köhler et al., 2003). Cependant, Tanaka et al. (2016) ont montré que le DOC et les composantes

optiques de la DOM auraient un comportement non conservatif avec la salinité, au sud de la mer de Chukchi. En effet, la composition et les caractéristiques de la matière organique dissoute (Amon et al., 1996) auraient un effet sur la réactivité et la dégradabilité du DOC (Moody et al., 2017). L'extrême hétérogénéité des apports en MO aux marges continentales par les sources ponctuelles (i.e. fleuves et rivières) et diffuses (i.e. ruissellement et apports souterrains) représente un défi majeur dans l'identification des sources, la quantification des flux et l'étude du devenir de cette matière.

Dans un contexte de changements climatiques, l'augmentation globale des températures atmosphérique engendre l'accélération du dégel du pergélisol. En dégelant, le pergélisol mobilise une quantité importante de DOM vers les écosystèmes côtiers de l'Arctique (Gruber et al., 2004; Schuur et al., 2008). La DOM est l'un des plus grands réservoirs de carbone organique (OC) sur Terre et de simples changements dans sa composition ont la capacité d'engendrer des perturbations importantes sur le cycle global du carbone (Hedges et al., 1997; Köhler et al., 2003). Il est donc primordial de mieux comprendre les différents processus impliqués dans le transport, la transformation et la séquestration de cette matière le long des marges continentales, des environnements clés pour le cycle du carbone.

LE PERGELISOL : UN RESERVOIR DE CARBONE QUI DEGELE

Le pergélisol est défini comme un sol maintenu à des températures inférieures à 0 °C pendant plus de deux années consécutives (French et al., 2007) et est constitué d'une combinaison de sédiments maintenus par de la glace. Le pergélisol se trouve entre une couche sous-jacente non gelée et une couche supérieure qui dégèle de manière saisonnière : la couche active (Fig. 3) (French et al., 2007; Williams et al., 1989).

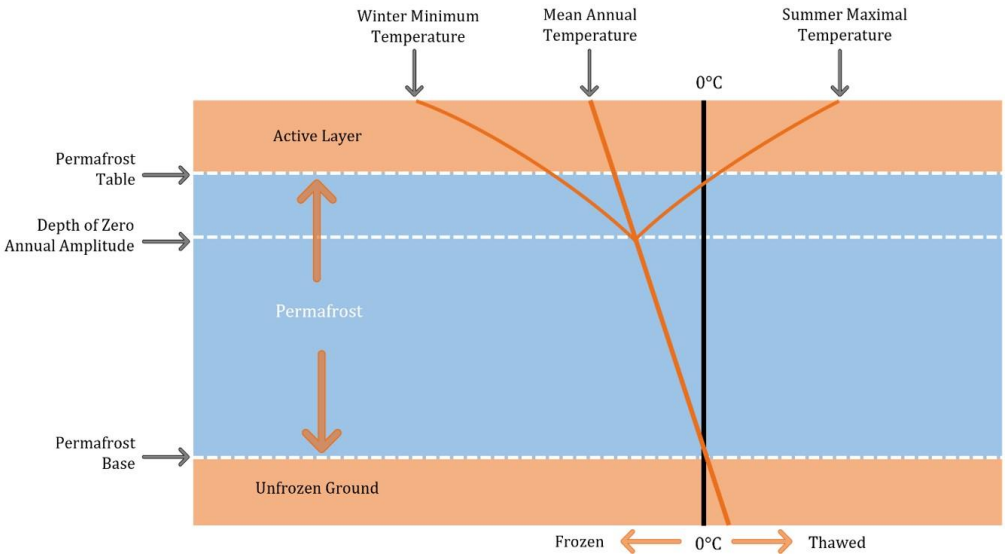

Figure 3. Profil vertical du pergélisol au cours des saisons (image adaptée de Palangi et al., 2017)

Le pergélisol est un réservoir de carbone terrigène important qui contient entre 1 460 et 1 700 PgC, soit le double de la quantité de carbone contenu dans l'atmosphère. Le pergélisol recouvre 15 % du sol mondial, mais accumule 60 % du stock mondial de carbone, dont une grande fraction (1 035 ± 150 PgC) serait comprise dans les trois premiers mètres seulement (Hugelius et al., 2014; Schuur et al., 2015; Schuur et al., 2018; Turetsky et al., 2020). Le pergélisol continental s'étend sur $13{,}9 \times 10^6$ km^2 et est distribué selon quatre types de zones : continue, discontinue, sporadique et isolé (Obu et al., 2019). Une zone de pergélisol continue est recouverte de plus de 90 % de pergélisol, discontinue de 50 à 90 %, sporadique de 10 à 50 %, tandis qu'une zone de pergélisol isolé est recouverte de 0 à 10 % de pergélisol (Fig. 4.) (Brown, 1970; Obu et al., 2019).

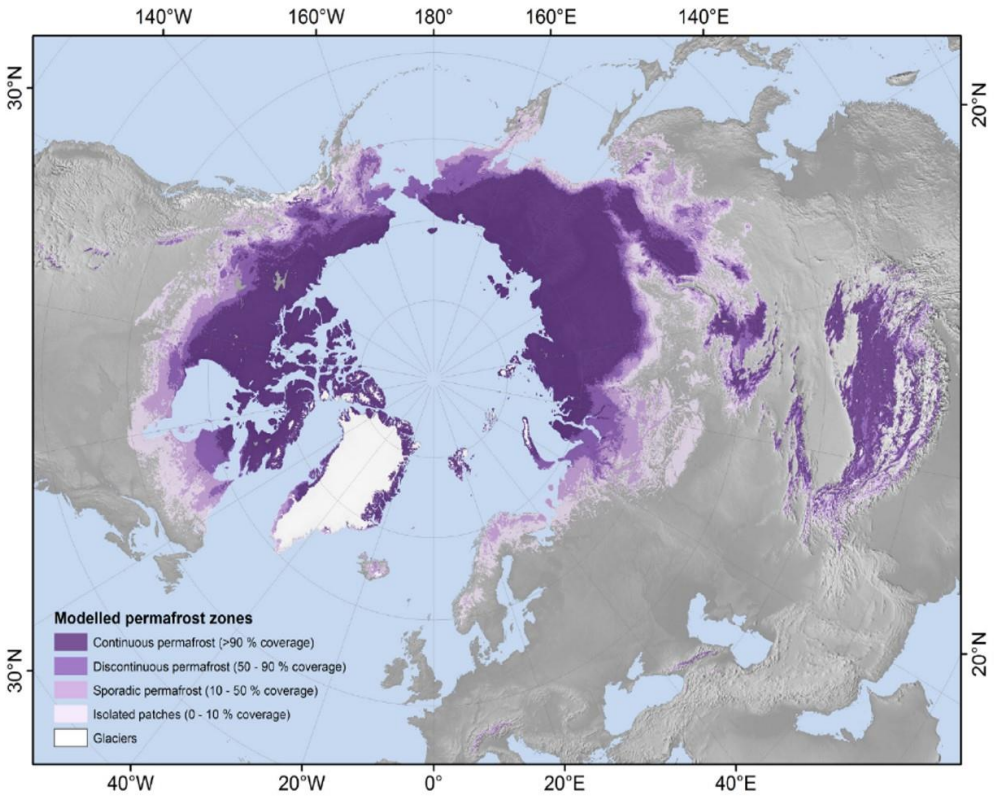

Figure 4. Distribution des zones de pergélisol dans l'hémisphère Nord (Granskog et al., 2012; Helms et al., 2008; Obu et al., 2019)

La majorité du pergélisol s'est formée lors de la dernière glaciation (Burn et al., 2009). L'âge du DOC issu du pergélisol a été estimé entre 40-50 kans et 115 kans en Sibérie et en Amérique du Nord (Lilleøren et al., 2012), pouvant aller jusqu'à ~650 kans dans le cratère de Batagaï, en Sibérie (Murton et al., 2022). Malgré son éventuel vieil âge, le DOC issu de sols de pergélisol serait hautement biolabile. En effet, la datation du tDOC issu des cinq fleuves majeurs qui se déversent dans l'océan Arctique a révélé que celui-ci était d'origine récente ; la matière issue du dégel du pergélisol, transportée par les grands fleuves, ne perdurerait pas dans les systèmes aquatiques (Mopper et al., 2015; Raymond et al., 2007). Nouvellement mobilisée, la vieille matière serait alors rapidement minéralisée et relâchée sous forme de gaz à effet de serre (CO_2, CH_4), par photooxydation et biodégradation (Drake et al., 2015; Spencer et al., 2015; Vonk et al., 2013). Sa biolabilité est estimée entre 24 à 71 % (avec une médiane à ~52 %) sur une période de plusieurs jours à plusieurs mois (Ma et al.,

2018). Ce fort pourcentage serait en partie expliqué par la composition chimique de la DOM issue du pergélisol, caractérisée comme étant de faible poids moléculaire et peu aromatique en comparaison de la DOM issue de la couche active (Fouché et al., 2020; Ward et al., 2015). En revanche, cette vieille matière ne serait pas aussi photosensible comparée à de la matière d'origine plus récente (Stedmon et al., 2011b; Stubbins et al., 2017).

LE PERGELISOL COTIER : DANS UN CONTEXTE DE CHANGEMENTS CLIMATIQUES

Entre 1950 et 2000, le pergélisol côtier arctique a subi un taux d'érosion moyen de - 0,5 m an^{-1}, avec un des plus hauts taux reportés dans la région de la mer de Beaufort, avec -1,1 m an^{-1} (Jones et al., 2020; Lantuit et al., 2012). Dans les deux dernières décennies, ce taux a augmenté de 80 à 160 %, notamment à cause de la diminution du couvert de glace, de l'augmentation de la température de l'air et de l'eau, de la montée du niveau marin et de l'augmentation de la récurrence et de l'intensité des tempêtes (Jones et al., 2020; Romanovsky et al., 2017). Selon le groupe intergouvernemental d'experts sur les changements climatiques (GIEC, 2013), l'Arctique subit une augmentation de température atmosphérique 1,9 fois supérieure au réchauffement global, soit un réchauffement de ~0,6 °C par décennie, et ce depuis 30 ans (Schuur et al., 2015). Il a été reporté qu'entre 2007 et 2016 les zones de pergélisol continues, en Arctique, ont subi une augmentation moyenne de température de 0,39 ± 0,15 °C, causant l'épaississement de la couche active, ainsi que l'accélération du dégel du pergélisol (Romanovsky et al., 2017). À Drew Point, en Alaska, le taux d'export de TOC (TOC pour *Total Organic Carbon*) à la mer de Beaufort a été évalué à 1 369 kgC an^{-1} entre 2002 et 2019, soit le double du flux reporté entre 1955 et 2002 (Bristol et al., 2021). L'amplification des flux de matière contenue dans le pergélisol peut perturber la chimie des eaux côtières, en affectant à la fois la réactivité et la composition de la matière organique déjà présente dans le milieu, tout en perturbant les réseaux trophiques (Vonk et al., 2015).

CARACTERISATION DE LA DOM

De nombreuses méthodes permettent de caractériser la DOM en milieu aquatique. Cependant, seulement 60 à 70 % de cette matière a été caractérisée (Carlson et al., 2015). En effet, l'hétérogénéité des composés de la DOM au sein d'un échantillon d'eau limite l'identification de certaines classes de molécules. Ces approches permettent soit de quantifier et d'explorer la composition au niveau moléculaire soit de qualifier les grandes caractéristiques des composés présents dans le mélange. Au niveau moléculaire, les biomarqueurs permettent de tracer la DOM à partir de son origine et son état diagénique (Hedges et al., 1982). Par exemple, la lignine, une composante majeure de la DOM d'origine terrigène (tDOM), peut être utilisée en tant que traceur dans les environnements aquatiques de par sa signature biochimique unique à caractère phénolique (Opsahl et al., 1999). La chromatographie en phase gazeuse couplée à un spectromètre de masse (GC-MS) permet de quantifier la lignine de la DOM (Opsahl et al., 1999). En ajoutant une analyse du rapport isotopique stable du carbone ($\delta^{13}C$), Opsahl et al., (1999) ont suivi la trace de la tDOM à haut poids moléculaire et ont déterminé que la couche de surface de l'océan Arctique avait une plus grosse fraction de tDOM (5-33 %) que les océans Pacifique et Atlantique (0,7-2,4 %). Kattner et al., (1999) ont également montré que 8-30 % du DOM de la mer de Laptev était d'origine riveraine.

La spectroscopie à résonance magnétique nucléaire (RMN), quant à elle, est une méthode qui permet d'étudier les groupes fonctionnels des isotopes ^{13}C et ^{1}H (Pavia et al., 2008; Ward et al., 2015). Les pics RMN propres aux groupes fonctionnels varient selon la localisation, la profondeur et le gradient de salinité de l'échantillon (Repeta, 2015). Par exemple, Ward et Cory, (2015) ont utilisé le ^{13}C RMN à phase solide afin de souligner la différence entre la composition de la DOM présente dans le pergélisol et dans la couche de matière organique qui la surplombe, la couche active. La DOM présente dans la couche de matière organique est plus enrichie en C aromatique, en groupes fonctionnels contenant des

atomes d'oxygène (groupe carboxylé, ketone et aldéhyde). Alors que la DOM issue du pergélisol était plus concentrée en groupes carbohydrates (Ward et al., 2015).

D'autres méthodes analytiques permettent de s'intéresser à des composés spécifiques. Par exemple, la chromatographie liquide à hautes performance (HPLC) permet de quantifier et d'identifier les acides aminés dissous qui composent les groupes protéiniques d'une solution (Repeta, 2015). Cette méthode permet notamment d'identifier la source du DOC dans les environnements côtiers (Shen et al., 2014).

Les méthodes mentionnées ci-dessus peuvent être limitées par certains facteurs. Plusieurs de ces instruments exigent une préparation supplémentaire de l'échantillon augmentant les risques de biais. Par exemple, la spectroscopie RMN nécessite une étape d'isolation et de concentration de la DOM présente dans l'eau afin de réduire les impuretés, une source d'interférences (Pavia et al., 2008). De plus ces méthodes peuvent nécessiter beaucoup de temps, ce qui peut être limitant lorsque l'analyse doit être faite rapidement après l'échantillonnage.

La spectroscopie d'absorbance et de fluorescence se démarque par sa simplicité d'utilisation, sa capacité à analyser un échantillon peu concentré et en petite quantité, son faible coût et sa rapidité (Pavia et al., 2008). Cette méthode d'analyse optique permet de qualifier la matière organique selon ces composées majeures, de par ces propriétés moléculaires et son origine (Ward et al., 2015). Plus précisément, elle permet de quantifier et caractériser la fraction colorée de la DOM (CDOM) en identifiant l'abondance de certains groupes fonctionnels, en indiquant le poids moléculaire relatif, l'aromaticité relative ou encore en identifiant la source de la DOM (e.g. marine, terrigène, microbienne). La DOM est composée de chromophores qui ont la capacité d'absorber de la lumière ultra-violette (200 - 400 nm) et visible (400 – 800 nm) (Stedmon et al., 2015). La capacité d'absorption d'un chromophore dépend de son intensité, de l'absorptivité molaire, de sa concentration (loi de Beer-Lambert), et de la nature de la lumière absorbée, qui va dépendre des transitions électroniques du chromophore (Stedmon et al., 2015). Ces techniques sont abondamment

utilisées dans les études de caractérisation de la DOM relâchée par le dégel du pergélisol. Par exemple Fouché et al., (2020) ont caractérisé la CDOM contenue dans le pergélisol comme étant à faible poids moléculaire et une faible aromaticité, ce qui pourrait suggérer une forte biodégradabilité.

L'absorbance d'un échantillon est obtenue par l'intermédiaire d'un spectrophotomètre qui mesure l'intensité des rayons qui passent à travers une cellule de référence (I_o) et l'intensité des rayons qui passant à travers une cellule contenant l'analyte (I). L'absorbance est ensuite calculée selon l'équation suivante :

$$A = log_{10} \frac{I_0}{I}$$

Un spectre d'absorption peut ensuite être calculé selon l'équation :

$$a_\lambda = \frac{2{,}303 A_\lambda}{l}$$

Le coefficient d'absorption spectrale (a_λ) est mesuré en fonction de l'absorbance à une certaine longueur d'onde (A_λ), qui correspond aux rayons transmis à travers l'échantillon, en prenant compte la longueur du trajet parcouru par la lumière dans la solution (l) et le facteur de conversion (2,303). Les spectres d'absorption permettent d'obtenir des renseignements qualitatifs et quantitatifs sur le CDOM contenu dans l'échantillon (Fig. 5 a). Il existe plusieurs indices qui permettent de caractériser le CDOM à partir des spectres d'absorption, dont le S_R, le $SUVA_{254}$ et le aCDOM. Le tableau 1 présente la formulation et la description de chacun de ces indices.

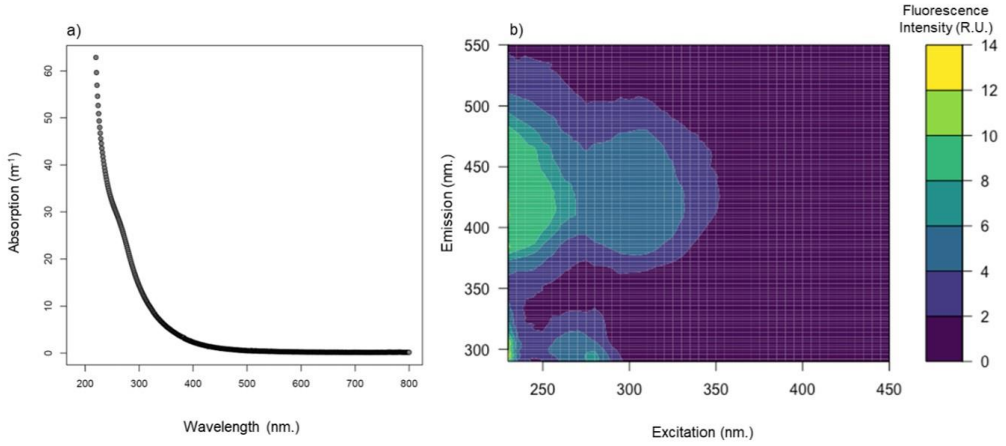

Figure 5. a) Exemple d'un spectre d'absorption, b) exemple d'une matrice d'émission et d'excitation (EEM)

Tableau 1. Indices optiques d'absorbance pour la caractérisation du CDOM (Del Vecchio et al., 2004; Granskog et al., 2012; Helms et al., 2008)

Indices	**Description**	**Formule**
Rapport de pente : S_R	- Origine du CDOM - Poids moléculaire du CDOM - Degré de dégradation photochimique du CDOM. S_R>1,5 : origine océanique ou terrigène fortement dégradée par la photochimie. S_R~1.1 : origine estuarienne et côtière. S_R~0.7 : origine terrigène.	$S_R = S_{275-295} : S_{350-400}$ S_R est la pente à λ 275-295 nm et 350-400 nm.
Abs. UV spécifiques : $SUVA_{254}$ (L mgC^{-1} m^{-1})	- Aromaticité du DOC - Poids moléculaire du DOC	$SUVA_{254} = a_{254} : DOC$ a_{254} est l'abs. à 254 nm et DOC est la concentration en carbone organique dissous.
aCDOM (m^{-1})	- Concentration du CDOM En rivière : $aCDOM_{375}$ =5-25 m^{-1}. - En milieu côtier : $aCDOM_{375}$ =0,5-5 m^{-1}.	Abs. à une λ spécifique (varie dans la littérature : $aCDOM_{350}$, $aCDOM_{375}$, $aCDOM_{412}$).

Finalement, la spectroscopie de fluorescence ou la fluorométrie repose sur la théorie des molécules fluorescentes ; molécules qui ont la capacité d'absorber des photons et de les émettre rapidement sous forme de lumière fluorescente, c'est une fraction du CDOM. Les mesures de fluorescence permettent de produire des matrices d'émissions et d'excitations (EEMs pour *Emission and Excitation Matrices*) (Fig. 5 b). Les EEMs sont des matrices en trois dimensions qui représentent l'émission selon l'intensité de la fluorescence, enregistrée à différentes longueurs d'onde d'excitation. L'intensité de fluorescence varie en fonction de la concentration du fluorophore (Murphy et al., 2013). En isolant les maximums de fluorescence, il est possible de comparer ces pics à la littérature dans le but d'identifier leur nature et leur origine (Coble, 1996). Tout comme pour l'absorbance, plusieurs indices de fluorescence peuvent être calculés pour fournir des indications sur la composition et la source de la DOM. Le tableau 2 présente trois d'entre-deux.

Tableau 2. Indice optique de fluorescence pour la caractérisation du CDOM (Cory et al., 2005; Fellman et al., 2010; Gabor et al., 2014; Huguet et al., 2009; McKnight et al., 2001; Ohno, 2002; Zsolnay et al., 1999)

Indices	Caractéristiques de la DOM	Formule
Indice biologique : BIX	>1 origine bactérienne aquatique ou biologique 0,8-1 forte composante autochtone 0,7-0,8 intermédiaire composante autochtone 0,6-0,7 faible composante autochtone	Intensité de fluorescence λ_{em} 380 nm : intensité de fluorescence λ_{em} 430 nm, à λ_{ex}310 nm.
Indice de fluorescence : FI	Distinction entre les sources des acides fulviques aquatiques. FI~1,8 et 1,9 = origine microbienne. FI~1,2 et 1,4 = origine terrestre.	λ_{em} 450 nm : 500 nm à λ_{ex} 370 nm.
Indice d'humification : HIX	Degré d'humification de la DOM. Plus grand HIX = plus faible ratio de liaison C-H et un plus grand dégrée d'aromaticité. Plus faible HIX = plus haut ratio de liaisons C-H.	λ_{em} 435-480 nm : (300-345 nm+435-480 nm

En plus de ces indices de fluorescence, un modèle statistique multivarié, appelé *PARAllel FACtor analysis* ou PARAFAC, permet de traiter les EEMs et d'identifier et quantifier les composantes principales présentes (Bro, 1997; Murphy et al., 2013; Stedmon et al., 2003). Le modèle PARAFAC repose sur l'équation suivante :

$$x_{ijk} = \sum_{f=1}^{F} a_{if} b_{jf} c_{kf} + \varepsilon_{ijk}$$

Où x correspond aux données mesurées selon l'émission (j) et l'excitation (k) de l'échantillon (i). La partie centrale de l'équation varie selon la concentration, l'émission et l'excitation de chaque composante. La dernière section (ε) permets de prendre en compte les résiduels, la fluorescence non expliquée (e.g. diffusion, bruit de l'instrument, signal non capturé par le modèle) (Murphy et al., 2013). Les composantes déterminées par l'analyse statistique sont ensuite testées et comparées sur une base de données internationale qui permet ainsi de définir chimiquement les composantes (Fig. 6). Par exemple, en combinant les concentrations de DOC et de CDOM avec les indices optiques ainsi que la méthode analytique PARAFAC, Olefeldt et al., (2014) ont pu montrer que, bien que la concentration de DOC riveraine diminuait au nord de la zone de pergélisol, la signature optique de la CDOM était plus marquée par les composantes protéiniques et moins marquée par les composantes d'acides fulviques et humiques, en comparaison avec la zone riveraine au sud de la zone de pergélisol.

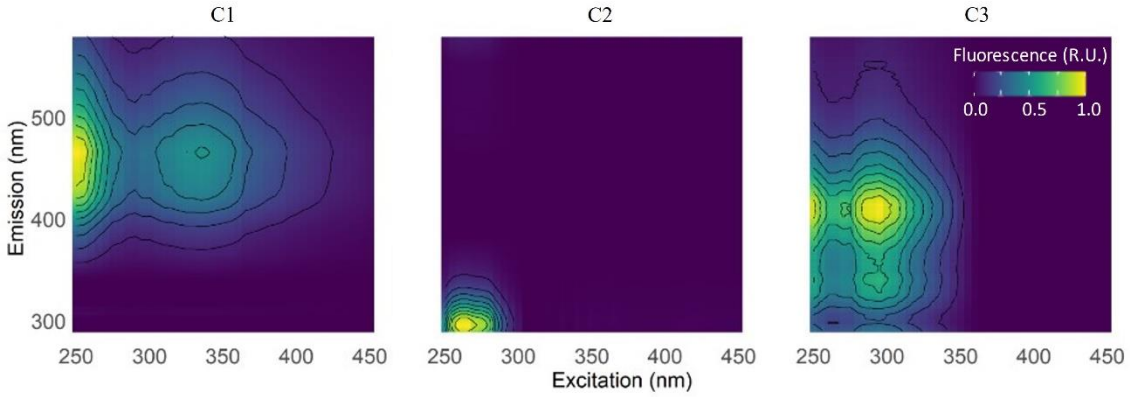

Figure 6. Matrices d'émission et d'excitation des trois composantes PARAFAC extraites d'un modèle de plus de 250 échantillons provenant de la zone côtière de la mer de Beaufort (77), l'estuaire du Saint-Laurent (118), et de la Baie des Chaleurs (62)

LE FER : UN REGULATEUR DE MATIERE ORGANIQUE

Plusieurs mécanismes sont impliqués dans la mobilité de la matière organique, dont les interactions entre la MO et les oxydes métalliques, par la floculation (ou coagulation), la coprécipitation ou encore l'adsorption de la MO sur des matrices minérales ; agissant comme un piège à plus ou moins long terme (Hedges et al., 1995; Kaiser et al., 2000; Lalonde et al., 2012; Linkhorst et al., 2017; Sholkovitz, 1976). Les interactions entre le C_{org} et les oxydes de fer réactif par coprécipitation ou adsorption auraient la capacité de piéger la MO à long terme, de manière presque irréversible, par l'intermédiaire de liaisons covalentes, sur des matrices d'argiles minérales et d'oxydes métalliques (Barber et al., 2017; Keil et al., 1994). Lalonde et al., (2012) utilisent le terme « rusty carbon sink » pour décrire ce phénomène. Les sédiments marins riches en oxydes de fer réactif (oxydes de fer amorphes) protégeraient ainsi la matière organique de la dégradation microbienne, augmentant sa préservation (Johnson et al., 1997; Kaiser et al., 2000). Près de 20 % du C_{org} présent dans les sédiments serait lié directement aux oxydes de fer réactifs, soit un stock de 19-45 PgC (Lalonde et al., 2012). 25 à 62 % du fer réactif total serait directement associé à du C_{org} par « direct inner-sphere complexation », agissant comme puits sédimentaire (Barber et al., 2017). Ces interactions C_{org}-Fe sont aussi observées dans les sédiments côtiers perméables. Dans les plages de la mer

du Nord, Linkhorst et al. (2017) ont montré qu'en précipitant expérimentalement des oxydes de fer, des agrégats se formaient préférablement avec des composés à hauts poids moléculaires (>450 Da), hautement aromatiques, riches en oxygène et d'origine terrigène. En suivant la signature isotopique du C_{org} piégé par les oxydes de fer réactifs, Sirois et al., (2018) ont aussi montré que ce processus de piégeage préférentiel se déroulait dans la zone de transition des plages de sable. En présence d'oxygène (ou d'autres oxydants), la forme réduite du fer (Fe(II)) précipite pour former des oxydes de fer réactif (Fe(III, IV)). Orem et Gaudette, (1983) ont montré que lorsque la MO, présente dans de l'eau porale anoxique, est exposée à l'oxygène, les concentrations de DOC chute, processus engendré par la coprécipitation avec les oxydes et hydroxydes de fer (Orem et al., 1984). Ce processus de séquestration serait nettement plus rapide (quelques minutes) (Zak et al., 2004) comparé au mécanisme de minéralisation. Cependant, une variation dans les conditions environnementales peut causer la réduction du Fe(III, IV), relâchant la MO (Canfield, 1997) (Fig. 7).

De nombreuses études se sont penchées sur la libération du carbone par le dégel du pergélisol, en posant comme hypothèse que la totalité du carbone relâché était minéralisée en CO_2 (Khvorostyanov et al., 2008; McGuire et al., 2018; Schaefer et al., 2014; Schaefer et al., 2011; Schuur et al., 2008; Turetsky et al., 2020). Vonk et al., (2013) ont cependant démontré que la séquestration, la sédimentation, la préservation sélective, la consommation microbienne (Vonk et al., 2013), l'adsorption ou encore l'association minérale atténuerait les émissions de CO_2 et CH_4, permettant une relocalisation temporelle et spatiale des émissions (Vonk et al., 2010). Dans une étude menée sur des milieux humides de pergélisol en Suède, Patzner et al., (2021) ont conclu que, lorsque le pergélisol dégèle rapidement, l'engorgement de l'eau et les limitations en O_2 engendrent la réduction des oxyhydroxydes de fer, mobilisant le carbone dans la phase dissoute. Cependant, le cycle d'oxydoréduction serait rythmé par les saisons. Au début de l'été, lorsque les conditions sont humides et anoxiques, les oxyhydroxydes de fer sont réduits et dissous pour précipiter à la fin de l'été, lorsque les conditions sont sèches et oxiques (Patzner et al., 2021). Cette oscillation redox agirait alors comme un puits transitoire, protégeant et remobilisant la MO saisonnièrement. Dans un

environnement où les conditions sont constamment oxiques, comme dans des sols de palses[1], par exemple, la formation d'oxyhydroxydes de fer peut se faire de manière continue agissant alors comme un piège à l'état stationnaire.

Qu'en est-il d'un environnement de pergélisol côtier, là où les marées, les vagues ainsi que le battement des tempêtes favorisent l'oscillation rédox ? En milieu côtier arctique, la MO issue du pergélisol est mobilisée rapidement d'un environnement anoxique à un environnement oxique. Les conditions oxiques favorisent non seulement la reminéralisation aérobique, mais aussi la précipitation des oxyhydroxydes de fer qui pourraient agir comme un puits, transitoire ou permanent de la MO nouvellement mobilisée.

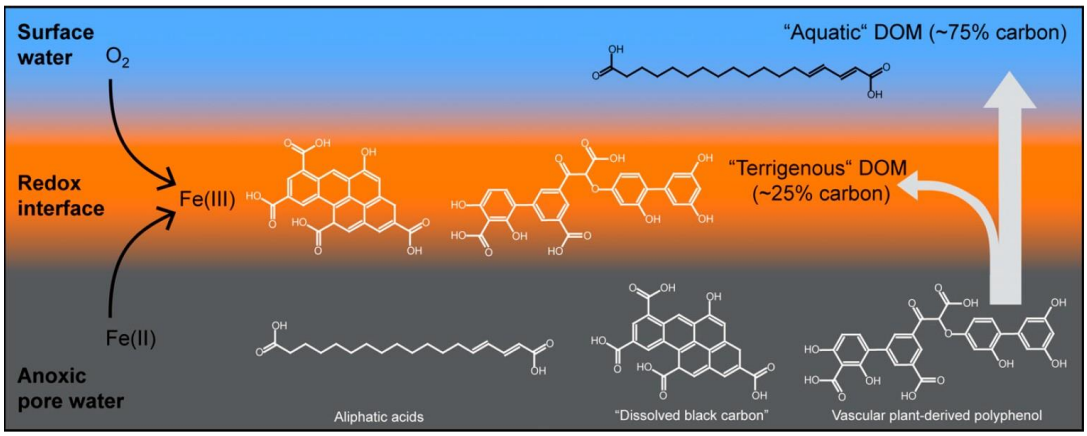

Figure 7. Exemple de mécanisme de piégeage de la DOM d'origine terrigène par les oxydes de fer réactifs (d'après Riedel et al., 2013)

[1] Les palsa sont des monticules de sol gelés de manière saisonnière superposant du pergélisol (source)

OBJECTIFS

L'objectif général de ce projet est de caractériser l'origine et le devenir de la MO issue du dégel du pergélisol côtier dans la zone côtière de la mer de Beaufort. Cette étude vise à mieux comprendre le rôle des marges continentales arctique dans le transfert de matière du continent à l'océan.

Plus spécifiquement, je souhaite :

1) **Caractériser et tracer la signature optique de la CDOM nouvellement mobilisée des falaises côtières de pergélisol à la zone infralittoral.**

2) **Évaluer expérimentalement l'affinité de la CDOM issue du pergélisol côtier avec les oxyhydroxydes de fer, en caractérisant et quantifiant la portion piégée.**

En raison des forts taux de dégel du pergélisol et d'érosion (Jones et al., 2020; Lantuit et al., 2012), la région côtière de la mer de Beaufort est un environnement idéal pour répondre à ces objectifs. Les conditions de recul du trait de côte favorisent une mobilisation importante de matière organique particulaire et dissoute (Solomon, 2005). De plus, cette région subit un apport important de MO et de C_{org} provenant du bassin versant du fleuve Mackenzie, le 4^{e} fleuve le plus important de l'océan Arctique, acheminant davantage de matière organique d'origine terrigène. Les quatre sites d'études principaux se situent le long de la côte de la mer de Beaufort : l'île de Tuktoyaktuk, Peninsula Point, Crumbling Point et North Head (voir Fig. 8). La côte se caractérise par des plaines composées de sédiments acheminés pendant l'Holocène et le Pléistocène, qui recouvrent une couche épaisse de pergélisol (épaisseur maximale : 700 m) (Judge, 1986; Solomon, 2005). Ce pergélisol riche en glace est composé de boue, sable, gravier et diamicton (Mackay, 1971; Rampton, 1988). L'île de Tuktoyaktuk est située à l'ouest de la communauté Inuvialuit de Tuktoyaktuk, dans la baie de Kugmallit. La face Nord de l'île abrite plusieurs glissements de terrain rétrogrades qui se déversent sur une plage recouverte d'une fine couche de sable et de gravier surplombant de l'argile provenant des coulées de boue de la falaise (Solomon, 2005). Il est prédit que d'ici

20 à 25 ans, l'île aura complètement disparu, exposant le havre de Tuktoyaktuk à de plus forts taux d'érosion (Jones et al., 2020). Peninsula Point se situe au sud-ouest de Tuktoyaktuk, et abrite un système important de glissements de terrain rétrogrades, tout comme Crumbling Point qui se situe au nord-ouest de la baie de Kugmallit. Finalement, North Head se situe au nord de l'île deltaïque Richards, et est entouré d'un système complexe de lagons et de lacs thermokarstiques, un lac formé à la suite de l'affaissement de terrain causé par le dégel du pergélisol.

Ce projet, financé par le réseau des centres d'excellence du Canada, ArcticNet, s'insère dans le programme international de recherche sur le pergélisol, Nunataryuk. Le programme Nunataryuk vise à comprendre comment le dégel du pergélisol sur terre, le long de la côte et sous la mer, modifie le climat mondial et la vie des habitants de l'Arctique.

CONTRIBUTION DE L'AUTEURE ET PUBLICATION

Le chapitre de ce mémoire est présenté sous forme d'article scientifique en anglais, intitulé, « *Characterization and fate of dissolved organic matter released by thawing coastal Permafrost (Beaufort Sea, NWT, Canada)* ». Cet article sera soumis à la revue *Arctic Science* au cours de la session d'hiver 2023. Je suis la première auteure de cet article, suivie de Jean-François Lapierre, Antoine Biehler, Dustin Whalen et Gwénaëlle Chaillou qui ont participé au traitement de données, au développement de la méthode, à l'analyse statistique, à la logistique de terrain, à l'échantillonnage et à l'édition de ce papier,

Les données présentées dans ce mémoire ont été collectées lors de deux campagnes d'échantillonnage dans la région de Tuktoyaktuk dans les Territoires du Nord-Ouest. Une première campagne a été réalisée par la Prof. Gwénaëlle Chaillou du 24 juillet au 6 août 2019 et a permis de récolter plus de 25 échantillons d'eau pour l'analyse du DOC, CDOM, fer total dissous (Fed_{tot}). À la suite d'une formation intensive sur le développement d'un modèle PARAFAC, j'ai traité les données récoltées lors des campagnes 2019 et 2021, mais aussi la base de données du laboratoire des hydrogéosytèmes côtiers (~250 échantillons). Ce qui m'a,

notamment, permis d'être coauteur de l'article Hébert et al., 2022, « *Origins and transformations of terrigenous dissolved organic matter in a transgressive coastal system* », publié en décembre 2022 dans la revue *Estuarine, Coastal and Shelf Science*. En 2021, j'ai organisé et participé activement à la seconde campagne d'échantillonnage à Tuktoyaktuk, du 22 juin au 31 août. Durant ces 2 mois et demi de terrain, j'ai récolté plus de 53 échantillons d'eau en suivant la méthodologie de la campagne de 2019. J'ai aussi prélevé des échantillons de carbone inorganique dissous, d'alcalinité et de méthane destinés au projet de maîtrise de Carole-Anne Guay. Dans le laboratoire, j'ai réalisé des expérimentations afin de tester l'affinité du DOC et du DOM avec des oxydes de fer. J'ai analysé tous les échantillons de 2021 pour le CDOM et le Fed_{tot}. De plus, lors de mon séjour sur le terrain j'ai rédigé un blogue de vulgarisation scientifique visant à partager mon expérience dans le Grand Nord canadien (audeflamand.wordpress.com).

Dans le cadre du projet Nunataryuk dans lequel mon projet de maîtrise s'intègre, j'ai pu participer à la préparation du rapport final sur la quantification des modifications récentes des processus de la matière organique dans l'océan Arctique. Ce dernier a été soumis en avril 2022. De même, la base de données compilant les données des campagnes de terrains de 2019 et 2021 a été publiée dans un article de type *data paper* intitulé « Nunataryuk field campaigns: Understanding the origin and fate of terrestrial organic matter in the coastal waters of the Mackenzie Delta region », qui est sous révision dans la revue *Earth System Science Data* et dans lequel je suis coauteur. J'ai rédigé la très grande majorité de ce mémoire avec l'aide de ma directrice Gwénaëlle Chaillou et de mon codirecteur Jean-François Lapierre.

De plus, lors de ma maîtrise j'ai participé à deux concours de vulgarisation scientifique « Mon Projet en 180 secondes » organisée par le comité REVUS de l'UQAR, où j'ai remporté la seconde place, et « Mon Projet Nordique », où j'ai remporté une place à la finale internationale qui a eu lieu en octobre 2022 lors de l'*Arctic Circle Assembly,* en Islande. J'ai présenté mon projet sous forme de conte de fées, que j'ai par la suite transformé sous forme de livre pour enfant « *The Tale of Sleeping DOM* », avec l'aide de Charlotte Tessier-

Larivière. J'ai aussi collaboré avec Betty Elias, une aînée de la communauté de Tuktoyaktuk. J'ai travaillé avec Betty lors d'un deuxième séjour à Tuktoyaktuk en 2022, lors duquel je me suis concentrée sur la communication de mon projet auprès de la communauté. En 2021 et en 2022, j'ai organisé des ateliers au centre des jeunes et des barbecues avec la communauté afin de montrer mes travaux et de discuter avec les membres de la communauté. Il est prévu que le livre soit publié en 2023

Les résultats de cette maîtrise ont également été présentés lors de différentes conférences sous forme d'affiches ou encore de présentation orale énumérées ci-dessous :

Présentations orales :

Aude Flamand, Jean-François Lapierre, Dustin Whalen, Gwénaëlle Chaillou, *The fate of dissolved organic matter released by thawing permafrost in the coastal Beaufort Sea*. 6 au 10 décembre 2021, ArcticNet, virtuelle.

Aude Flamand, Jean-François Lapierre, Dustin Whalen, Gwénaëlle Chaillou, *Devenir de la matière organique dissoute issue de la fonte du pergélisol côtier dans la Mer de Beaufort*, 31 janvier au 3 février 2022, AGA Québec-Océan 2022, virtuelle, prix de la meilleure présentation orale.

Aude Flamand, Jean-François Lapierre, Dustin Whalen, Gwénaëlle Chaillou, *Devenir de matière organique dissoute issue de la fonte du pergélisol côtier dans la Mer de Beaufort*, 17 au 18 février 2022, AGA Centre d'étude Nordique du Québec, virtuelle.

Aude Flamand, Jean-François Lapierre, Dustin Whalen, Gwénaëlle Chaillou, *The fate of dissolved organic matter released by thawing permafrost in the coastal Beaufort Sea*. 24 février au 4 mars 2022, Association for the Sciences of Limnology and Oceanography, virtuelle.

Présentations par affiches :

Biko Brideau, Thomas Durizot, **Aude Flamand**, Camille Gravel-Brunet, *Conditions environnementales et biodiversité de l'estuaire de la rivière du BIC*, 8 février 2021, AGA Québec-Océan 2021, virtuelle.

Aude Flamand, Jean-François Lapierre, Dustin Whalen, Gwénaëlle Chaillou, *Characterization of an optical signature of the DOM of the coastal permafrost in the Mackenzie delta, by PARAFAC analysis*. 8 février 2021, AGA Québec-Océan 2021, virtuelle.

Aude Flamand, Jean-François Lapierre, Dustin Whalen, Gwénaëlle Chaillou, *Characterization of an optical signature of the DOM of coastal permafrost, by PARAFAC analysis*. 19 au 30 avril 2021, European Geosciences Union, virtuelle.

CHAPITRE 1 : CARACTÉRISATION ET DEVENIR DE LA MATIÈRE ORGANIQUE DISSOUTE ISSUE DU DÉGEL DU PERGÉLISOL CÔTIER (MER DE BEAUFORT, TNO, CANADA)

1.1 RÉSUMÉ EN FRANÇAIS DU PREMIER ARTICLE

Aux hautes latitudes, les changements climatiques accentuent l'épaississement de la couche active ainsi que les taux d'érosion côtière et de dégel du pergélisol, entraînant une augmentation de la mobilisation de la OM. Cette matière, relâchée à l'océan Arctique par l'intermédiaire de rivières, de ruissellements et d'eaux souterraines, constitue une source importante d'OM terrigène vers l'environnement côtier. Ces apports massifs modifient non seulement la chimie des eaux côtières, mais entraînent aussi des changements dans la dynamique des réseaux trophiques et des processus biogéochimiques de l'environnement. Caractériser et suivre le devenir de cette matière est crucial afin de mieux comprendre le rôle des marges continentales arctique dans le transfert de matière du continent à l'océan. Les deux principaux objectifs de cette étude consistent à caractériser et tracer la signature optique de la DOM nouvellement mobilisée des falaises côtières de pergélisol à la zone infralittorale et d'évaluer expérimentalement l'affinité de cette matière avec les hydroxydes de fer, en caractérisant et quantifiant la portion piégée. La spectroscopie d'absorbance et de fluorescence sont ici utilisées pour identifier une signature optique spécifique de la DOM dérivée du pergélisol côtier. Une cinquantaine d'échantillons, incluant de l'eau de fonte de pergélisol, de l'eau souterraine de plage et de l'eau de mer, a été récoltée sur des falaises le long de la zone côtière de la baie de Kugmallit, dans la mer de Beaufort. Une analyse factorielle parallèle (PARAFAC) indique que cette DOM perd rapidement ses caractéristiques et qu'elle est difficilement traçable dans la zone côtière. L'eau issue du dégel du pergélisol a été caractérisée comme étant riche en DOC (>900 à 3210 µM) et en CDOM ($aCDOM_{350}$ >19 à 60 m^{-1}) et comme étant humique, à HMW et terrigène, alors que l'eau

issue de l'océan côtier, a été caractérisée comme étant plus faible en DOC et CDOM, et plutôt protéinique, à LMW et d'origine biologique. À l'aide d'expérimentation en laboratoire, nous démontrons, que des mécanismes de séquestrations sont mis en place dès la mobilisation de la matière dans la fraction dissoute. La DOM a plus haut poids moléculaire, aromatique et terrigène se ferait préférablement piéger, par coprécipitation, avec les hydroxydes de fer réactifs, contrairement à la DOM de plus petit poids moléculaire et moins aromatique qui se ferait exporter vers l'environnement côtier. De plus, le DOC ne serait que faiblement adsorbé sur les hydroxydes de fer, favorisant sa remobilisation dans la fraction dissoute. Globalement, cette étude a permis de montrer que des processus de régulation impliquant le cycle du fer, pourraient prendre place dès la mobilisation de la MO issue du dégel du pergélisol côtier, contrôlant ainsi les flux de carbone terrigène dans les eaux côtières arctiques.

1.2 CHARACTERIZATION AND FATE OF DISSOLVED ORGANIC MATTER RELEASED BY THAWING COASTAL PERMAFROST (BEAUFORT SEA, NWT, CANADA)

Aude Flamand[1], Jean-François Lapierre[2], Antoine Biehler[1], Dustin Whalen[3], Gwénaëlle Chaillou[1]

[1] Institut des Sciences de la Mer de Rimouski, Université du Québec à Rimouski, 310 Allée des Ursulines, Rimouski, (Québec), Canada, G5L 3AL.

[2] Université de Montréal, 1375 Avenue Thérèse-Lavoie-Roux, Montréal, (Québec), Canada, H2V 0B3.

[3] Natural Resources Canada, 1 Challenger Drive, Dartmouth, (Nova Scotia), Canada, B2Y 4A2.

1.3 INTRODUCTION

Permafrost stores around 1 300 Pg of organic carbon (OC) within its 13.9 × 10^6 km^2 surface area, which represents 60 % of the world's carbon stored in 15 % of the world's soil (Hugelius et al., 2014; Obu et al., 2019; Schuur et al., 2015). The Arctic permafrost coastline is greatly impacted by the global changes inducing unprecedented thawing rates, along with the deepening of the active layer (e.g. top layer of soil that thaws during the summer and freezes again during the autumn), increasing subsurface transport (Jones et al., 2020; Lantuit et al., 2012). Unlithified and ice-bonded permafrost cliffs, such as those that span along the Beaufort Sea, are particularly sensitive to coastal erosion, experiencing one of the highest coastal erosion rates recorded across the Arctic, over the past twenty years (i.e., 1.1 m yr^{-1} recorded between 1950 and 2000 and increased by 80–160 % in the last two decades; (Jones et al., 2020; Lantuit et al., 2012). Accelerating coastline erosion is supplying increasing quantities of terrestrial materials (Kipp et al., 2018), associated nutrients (Fritz et al., 2017), carbon (Bristol et al., 2021), and contaminants (Kwasigroch et al., 2018) to the coastal ocean. This additional, non-point source of solutes rapidly reaches near-shore waters and is remobilized in late summer mostly when thaw depths are at a maximum (Walvoord et al.,

2007). Dissolved organic matter (DOM) represents a fundamental link between terrestrial and aquatic carbon cycles and plays a significant role in the biogeochemistry of aquatic ecosystems (Hedges and Keil, 1995). River transported terrestrially derived dissolved organic matter (tDOM) is well known to strongly influence coastal ecosystem functioning (Vonk et al., 2015), food web dynamics (McMeans et al., 2015; Thingstad et al., 2008), ocean chemistry (Guo et al., 2007; Stedmon et al., 2011a; Vonk et al., 2014) and optical conditions (Fichot et al., 2013; Matsuoka et al., 2012). A fraction of this tDOM can be rapidly mineralized through microbial and photochemical processes, affecting nutrient budgets, air-sea CO_2 exchanges, biological productivity, as well as acidification, in coastal waters (Kaiser et al., 2017a; Kaiser et al., 2017b). For example, Kaiser et al. (2017a) showed that ~50 % of the annual tDOC discharged by Siberian rivers was mineralized along the land-sea continuum: tDOC is strongly removed and lost as CO_2 along the transport. Therefore, only a small fraction potentially persists in the ocean over centuries and millennia (Fichot et Benner, 2014; Kaiser et al., 2017a). While the export of riverine-derived tDOM is known to strongly influence the arctic marine ecosystem, little is known about the role and importance of erosional and thawing inputs on shaping the ecology and chemistry of nearshore coastal waters. This is largely due to the stochastic nature of erosion and thaw related inputs and current lack of adequately resolved datasets of coastal chemistry and environmental conditions.

Absorbance and fluorescence spectroscopies are commonly used to characterize the origin, the reactivity, and the transformations of DOM along the land-sea continuum (Fichot et al., 2014; Meilleur et al., 2023; Stedmon et al., 2003). In this study, the absorption coefficient at 350 nm ($aCDOM_{350}$) has been used as a proxy of the amount of DOM (Li et al., 2014; Müller et al., 2011), while fluorescent dissolved organic matter (FDOM) was used to discriminate allochthonous (terrestrial-derived DOM) and autochthonous sources (biological activity) (Coble, 2007). The application of excitation-emission matrices (EEM) along parallel factor analysis (EEM-PARAFAC) of FDOM (Bro, 1997) allowed to assess the composition and sources of permafrost-derived CDOM delivered to coastal arctic waters. Recently, Fouché et al., (2020) characterized the permafrost-derived DOM as low molecular

weight (LMW), proteinaceous and with low aromaticity, a signature which fades rapidly during lateral flow downslope of the permafrost table and within the fluvial continuum: suggesting high biodegradability. The chemical composition of the DOM components mainly drives its lability and transformation (Fouché et al., 2020); larger molecules such as humic substances take a longer time to degrade than simpler organic compounds (i.e., amino acids, carbohydrates, and fatty acids) (Abbott et al., 2014). These approaches, used to trace of tDOM, suggest a rapid turnover or loss of optical signature once mixed with coastal sea water.

In addition to the intrinsic chemical composition of DOM, physicochemical processes such as the presence of some minerals and the redox conditions, also shape the concentrations and compositions of DOM that transits to near-shore waters. Selective interactions between tDOM and soil minerals occur in soils and sediments (Kaiser et al., 2003; Lalonde et al., 2012; Shen et al., 2014), as well as in surficial (Hedges et al., 1986; Hedges et al., 1994) and subterranean estuaries (Linkhorst et al., 2017; Sirois et al., 2018). This results in differential retention of some DOM components during the DOM transport from land-to-sea. Adsorption of DOM on iron minerals occurs when source water passes through iron (Fe) oxide-rich sediments and the DOM compounds are then filtered out (Kaiser et al., 2000). Coprecipitation into ferric oxyhydroxide favorizes the permanent sequestration of carbon; this reduces its concentrations in the water column and protects it from mineralization (Meredith et al., 2019; Vonk et al., 2013). At the shoreline, the redox oscillation induced by tides, waves, seasonal water table levels, and long-term sea level changes control the location of Fe-oxyhydroxide formation (Charette et al., 2002). This Fe curtain acts as a barrier for redox-sensitive elements and elements with a high affinity for Fe-hydroxides, such as OM (Lalonde et al., 2012; Riedel et al., 2013). The strong affinity between DOM and ferric hydroxides, through several mechanisms, directly affects both the mobility (Kaiser et al., 2000) and molecular properties (Poulin et al., 2014) of exported DOM. A recent study showed that a significant amount of Fe-OC binding (<10 %) formed on land, during the transport to the seafloor or at the sediment-water interface prior to deposition (Faust et al., 2021). Additionally, Lalonde et al. (2012) showed that nearly 20 % of the OC present in

marine sediments was directly linked to ferric hydroxides, acting as a "rusty carbon sink" protecting OM from microbial degradation. To date, such Fe–OM interactions have been observed in soils (Jones et al., 1998; Kaiser et al., 2000; Wagai et al., 2007) and in both cohesive and non-cohesive coastal sediments (Barber et al., 2017; Keil et al., 1994; Lalonde et al., 2012; Sirois et al., 2018; Waska et al., 2021). There is, however, limited information on the potential permafrost-derived tDOM sink which could then stabilize large, oxidized, aromatic and lignin-type molecules before even reaching the coastal waters and undergoing mineralization. We hypothesize that the composition of DOM affects its affinity with Fe, as well as the composition of the non-Fe-stabilized molecules in the coastal permafrost environment.

The aim of the present study is to characterize the sources and transformations of DOM released from the thawing of coastal permafrost cliffs, while better understanding the role of arctic coastline in the transfer of tDOM from the continent to the ocean. More specifically, we have developed a site-specific scale approach in the Kugmallit Bay (NWT, Canada) to 1) optically characterize and follow the behaviour of the newly mobilized permafrost-derived DOC and DOM (CDOM and FDOM), in a near-shore coastal permafrost environment, and to 2) experimentally test the affinity of Fe-oxyhydroxides with permafrost-derived DOM and DOC, upon release from an anoxic to oxic environment.

1.4 MATERIALS AND METHODS

1.4.1 Site Description

The study area is located in the Inuvialuit Settlement Region of the Northwest Territories adjacent to the Mackenzie Delta region, the 4th largest river draining in the Arctic Ocean (Macdonald et al., 1998). A first sampling campaign took place from July 24th to August 6th, 2019, and a second campaign from June 22nd to August 31st, 2021, when thaw rates were at a maximum. About 60 samples were collected at four sampling sites characterized by continuous permafrost coastal cliffs with thaw slumps surrounded by sandy

and clay beaches: Tuktoyaktuk Island, Peninsula Point, Crumbling Point and Reindeer Island (Fig. 8). Tuktoyaktuk Island, the main sampling site (N=27), is characterized by a coastal bluff of approximately 9 m high, 1.5 km length and 100 m width (Ouellette, 2021) and is located across the Hamlet of Tuktoyaktuk, in the south-east of the Kugmallit Bay. The island loses ~1.8 m of shore per year due to erosion induced by storms, erosion, and thawing permafrost, an increase of 22% since the last 15 years (Berry et al., 2021; Tanguy et al., 2023; Whalen et al., 2022), and is projected to entirely disappear within 20–30 years (Jones et al., 2020). Peninsula Point is located in the Pingo Canadian Landmark, southwest of Tuktoyaktuk Island, and forms a complex retrogressive thaw slump system. Crumbling Point is also a retrogressive thaw slump system, located at the extreme northwest of the Kugmallit Bay. Finally, Reindeer Island is located at the north of Richards Island, in an important lagoon system formed by thermokarst lakes surrounded by coastal bluffs. According to our knowledge, there are no published data on the coastal retreat in these zones, but it could be similar, at least, to what is reported in the Canadian Beaufort-sea region (~0.5 m yr^{-1}; (Solomon, 2005)) and likely reaches locally very high retreat rates as presently observed in some location, as for example in Pullen Island (>12 myr-1, Berry et al., 2021).

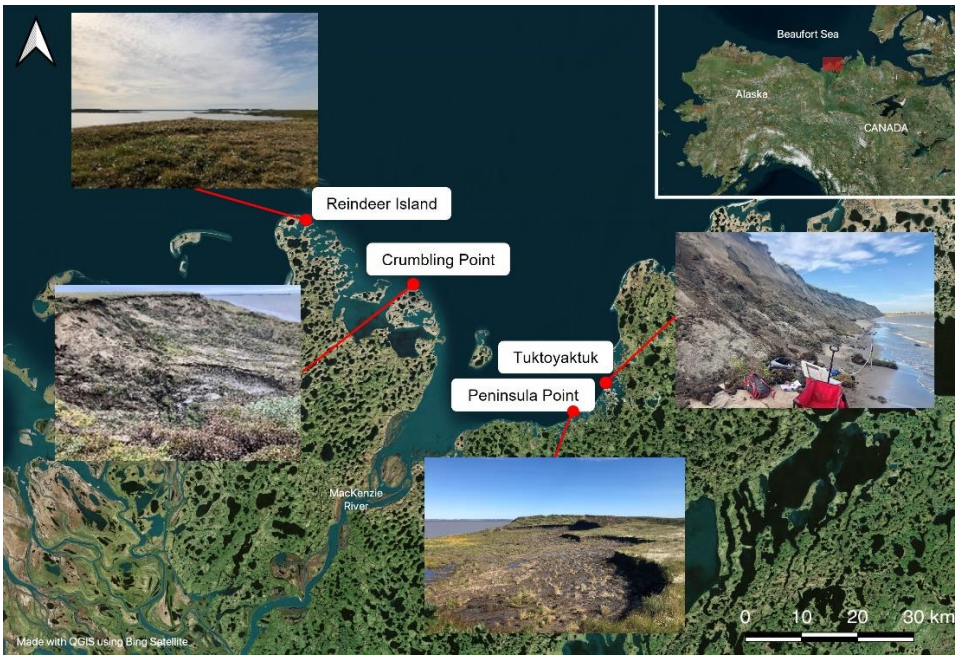

Figure 8. Map of the four sampling sites (red dots) located in the Northwest Territories, Canada

1.4.2 Water and Sediment Sampling

In each site, we carried out a site-specific scale approach where different water sample types were collected along a transect, from the coastal permafrost cliffs, through the sandy intertidal zones, to the near-shore seawater. Meltwater and groundwater (here defined as porewater into sandy coastal sediment) samples were collected on coastal permafrost slumps and on the adjacent sandy shore, respectively, while seawater samples were collected in front of each study site between 0.5 to 2 km from the coastline. Meltwater was directly sampled in puddles formed on the slope of thaw slumps using a submersible pump. For beach groundwater, push-point piezometers were inserted to ~50 cm depth into the sandy ground in front of thaw slumps in the intertidal zone and water was continuously pumped by a Solinst® peristaltic pump. Finally, bay water was collected directly in the Kugmallit Bay using a submersible pump placed between 0.5 and 1 m depth below the surface. For each location, water samples were pumped into an on-line flow cell where practical salinity (S), temperature and oxygen saturation were monitored using a calibrated multiparametric probe

(600QS, YSI Inc.). After these parameters stabilized, water samples were collected for CDOM/FDOM into acid-washed 60 mL glass amber bottles after on-line filtration through a 0.22 µm Millipore Opticap® XL4 cartridge with a Durapore® membrane. The samples were stored in the dark at 4 °C. Total dissolved Fe samples were collected in 60 mL metal-free Falcon® tubes after filtration through the same 0.22 µm Millipore Opticap cartridge. The samples were acidified with 3 drops of 70 % nitric acid to prevent the re-oxidation of reduced trace-metals and stored at 4 °C. DOC samples were taken using 60 mL acid cleaned polypropylene syringes and rapidly filtered with pre-combusted (450 °C for 5–6 hours) 0.7 µm glass microfiber filters GF/F Whatman™ and stored in pre-combusted and acid-washed 12 mL borosilicate EPA tubes with PTFE caps. The DOC samples were acidified to pH <2 with high purity HCl 2N and stored in the dark at 4 °C until analysis.

1.4.3 Chemical and Optical Analysis

DOC samples were analyzed a few weeks after data collection by Total Organic Carbon analyzer (TOC-V_{cpn} Shimadzu). The analytical uncertainty was less than 4 %, while the detection limit was of 5.8 µM. Fresh acidified deionized water (blank) and a standard solution (86.6 ± 1.7 µM) were analyzed every seven samples to ensure the stability of the instrument. The concentration of total dissolved iron (Fe_{tot}) was measured according to the ferrozine method proposed by Stookey (1970) and adapted by Viollier et al. (2000). The iron concentration was measured to ensure that it was low enough to not interfere with the absorption and fluorescence measurement of ultraviolet and visible radiation (Poulin et al., 2014). The detection limit of the method was 0.4 µM and the reproducibility was better than 0.3 %.

Absorbance and fluorescence spectroscopy were used for the measurement of the chromophoric fraction of DOM (CDOM/FDOM) a few weeks after sampling. The CDOM absorbance was measured using a Lambda 850 UV-VIS Perkin Elmer spectrophotometer with two paired 1 cm path length quartz cuvettes, for the reference and for the sample. Measurements were taken from 220 to 800 nm at 1 nm intervals with a scanning speed of

100 nm min^{-1} and a 4 nm slit width. Blanks and references were measured using fresh Milli-Q water. Every five samples, the reference cell content was discarded and refilled with fresh Milli-Q water to prevent warming. The sample cuvette was flushed with fresh Milli-Q water three times and with the sample one time. The spectral absorption coefficient (a_λ) was obtained based on the following equation:

$$a_\lambda = \frac{2.303 A_\lambda}{l} \qquad \text{Eq (1)}$$

where (A_λ) corresponds to the absorbance at a specific wavelength and (l) to the length of the path travelled by the light in the solution (in m). The FDOM fluorescence was measured concomitantly using a Varian Cary Eclipse spectrofluorometer. Fluorescence spectra were measured within the emission wavelengths of 220 to 600 nm and within the excitation wavelengths of 220 to 450 nm at 5 nm intervals as described by Couturier et al. (2016). Similarly, fresh Milli-Q water was used as a blank and to rinse the cuvette in between samples. Fresh deionized water was used as a blank and absorbance measurements of the samples were used to correct the inner-filter effect and the dataset was corrected for Rayleigh and Raman scattering, according to the method used by Pucher et al. (2019). The collected data were then described as excitation-emission matrices (EEMs).

Absorbance and fluorescence indices were extracted using the staRdom toolbox on the R Studio Software (Pucher et al., 2019). In this study we used the $aCDOM_{350}$ to track the relative concentration of CDOM in the continuum. The S_R (slope ratio) was used as an indicator of the origin of the CDOM and was calculated as the ratio of the spectral slopes 275 - 295 nm and 350–400 nm (Helms et al., 2008). S_R values of ~0.7 correspond to more terrestrial CDOM, while larger values, ~1.1 correspond to more estuarine and coastal CDOM (Helms et al., 2008). The S_R is also used as an indicator inversely proportional to the average molecular weight of CDOM referring to molecules with high molecular weight (HMW) and low molecular weight (LMW) of CDOM (Helms et al., 2008). The specific UV absorbance, $SUVA_{254}$, was calculated by dividing the absorbance at 254 nm by the DOC concentration (mgC L^{-1}) and was used to track the CDOM aromaticity (Weishaar et al.,

2003). Greater $SUVA_{254}$ values correspond to a greater degree of aromaticity (Helms et al., 2008). Lastly, the biological index, BIX, was used as a relative CDOM freshness indicator (Huguet et al., 2009). A lower BIX (~0.6) indicates an older, more decomposed CDOM, while a higher BIX (~1.0) indicates a fresher CDOM mostly associated with microbial degradation (Huguet et al., 2009). The BIX is calculated by dividing the emission fluorescence intensity (FI λ_{ex}) at 380 nm by the FI λ_{ex} at 430 nm, at an excitation wavelength of 310 nm (Huguet et al., 2009).

In combination with the absorbance and fluorescence indices, PARAFAC model was used to further investigate the composition and the sources of FDOM across samples. The PARAFAC multivariate statistical model was built to decompose the emission and excitation matrices fluorescence signals into distinct unique components (Bro, 1997; Murphy et al., 2013; Stedmon et al., 2003), using a combination of more than 250 samples from coastal arctic and subarctic coastal regions. This approach could lead to a loss of information specific to the tested dataset. However, by integrating it into a model based on a diversified database, but still in coastal and nearshore environments, the robustness of the model is assured. While only 59 samples were analyzed in this article, the 191 samples were taken from previous cruises in the St-Lawrence estuary and gulf system, including the Saguenay Fjord and the Baie des Chaleurs in the Gulf. These samples were only used to build the PARAFAC model and will not be further mentioned. Most of these samples were already published in previous articles (Hébert et al., 2022; Lizotte et al., 2022). Three major components were extracted from the validated model (split-half and core consistency) using the method adapted by Pucher et al., (2019), in R studio (R^2>92 %). The components were also matched with the literature for identification and external validation, using OpenFluor (Murphy et al., 2013). The three fluorescing OM peaks (C1-3) identified are presented in figure 9 and their theoretical characteristics based on the literature are summarized in Table 3. Component 3 appears to include more than one fluorophore, but a 4-component model could not be validated and explained only ~1 % additional variance, suggesting that if C3 includes more than one fluorophore, the molecules. associated to these very strongly co-vary among samples.

Tableau 3. Description of the EEM-PARAFAC modelled FDOM components based on the literature results of literature references. PARAFAC components and their characteristics

Comp.	Peak max Ex/Em	Coble peak	Description	Literature
C1	250-335/466	A, C	Humic-like terrestrial, HMW, aromatic	C_C : <240-340/452 (Olefeldt, Persson et al. 2014) ALL1: 250-350/459 (Pitta and Zeri 2021) C3: <240-355/476 (Stedmon and Markager, 2005a) C3: 260-370/490 (Murphy et al., 2018)
C2	265/296	B	Protein-like, tyrosine, biological, microbial autochthonous origin. LMW phenolic compounds.	C_{Ty}: 270/<300 (Olefeldt, Persson et al. 2014) ACT-10 C3: 270/302 (D'Andrilli and McConnell 2021) C6: 280/338 (Stedmon and Markager, 2005a) C1:275/<300 (Murphy et al. 2008)
C3	250-295/414	A, M	Humic-like, terrestrial, autochtonous production and microbial processing, LMW.	C_M :<240,305/404 (Olefeldt, Persson et al. 2014) C2: <300/396 (Søndergaard, Stedmon et al. 2003) C2 : 315/418 (Murphy et al., 2008)

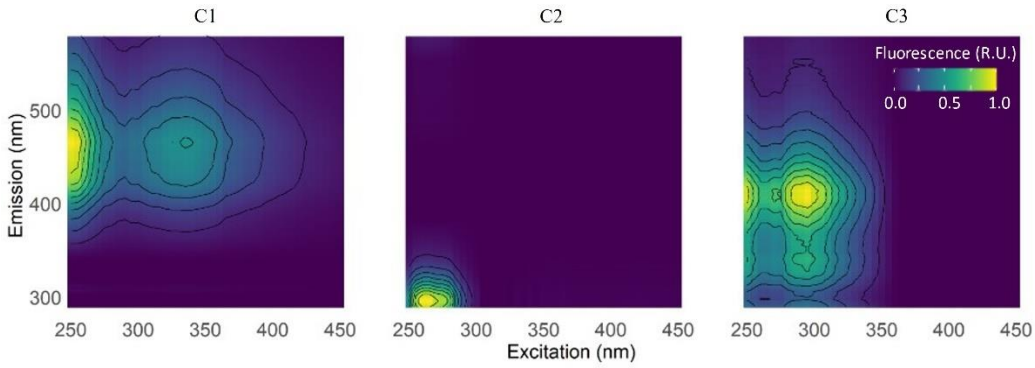

Figure 9. EEMs of the 3-components PARAFAC model. Fluorescence is expressed in Raman Unit (R.U.)

1.4.4 Affinity of Permafrost derived DOM with Iron Oxides

Experiments were performed to assess the affinity of mobilized DOM with Fe-oxyhydroxides. Beach groundwater, seawater and meltwater samples were collected in 1-L acid-washed glass bottle with a Pall® GWV High-Capacity Groundwater Sampling Capsule (0.45 µm porosity) to retain the particulate fraction. In the laboratory, ~20 mM of $FeCl_2 \cdot 4H_2O$ were added to filtered water samples. The experimental bottles were kept in the dark, at room temperature (~ 21°C) and continuously air-bubbled to maintain well-oxygenated conditions during the experiment. Sub-samples for DOC and CDOM analysis were collected at time 0, 6, 12, 24 and 48 hours as described in section 1.4.2. Briefly, DOC

samples were collected using acid cleaned polypropylene syringes and filtered with pre-combusted 0.7 µm glass microfiber filters GF/F Whatman™. The DOC samples were acidified with high purity HCl 2N and stored in the dark at 4 °C until analysis. Other indices could have been used to describe the aromaticity (SUVA) and relative molecular weight (S_R) of the OM since UV-vis absorption increases linearly with increasing iron (Poulin et al., 2014). However, in this study, we only focused on the DOC and CDOM concentrations.

1.4.5 Statistical Analysis

A multivariate approach was used to better understand the distributions and the relationships between the different optical characteristics of the CDOM dataset. The tests were performed on selected samples collected in 2021 (N=32). The database included the PARAFAC components C1, C2, and C3, as well as the S_R, $SUVA_{254}$, $aCDOM_{350}$ and BIX values. For the hierarchical cluster analysis (HCA), the database was standardized using the "normalize" function of the "vegan" package and the Euclidean dissimilarity index was used along with the agglomeration method "ward.D2" (Murtagh et al., 2014) in R. Three clusters represented optimally the dataset according to the kmeans test.

1.5 RESULTS AND DISCUSSION

1.5.1 Distribution of the physical and chemical parameters along the salinity gradient

Within the whole dataset (N=59), the concentration of Fe_{tot} ranged from 0 up to 11 µM with a mean of 1.1 ± 2.1 µM. Higher concentrations (>3 µM) were mostly found in beach groundwater. Six samples with a molar ratio of Fe_{tot}: DOC > 0.03 were excluded from the dataset as it has been shown, Fe can lead to important interference in the DOM optical properties (Poulin et al., 2014). These samples were collected in meltwater and seawater samples collected near the shoreline (~0.5 km). The practical salinity varied between ~0 and 20 (with a mean value of 3.5 ± 4.2) over the rest of the dataset (N=53), the low salinities (S<5.4) were measured in beach groundwater and meltwater samples. The

temperature varied between 8.1 and 16.7 °C (with a mean value of 13.0 ± 2.6 °C) with the higher temperatures measured in meltwater and some beach groundwater and sea water samples at the Tuktoyaktuk island site. Oxygen saturations ranged from 6.3 to 141.0 %. The nearshore surface seawater and the meltwater samples were all over saturated. However, the low salinity beach groundwater samples (N=8, S≈ 1-5) exhibited low oxygen saturation (6.3-48.1 %) indicating the occurrence of suboxic to anoxic conditions. Redox oscillations and transitory oxygen-depleted conditions are often observed in microtidal sandy intertidal zone (Hébert et al., 2022; Sirois et al., 2018; Waska et al., 2021) where the tidally input oxygen is rapidly consumed by heterotrophic respiration (Chaillou et al., 2018).

The DOC and the $aCDOM_{350,}$ here used as a proxy of the terrestrial CDOM amount (Li et al., 2014; Müller et al., 2011), exhibited a non-conservative behaviour along the salinity gradient with a rapid decreases of the concentrations in the low salinity samples, which could not be only explained by the processes of dilution (Fig. 10). DOC and $aCDOM_{350}$ exhibited however different behaviours along the gradient, the DOC concentrations dropping drastically as soon as it reaches salted water (S>1). DOC concentrations varied between 221 and 3210 µM with the highest concentrations (> 900 to 3210 µM) in the meltwater samples (S≈ 0) and lower DOC concentrations (<900 µM) in samples with higher salinity (S>1). The $aCDOM_{350}$ values exhibited a large variation from 2 to 60 m^{-1}, with a mean of 13.7 ± 10.7 m^{-1}. The highest $aCDOM_{350}$ values are consistent with permafrost studies. For example, Wauthy et al., (2018) recorded values between 45 and 55 m^{-1} in thaw pond samples at $aCDOM_{320}$. As for DOC, meltwater samples had the highest CDOM concentrations (>19 m^{-1}) at the low salinity (S≈ 0) samples, excepted for a few groundwater and seawater samples that also exhibited high CDOM concentrations (11–30 m^{-1}) (Fig. 10 b), whatever their salinities (S varying between 1 and 20). The decoupling between the $aCDOM_{350}$ vs DOC distribution along the salinity gradient suggests that they are implicated in different processes.

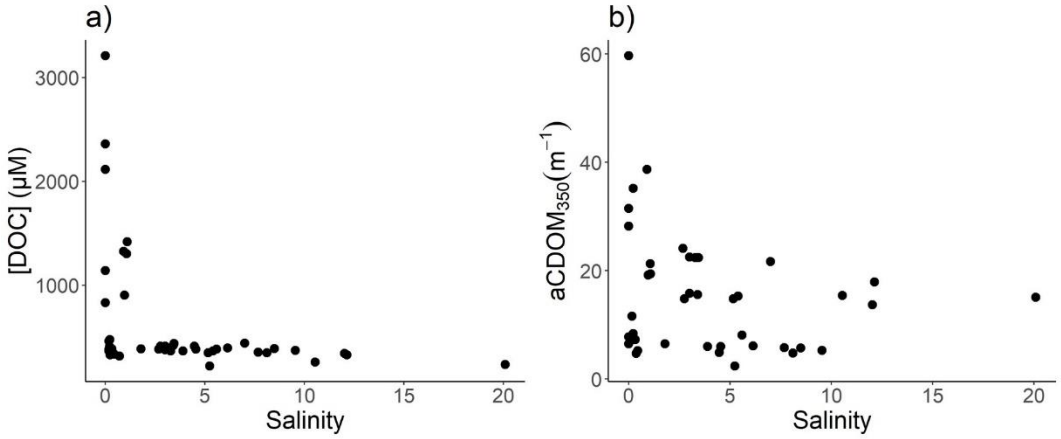

Figure 10. (a) Relationships of DOC concentration and (b) aCDOM350 with practical salinity, across the whole dataset (N = 53). The samples with a Fe/DOC molar ratio > 0.03 were excluded

The $SUVA_{254}$ values were high ranging from 1 to 7 L mgC^{-1} m^{-1} (with a mean of 3.2 ± 1.1 L mgC^{-1} m^{-1}, Fig. 11 a) which are in agreement with the $SUVA_{254}$ values of 3.4 L mgC^{-1} m^{-1} reported by Wauthy et al., (2018) for thaw pond samples. The highest values (> 4 L mgC^{-1} m^{-1}) were measured in beach groundwater samples and in nearshore seawater samples, whatever their salinities, indicating a greater aromatic content of humic substances in these samples (Weishaar et al., 2003). The lowest values (~2.3 L mgC^{-1} m^{-1}), measured in meltwater and groundwater, indicate lower aromaticity in the samples. The slope ratio (S_R) range is large, from 0.2 to 2.3, with a mean ratio of 1.1 ± 0.3 (Fig. 11 b) that likely refers to higher molecular weight CDOM of terrestrial origin. As for $SUVA_{254}$, S_R higher than 1.1 were observed in beach groundwater and nearshore seawater samples. The fluorescent index (FI) ranged from 0.3 to 3.2 with a mean value of 1.4 ± 0.4 and it exhibited the same distribution along the salinity gradient (Fig. 11 c). The highest FI values, associated with microbial-derived CDOM (>1.7), were only observed for five seawater and beach groundwater samples, while most of the other samples showed lower values (<1.5) associated with terrigenous OM (McKnight et al., 2001). This is in agreement with the biological index (BIX) which was mainly comprised between 0.5 and 0.9 (except for 3 samples, Fig. 11 d). This suggests the occurrence of more decomposed CDOM (Huguet et al., 2009). HIX showed a more complex behaviour along the salinity gradient (Fig. 11 e). The large range of

variations of the different optical indices points out the occurrence of DOM with distinct optical signatures that probably lead to different reactivities and fate in coastal waters. Globally, the values tended to decrease when the salinity increases, suggesting CDOM is fresher, less humified and lowering MW compounds in coastal waters. In the other hand, the large range of HIX (from 0.1 to 6.3) suggests highly variable humification states in low salinity samples.

According to the PARAFAC model, C2 dominated the FDOM pool. The fluorescence intensities of the component varied between 0.2-4.5 R.U. for C1 (2.6 ± 1.5 R.U.), 0.3-9.8 R.U. for C2 (5.6 ± 3.6 R.U.) and 0.1-2.4 R.U. for C3 (1.2 ± 0.6 R.U.). The two humic-like (C1-C3) components were well correlated with each other (r^2=0.83, $p < 0.05$) and with HIX (r^2=0.84 and 0.73, respectively, $p < 0.05$). In contrast, the protein-like compound C2 is only significantly negatively correlated to C3 (r^2=-0.89, $p < 0.05$) and HIX (r^2=-0.93, $p < 0.05$).

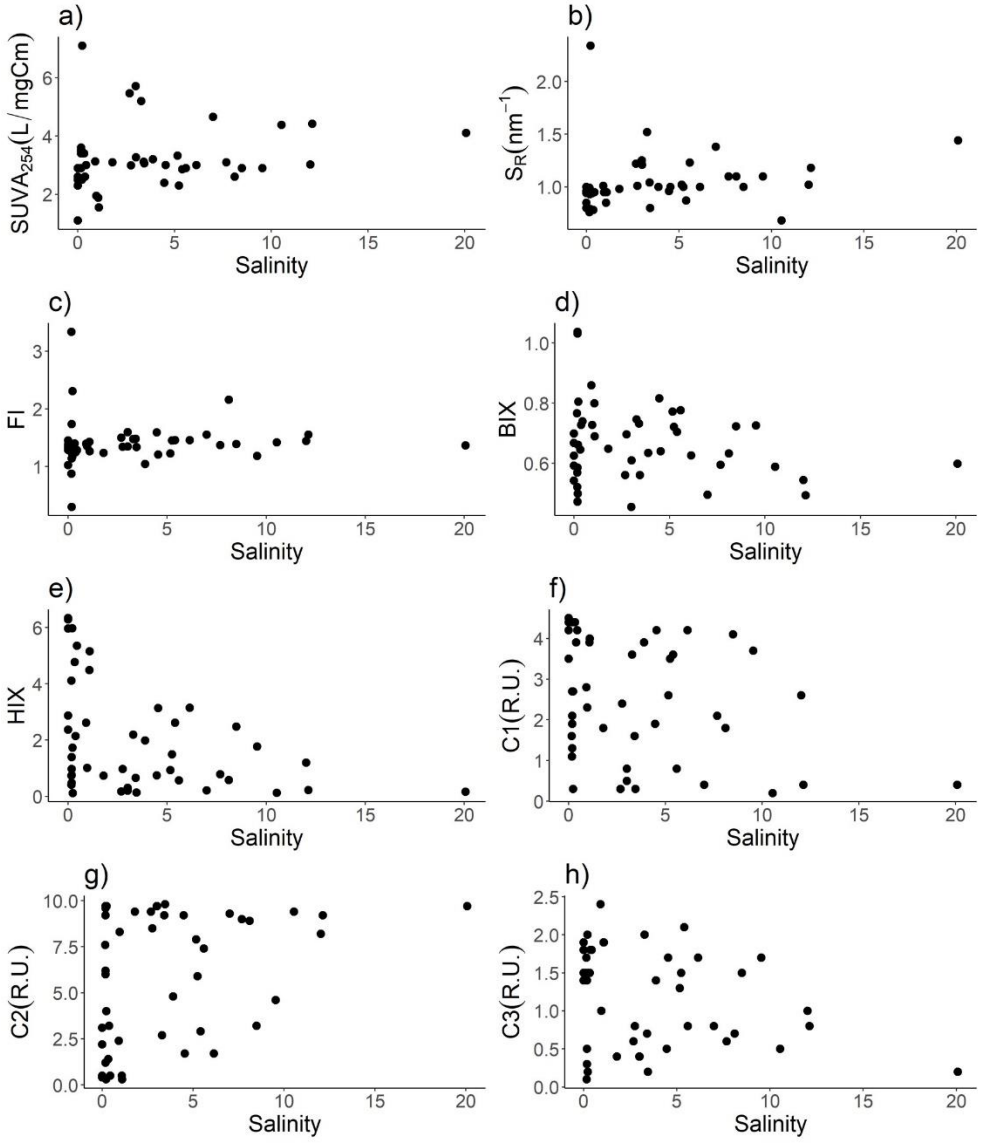

Figure 11. Relationships of (a) SUVA254 (L mgC-1m-1), (b) SR (nm-1), (c) FI, (d), BIX, (e) HIX, and the fluorescence intensity of the PARFAC components (f) C1 (R.U.), (g) C2 (R.U.) and (h) C3 (R.U.), with practical salinity, across the whole dataset (N = 53). The samples with a Fedtot/DOC molar ratio>0.03 were excluded

1.5.2 DOM characterization

To further explore the behavior of the DOM, a hierarchical cluster analysis (HCA) was achieved on the 2021 dataset based on eight optical properties (DOC, $aCDOM_{350}$, BIX, $SUVA_{254}$, S_R, and C1, C2 and C3), HIX was excluded from the selected parameters because

of the strong correlations with humic-type components C1 and C3. The salinity was not included in the HCA but was used *a posteriori* to characterize the groups along the continuum (Fig. 12 a). The HCA result separated the samples into three distinct groups: G1, G2 and G3. The distance between G1 and G2 was the smallest, while the distance between G1 and G3 was the largest. Figure 12 presents the distribution of the values of the optical parameters for each group. G1 (N=5) includes the terrestrial samples with a practical salinity of 0. It regroups all the meltwater samples collected on the slopes of thaw slumps. On the opposite, G3 (N=11) includes seawater samples only (S=3.4±3.2). G2 (N=14) includes the samples collected at the nearshore (S=2.9±3.5) and regroups beach groundwater and a few seawater samples. It is to be noted that the salinity varies greatly for G2 and G3 samples mainly in response to the tide level at the sampling time. Across the selected dataset, the fluorescence and absorbance indices remained almost stable with a low coefficient of variation (mean SUVA=3.0±0.7 L mgC^{-1} m^{-1}, mean S_R=1.0±0.1 and mean BIX=0.7±0.1 (Fig. 12 d, e, f). For the 3 groups, the CDOM is terrigenous, decomposed (BIX~0.7) (Huguet et al., 2009) and aromatic with compounds close to estuarine/coastal CDOM properties (S_R~1.1) (Helms et al., 2008). These indices suggest that the pool of CDOM, and the associated DOC present in the sampling area, mainly originated from a common terrestrial derived-OM. Indeed, while different types of OM are present in the environment and characterized by different PARAFAC components (mentioned below), they all originated from the same terrestrial source before undergoing any alteration.

In contrast to the optical indices, the modeled PARAFAC components showed more contrasted distribution within the three groups. Both humic-like components C1 and C2, showed similar distribution, with higher fluorescence intensities (F.I.) in the terrestrial groups of G1, and lower F.I. in the marine group of G3. On the other hand, the protein-like component, C2, was inversely correlated and increased greatly from G1/G2 to G3, showing an increase in the protein-like component in the marine samples. Based on these modeled components, samples included in G1 are characterized as a humic-like, high molecular weight (HMW) and terrestrially derived FDOM (C1), which agrees with Fouché et al. 2020, who characterized the active layer-derived FDOM as HMW, aromatic and terrestrially

derived. G2 corresponds to transitory FDOM, mostly collected in the intertidal zone or nearshore. While the optical signals of G2 samples are mostly similar to those of G1, the DOC and CDOM concentrations are much lower. In contrast, G3 is characterized as a tyrosine-like FDOM from biological origin, which corresponds to the signature of riverine drained permafrost derived FDOM (Olefeldt et al., 2014). Overall, G1 varied mostly according to $aCDOM_{350}$ and DOC concentrations, G2 according to C1 and C3 and G3 varied mostly according to C2.

The rapid and important decrease of DOC and CDOM from G1 (1931.0 ± 960.7 µM and 26.7 ± 21.7 m^{-1}, respectively) to G2 (390.4 ± 39.5 µM and 6.8 ± 1.7 m^{-1}, respectively), and the persistence of the humic-like components (C1 and C3) between these two groups, indicate that the CDOM released by coastal permafrost is subject to an important and rapid attenuation mechanism; during its transit, the CDOM concentrations dropped without apparent molecular transformation. This trapping is likely selective, explaining the decoupling observed between $aCDOM_{350}$ and DOC. Heterotrophic mineralization and photooxidation are not totally excluded with regards to the high DIC concentrations measured in G2 samples (DIC~1200 µM, data not shown). However, we suspect that an important fraction of the permafrost-derived tDOM is rapidly sequestrated in the iron-rich intertidal sediment, through the precipitation of iron-oxyhydroxides (Kaiser et al., 2000), which is explored in the next section.

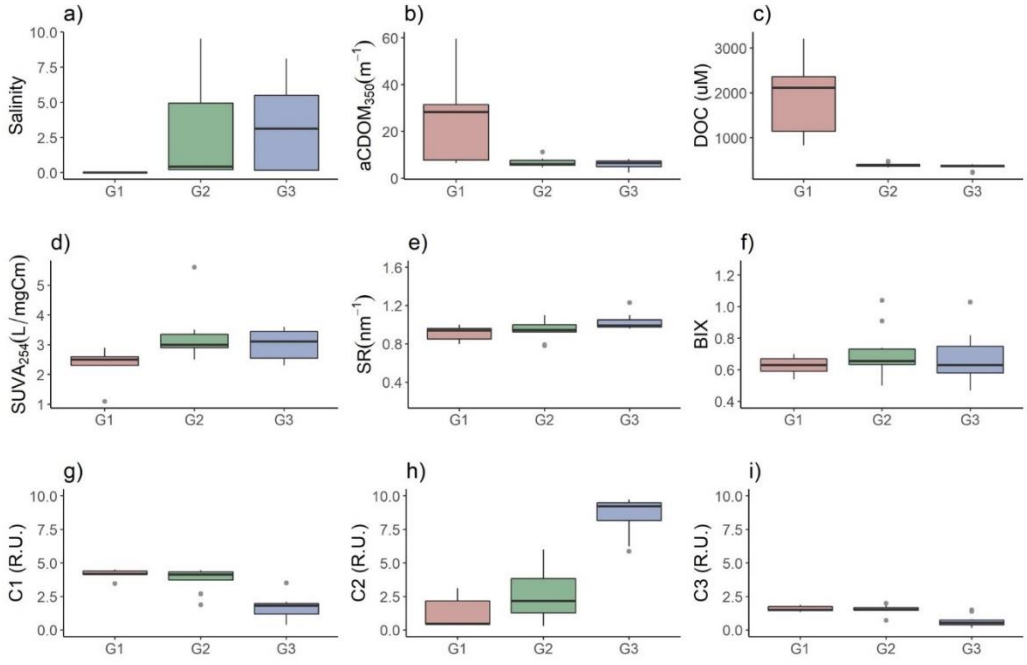

Figure 12. Box plots of the distribution of (a) salinity, (b) $aCDOM_{350}$, (c) DOC concentration, (d) $SUVA_{254}$, (e) S_R, (f) BIX, (g) C1, (h) C2, (i) and C3 across the three HCA groups. The red, green, and blue boxes represent the group 1 (G1, n=5), 2 (G2, n=14) and 3 (G3, n=11), respectively. The black lines represent the median, the whiskers represent the extent of the data, and the grey points represent the outliers

1.5.3 Affinity of Iron-Hydroxides with CDOM and DOC

To better understand the trapping mechanism of permafrost-derived CDOM and DOC by iron-hydroxides, incubations of meltwater, beach groundwater and seawater samples (from G1, G2, and G3 groups, respectively) were done by adding excess Fe^{2+} along with constant oxygen bubbling. The incubations were done with filtered (0.45 µm) and non-filtered water samples, to study the impact of particles naturally present in water, on the trapping mechanism, the occurrence of a clay mineral particle enhancing the trapping of permafrost derived-OM through sorption (Kaiser et al., 2000).

Before the addition of iron in excess, the initial DOC concentration of the seawater, beach groundwater and meltwater samples were of 383, 334 and 1019 µM, respectively, in agreement with the mean DOC values of the different HCA groups. As soon as iron was

added in excess (~20 mM), the DOC concentrations dropped rapidly in both filtered and non-filtered samples. During the next 6-hours, the DOC decreased gradually and reached its lowest concentration (Fig. 13 a and b). However, after 48-hours, a portion of the DOC was released in solution to reach a final concentration of 335, 280 and 775 µM for the filtered seawater, beach groundwater and meltwater samples, respectively. The final concentrations were slightly lower for the non-filtered samples with respective concentrations of 259, 219 and 710 µM. Furthermore, $aCDOM_{350}$ measured to evaluate the affinity of tDOM with iron-oxyhydroxides, was not corrected for iron interference as this study aims to monitor the tendency of CDOM over the experiment, rather than accurately quantifying the amount present in solution. The results revealed that, within the first 6 hours, most of the tDOM was rapidly and completely trapped by iron-oxyhydroxides for both filtered and non-filtered samples. After 48 hours, only a small portion of this initial CDOM was released back in solution (Fig. 13 c and d). DOC and CDOM did not significantly interact with the mineral surface of the particles present in the non-filtered incubation, as relatively similar DOC concentrations were present in both experiments.

Iron-oxyhydroxides showed a stronger affinity with tDOM than DOC. Our results suggested that DOC was only weakly adsorbed on the surface of the amorphous Fe-minerals formed during the experiment, while tDOM was likely completely trapped within a Fe-OC mixture. We suspect that, after desorption, *in situ* DOC undergoes rapid mineralisation, making it difficult to trace in the coastal aquatic environment. Spencer et al., (2015) showed that permafrost-derived DOC was rapidly utilized by microbes, in Arctic Rivers. Furthermore, we observed higher concentrations of *in situ* CDOM persisting along the salinity gradient (Fig. 10 b), in comparison to DOC (Fig. 10 a), The difference between these two observations could be explained by the presence of limited iron in the ambient environment, only HMW, terrestrial and aromatic CDOM are favorably trapped by iron hydroxides, letting LMW, biologically derived and less aromatic CDOM pass through (Linkhorst et al., 2017; Riedel et al., 2013; Shields et al., 2016; Waska et al., 2021). In the lab experiments, the presence of excess Fe prevented this selective affinity. The oxidative precipitation of excess Fe^{2+} (~0.02 mM) act as a natural chromatography, rapidly dragging

the suspended clay mineral in the particulate fraction and preventing further interaction between the mineral surface and the OC over the experimental time. The persisting higher CDOM concentration could also be explained by the contribution of an additional source of DOM to the coastal aquatic system.

Our findings highlight the very strong affinity of permafrost derived-OM with Fe-minerals which can act as a sink of tDOM when source water transits from an anoxic to an oxic conditions. In fact, right upon release, the permafrost derived-OM transits from an anoxic to an oxic environment, where it can rapidly interact with reactive Fe through co-precipitation, adsorption or even flocculation, trapping the OM short to long term (Hedges et al., 1995; Kaiser et al., 2000). Sirois et al. (2018) showed that Fe-OC interaction preferentially trapped terrigenous and lignin-type compounds, independently of the DOC origin, where redox processes are favored (Lalonde et al., 2012; Linkhorst et al., 2017). *In situ*, the CDOM and DOC did not follow a conservative relationship with salinity, due to the dependence of iron precipitation and redox conditions, acting independently of salinity. Riedel et al., (2013) showed that, in peatlands, redox interfaces act as an important and selective barrier for terrestrially derived OM. Furthermore, molecular composition studies revealed that HMW compounds of terrestrial origin, enriched in aromatic and hydroxyl moieties such as altered lignin and polysaccharides were strongly stabilized by Fe minerals (Linkhorst et al., 2017; Riedel et al., 2012; Shields et al., 2016; Waska et al., 2021). The increase of the protein-like component (C2) and the fading of the humic-like components (C1 and C3) in the continuum can then result from the microbial degradation of the non-Fe-stabilized molecules. Indeed, the fraction of the permafrost derived-OM which escaped the "iron curtain" must get transformed through microbial degradation and is then diluted with the DOM pool drained by the Mackenzie River.

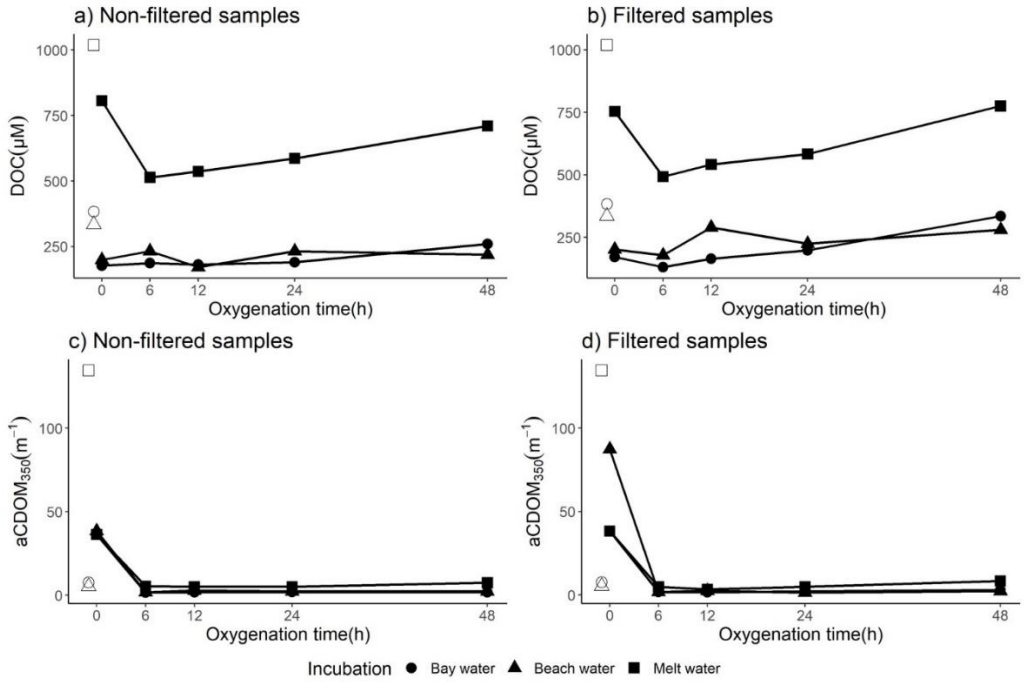

Figure 13. Variation of DOC and $aCDOM_{350}$ concentration with excess iron and constant oxygenation in bay, beach and melt water samples incubation over 48 hours. a) DOC concentration variation in non-filtered water sample b) DOC concentration variation in filter water sample (0.45 µM). c) $aCDOM_{350}$ variation on non-filtered water samples, d) $aCDOM_{350}$ variation in filtered water samples (0.45 µM). The non-colored points represent the water samples collected *in situ* without added excess iron. The black colored points represent the water samples with added excess iron and with constant oxygenation. The round, triangle and square points represent the bay, beach, and melt water respectively

1.6 CONCLUSION

In this study, chemical and optical analyses as well as iron spiked experiments were combined to better understand the biogeochemical processes involved in the regulation of coastal permafrost derived DOM, in a near-shore environment. The rapid decrease of DOC and CDOM concentrations within a short spatial scale showed that rapid processes were taking place upon permafrost thaw. However, the optical analysis revealed that the sharp drop in CDOM concentration, within the infralittoral zone, did not correspond with a changing fluorescence. These results suggest that an important and rapid trapping mechanism was taking place, rather than a transformation mechanism (e.g., photooxidation,

biodegradation), which would alter the original DOM optical properties. Additionally, while terrestrially, aromatic and HMW CDOM were favorably and rapidly coprecipitated with iron-hydroxides, DOC was only weakly adsorbed on the surface of the precipitating Fe-hydroxides, favoring a rapid desorption. The PARAFAC analysis revealed that the permafrost-derived FDOM had a heterogeneous signature due to the presence of numerous sources in a coastal permafrost environment. In the land to nearshore ocean continuum, the optical signal fades rapidly from a humic, HMW, aromatic terrigenous FDOM to a more protein-like, tyrosine biological, microbial/biological FDOM. The increasing proteinaceous optical signature but the low CDOM concentration in the more marine samples revealed a potential additional non-colored DOM source, in the estuarine/coastal environment, comparatively to the terrestrial derived DOC and CDOM, which is rapidly lost and not replaced in the continuum. Our findings, at the continental to coastal ocean interface, highlight how the combination of experiments on the effect of Fe on DOC and CDOM removal, and of field observations on FDOM composition, across a salinity gradient, suggest a shift in FDOM composition from terrestrial humic-like to protein-like material, likely produced in more marine environments. This is likely due to the rapid and preferential loss of terrestrial DOM, which settles with Fe in the coastal sediments.

CONCLUSION GÉNÉRALE

Ce mémoire a permis, de caractériser et d'étudier le devenir de la CDOM issue du dégel du pergélisol dans un continuum continent à océan côtier. Ceci a été réalisé par l'intermédiaire d'analyse optique et en testant l'affinité des oxyhydroxydes de fer réactifs avec le DOC et la CDOM issus d'un environnement de pergélisol côtier. Les résultats ont révélé que la signature optique à caractère humique, aromatique, de haut poids moléculaire (HMW) et d'origine terrigène de la FDOM issue de l'eau de fonte, s'estompait rapidement dans le continuum (Fig. 14), pour laisser place à une signature plus protéinique, de faible poids moléculaire (LMW) et dérivé de l'activité biologique dans l'environnement côtier. Cette étude montre que des processus d'atténuation et de séquestration, causés par la formation d'oxyhydroxydes de fer réactifs, seraient impliqués dans la séquestration de la MO, piégeant rapidement le DOC et la CDOM. Les expériences d'enrichissements en fer ont notamment permis de montrer que la CDOM était rapidement et complètement piégée par les oxyhydroxydes de fer nouvellement précipités, alors que le DOC serait plutôt faiblement adsorbé, favorisant leur remobilisation et leur transport dans le milieu aquatique. De plus, la portion de CDOM qui ne serait pas stabilisée par les oxyhydroxydes de fer réactifs (plus faible en oxygène, faible aromaticité, faible poids moléculaire, (Linkhorst et al., 2017) pourrait ensuite se mélanger à la MO déjà présente dans l'environnement.

Dans un contexte de changements climatiques, d'augmentation des taux d'érosion côtière et d'épaississement de la couche active, les flux latéraux de matière organique ne cessent d'augmenter (Jones et al., 2020; Lantuit et al., 2012). Il est donc primordial de mieux comprendre les processus de régulation de carbone et de matière organique qui prennent place dans les zones de pergélisol côtier. Globalement, cette étude a permis de montrer que la signature optique de la FDOM s'estompait rapidement dans le continuum continent à océan côtier et que, dès sa mobilisation, d'importants processus biogéochimiques tels que la biodégradation, la photo dégradation et/ou la séquestration, participaient à la régulation de

ces apports vers l'environnement aquatique. Le processus de séquestration affecterait autant la quantité de MO exportée que sa composition. Nos résultats sont en accord avec l'hypothèse du « rusty carbon sink », agissant comme piège transitoire lors de l'export de la matière à l'environnement aquatique côtier (Lalonde et al., 2012).

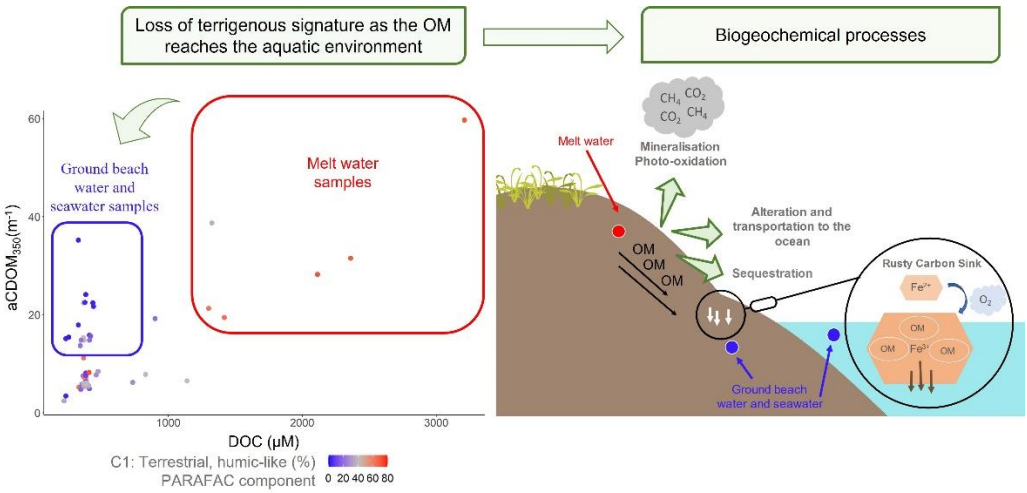

Figure 14. Évolution de la signature optique de la DOM issue du pergélisol côtier, dans un continuum continent-océan côtier. C1 correspond à la première composante extraite du modèle PARAFAC, et représente une DOM humique, terrigène, HMW et aromatique

LIMITES DU PROJET

Pendant cette étude, plusieurs aspects n'ont pas pu être abordés. Tout d'abord, 1) afin de mieux comprendre l'origine de la matière organique, une datation du DOC au carbone 14 (Δ^{14}C-DOC) aurait pu être réalisée, afin de dater le carbone qui est relâché par le dégel du pergélisol le long de son transport à l'environnement côtier (Mann et al., 2015). En effet, il est impossible, ici, de confirmer, par caractérisation optique, que la matière organique échantillonnée correspond à de la « vieille » matière issue du pergélisol. De plus, cette analyse permettrait de mieux comprendre les processus de mobilisation de la DOM entre le pergélisol et la couche active et de suivre cette matière sur une courte échelle spatiale. En effet, l'analyse optique ne permet pas de distinguer la matière lorsqu'elle est mélangée au DOM drainé par le fleuve Mackenzie. De plus, 2) il aurait été pertinent, de mesurer la

concentration de fer particulaire présent dans le sédiment et de caractériser la matière déjà piégée dans celui-ci (Chen et al., 2018; Sirois et al., 2018). Cette analyse aurait pu permettre de mieux comprendre la dynamique de cette zone transitoire. Finalement, 3) une analyse moléculaire aurait permis de compléter l'analyse optique afin de renforcer, confirmer et préciser les observations faites lors de cette étude. Par exemple, Ward and Cory, 2015 ont combiné l'analyse ^{13}C RMN à l'optique afin de caractériser la DOM issue de différentes couches de pergélisol.

PERSPECTIVES

Dans un contexte d'amplification d'érosion côtière, ainsi que d'épaississement de la couche active, de plus en plus grande quantité de vieille matière organique sera acheminée à l'océan Arctique dans les prochaines décennies (Jones et al., 2020; Lantuit et al., 2012). Il importe de mieux comprendre la composition de la matière, susceptible de perturber les stocks globaux de carbone. De même, il importe de mieux comprendre les processus impliqués dans la séquestration de cette matière nouvellement mobilisée et acheminée par apports latéraux. En effet, la présente étude a permis de démontrer que l'eau de fonte de pergélisol, qui est très riche en matière organique, est affectée par divers processus, affectant sa concentration et sa composition. Une meilleure compréhension de ces processus biogéochimiques côtiers, qui agissent sur la régulation de la matière organique, permettrait de prévenir les répercussions du dégel massif du pergélisol, prédit dans les prochaines décennies (Chadburn et al., 2017).

En perspective de ce projet de maîtrise, il serait pertinent de s'intéresser à la quantité de matière inorganique qui est issue du transport latéral de la matière dérivée du pergélisol. Plusieurs études (Schaefer et al., 2014; Tanski et al., 2019; Tesi et al., 2016) se sont déjà intéressées sur les gaz à effet de serre relâchés par le pergélisol. Cependant, une meilleure compréhension de la fraction minéralisée, sur une courte échelle spatiale, permettrait de mieux concevoir l'impact du mécanisme de séquestration et de protection, le long de son transport à l'environnement côtier. Il pourrait aussi être intéressant d'étudier l'impact de la

formation de radicaux hydroxyles (·OH), un oxydant puissant résultant de l'oxydation du fer et de la DOM réduite, sur la matière organique issue du pergélisol côtier (Page et al., 2013). En effet, ces radicaux ont la capacité de réagir avec des substances organiques affectant à la fois leur arrangement moléculaire ainsi que leur composition (Page et al., 2012). Encore très peu d'études se sont intéressées à l'impact de ce mécanisme sur le devenir de la MO, en milieu de pergélisol côtier. De plus, il pourrait être utile de caractériser des microorganismes (bactéries) dans le gradient de salinité, afin de mieux comprendre les processus microbiens potentiellement impliqués dans la transformation de la DOM dans un environnement de pergélisol côtier. Finalement, en perspective de ce projet il serait pertinent de pouvoir interpoler nos résultats, de passer d'une approche locale, spécifique à des sites d'étude, à une intégration régionale des résultats. Le développement d'une méthode d'extrapolation de résultats observés localement permettrait d'améliorer les bilans sur une plus grande échelle.

ANNEXE 1: ORIGINS AND TRANSFORMATIONS OF TERRIGENOUS DISSOLVED ORGANIC MATTER IN A TRANSGRESSIVE COASTAL SYSTEM

Hébert, A.-J., Flamand, A., & Chaillou, G. (2022). *Origins and transformations of terrigenous dissolved organic matter in a transgressive coastal system. Estuarine*. Coastal and Shelf Science. 279, 108137-108137. https://doi.org/10.1016/J.ECSS.2022.108137

Estuarine, Coastal and Shelf Science 279 (2022) 108137

Contents lists available at ScienceDirect

Estuarine, Coastal and Shelf Science

journal homepage: www.elsevier.com/locate/ecss

Origins and transformations of terrigenous dissolved organic matter in a transgressive coastal system

Anne-Josée Hébert, Aude Flamand, Gwénaëlle Chaillou *

Québec Océan, Institut des Sciences de la Mer de Rimouski, Université du Québec à Rimouski, 310 Allée des Ursulines, Rimouski, Québec, G5L 3A1, Canada

ARTICLE INFO

Keywords:
Dissolved organic matter
Carbon
Transgressive coastal system
Submarine groundwater discharge
Radon-222
EEM-PARAFAC model

ABSTRACT

Hydrogeological, geochemical, and optical approaches were combined to explore how a transgressive coastal system, where 2-kyr-old organic matter is preserved, contributes to dissolved organic matter (DOM) and dissolved organic carbon (DOC) flux to coastal waters. The sand spit system, located on the St. Lawrence shore (Chaleur Bay, Québec, Canada), was mainly composed of saline groundwater from seawater recirculation, and we estimated submarine groundwater discharge (SGD) velocities fluctuating from 0 during the rising tide to 106 cm d^{-1} during the ebb tide. The radon-222 (^{222}Rn) activities revealed the presence of two distinct water masses in the spit: a surface recirculated saline groundwater cell with a short residence time and low or no ^{222}Rn activity, and a deeper recirculated saline groundwater with a longer residence time, from a few hours to a few days, and thus exhibited higher ^{222}Rn activities. At the falling tide, the upward flow of this ^{222}Rn-rich groundwater contributes to volumetric discharges ranging from ~6 to ~17 m^3 d^{-1}, corresponding between 10 and 30% of the total SGD. Both DOC and DOM were produced in the subsurface. However, despite the concentrations being high in the discharge zone, the DOC export remained weak, with mean fluxes of 60.7 (±15.5) and 55.8 (±36.5) mol C yr^{-1} in 2018 and 2019, respectively. While surface recirculated saline groundwater dominates the SGD, absorbance and fluorescent indices indicated a strong terrestrial character in the DOM pool likely originated from material sources with a high degree of humification. An EEM-PARAFAC model reveals the dominance of humic-like components of high molecular weights and the occurrence of degraded material, whatever the tidal regime. When the residence time of the groundwater was longer, with higher radon activities, protein-like components with lower molecular weights were microbially produced, probably enhancing the bioavailability of the DOM exported to surrounding seawater. Our results suggest that transgressive coastal systems can be a hot spot for terrigenous DOM transformation which could affect the optical and chemical properties of coastal waters.

1. Introduction

Eastern Canada has been subjected to a sea-level rise since the Late Holocene (Gehrels et al., 2004; Barnett et al., 2017, 2019). This rise comes from two distinct processes, the first being the global sea-level rise associated with climate change and the second being the post-glacial rebound of Earth's crust since the last glaciation in North America (Henton et al., 2006). This recent sea-level rise has caused a marine shoreline transgression across northeast North America, resulting in the submersion of terrestrial vegetation on the coast (Barnett et al., 2019).

Terrigenous organic matter (OM) is a major source of phosphorus, nitrogen, and carbon to the coastal ocean, affecting its biogeochemistry and the primary productivity of its ecosystems(McCoy et Corbett, 2009; Stedmon et Nelson, 2015; Ward et al., 2017; Wagner et al., 2020). Although the contribution of submarine groundwater discharge (SGD) to OM fluxes remains poorly understood to this day, recent advances in technologies and techniques have allowed to better understand the impacts of SGD on the chemistry of coastal waters (Burnett et al., 2003, 2006; Povinec et al., 2012; Wu et al., 2013). The term SGD is defined as any pore water flow towards the coastal ocean, regardless of its salinity, and it thus includes seawater recirculation driven by tidal pumping or a pressure gradient through subterranean estuaries (Burnett et al., 2003). These systems are considered key ecosystems along the groundwater-seawater continuum for biogeochemical processes such as nutrient and carbon cycling (Beck et al., 2007; Anschutz et al., 2009; Moore, 2010; Chaillou et al., 2014, 2016; Couturier et al., 2016) where solutes vary in nature and concentration according to production,

* Corresponding author.
E-mail address: Gwenaelle_Chaillou@uqar.ca (G. Chaillou).

https://doi.org/10.1016/j.ecss.2022.108137
Received 7 March 2022; Received in revised form 20 October 2022; Accepted 28 October 2022
Available online 4 November 2022

transformation, and removal processes along the flow path, which mostly depends on the subsurface redox conditions (Charette and Sholkovitz, 2002; Charette et al., 2005). Different parameters can be used to investigate the source and fate of dissolved organic matter (DOM) along the groundwater-seawater continuum. In this study, we used dissolved organic carbon (DOC) to analyze the behaviour of DOM and evaluate its potential impact on coastal ecosystems. Several studies have investigated the behaviour of DOC along the groundwater flow path (Beck et al., 2007; Santos et al., 2009; Kim et al., 2012, 2013; Couturier et al., 2016; Sirois et al., 2018). Both conservative (Beck et al., 2007; Kim et al., 2013) and non-conservative (Santos et al., 2009; Couturier et al., 2016) behaviours have been observed for DOC, suggesting a high variability of production and removal processes between and within each system. However, we still have little understanding of the sources and fates of DOM. Some studies have shown that marine particles were the main source of carbon in high-energy meso to macro tidal subterranean estuary (Anschutz et al., 2009; Kim et al., 2012; Charbonnier et al., 2022) while others showed evidence that more humic-like organic compounds were dominant, as for example in the microtidal sandy Martinique Beach (Couturier et al., 2016; Qi et al., 2018). Furthermore, Kim and Kim (2017) revealed the importance of SGD-derived terrigenous organic matter in controlling the optical properties of coastal waters of a volcanic island in Jeju (Korea), and its impacts on coastal ecosystems, more specifically on corals and marine microorganisms. More recently, Waska et al. (2021) showed that buried peat lenses imprinted onto the molecular composition of DOM in the Spiekeroog beach porewaters (Germany).

Chromophoric dissolved organic matter (CDOM) is the DOM fraction able to absorb ultraviolet and visible light and can provide information about DOM's origin based on several indicators obtained from absorbance spectra (Blough and Del Vecchio, 2002). Similarly, fluorescent dissolved organic matter (FDOM) is the fraction of DOM that has the ability not only to absorb light but also to emit back fluorescent radiation. Fluorescence can be used to obtain excitation-emission matrices (EEM) which also provide indications about DOM's composition (Coble, 1996; Stedmon et al., 2003). EEM allows FDOM components, such as fulvic-like and humic-like or protein-like (tryptophan-like and tyrosine-like) substances, to be identified and distinguished between the different DOM sources (Coble, 1996). Furthermore, the application of EEM with parallel factor analysis modelling (EEM-PARAFAC), a multivariate technique commonly used to evaluate and characterize the complex mixtures of FDOM (Bro, 1997), may help better understand DOM dynamics during groundwater-seawater exchange processes. CDOM and FDOM analysis are commonly used to estimate DOM sources in coastal ocean (Coble, 1996, 2007; Helms et al., 2008; Stedmon and Nelson, 2015; Zhou et al., 2017). More recently, these techniques have also been applied to inland (Shen et al., 2015) and coastal groundwaters (Kim et al., 2012, 2013; Stedmon and Nelson, 2015; Couturier et al., 2016; Qi et al., 2018).

The source and the behaviour of DOM profoundly affect the optical and biogeochemical processes in coastal waters. Despite the recognized ecological and environmental importance of DOM in surface water, little attention has been devoted to understanding and quantifying SGD-derived DOM, more specifically in transgressive coastal systems where long-term preserved organic matter is buried. In the present study, we combined water levels, radon-222, DOC concentrations and optical properties of DOM in the discharge zone of a sand spit located in Chaleur Bay (Quebec, Canada) that formed over a 2-kyr-old paleosol as a result of recent seawater transgression. The main objective was to determine the dynamics of groundwater and derived carbon fluxes in such a system. More specifically, we aimed to quantify SGD fluxes and associated DOC exports and characterize the optical properties and transformations of DOM at the discharge zone.

2. Material & methods

2.1. Study site

This study was conducted on a sand spit located in St-Siméon-de-Bonaventure (Quebec, Canada) (Fig. 1A). There is a salt marsh to the northwest of the sand spit and the sand spit itself is surrounded by seawater. The spit is composed of coarse sands and pebbles overlying an old organic-rich soil horizon and glaciomarine clays located at a depth varying between 20 and 60 cm in the intertidal zone. The sediments found in the intertidal zone released a strong smell of sulphur and appeared coloured from dark grey to black, suggesting that the transport of oxygen in the subsurface sediments is limited. Barnett et al. (2019) recently dated the organic matter from this paleosol to over 2000 cal yrs BP, as revealed by ^{14}C dating of lignose fragments and conifer needles. The paleosol is associated with the recent sea-level rise that has been observed in eastern Canada since the Late Holocene. The relative sea level in St-Siméon-de-Bonaventure rose from −3.0 to −1.5 m from −1000 to 500 years CE and has risen at a mean rate of 0.93 (±1.25) mm yr^{-1} over the past 500 years (Barnett et al., 2019). The sand spit had a maximum elevation of 1.6 m according to Differential Global Positioning System measurements (Fig. 1B) and an approximate width and length of 25 and 425 m, respectively. The mean tidal range during the study was 1.00 (±0.37) m. The tidal dynamic is characteristic of semi-diurnal tides with low amplitudes varying from a microtidal to mesotidal scale. The tidal range varies from 1.5 m at neap tide to 2.1 m during spring tide, with mixed semidiurnal tides.

2.2. Determination of discharge rates

Two piezometers were inserted into the sand spit: one at the top of the sand spit (P_1) and one at the flexure of the beach (P_2) (Fig. 1). The piezometers were made from 3.8 cm ID PVC pipe with a 30 cm long screened end. The piezometers extended −1 m below the beach surface so that the screened bottom end was always below the water table. Automated pressure loggers (HOBO, U20-001-01) were inserted into the piezometers to monitor water-level variations every 5 min from 17 to 20 July 2018 and 1–5 July 2019. The piezometers were separated by 11 m in 2018 and by 16 m in 2019. Water table levels were corrected using barometric pressure from a logger located at the study site and were used to estimate the hydraulic gradient component perpendicular to the shore. A permanent water-level station located 25 km from the study site on the southern shore of the bay (Government of Canada; Belledune, New Brunswick; instrument #2145) was used for the tide level reference. In addition, permeability measurements (N = 10) were conducted using a Guelph permeameter to estimate the local hydraulic conductivity of the unsaturated surficial sandy sediment. Hydraulic conductivity was assumed to be homogeneous for the paleosol and permeable sediment layers. Based on Darcy's law, and assuming the hydraulic gradient component parallel to the coastline is null, groundwater fluxes from the sand spit's aquifer (q, in cm d^{-1}) were calculated as:

$$q = K \times gradH \quad \text{(Eq1)}$$

where K is the hydraulic conductivity of sand spit sediment and *grad*H is the hydraulic gradient component perpendicular to the shoreline calculated between P_1 and P_2. The q values were multiplied by the estimated vertical surface of the sand spit aquifer to determine the volumetric SGD rates (Q, in m^3 d^{-1}).

2.3. Water and sediment collection

SGD samples were collected from a 1.2 m long PVC pipe (P_5) inserted into sediments a few decimeters beside P_2 (Fig. 1) to a depth of 50 cm below the surface, at the top of the glacio-marine clay horizon. The PVC pipe was sealed at the base and equipped with a 0.3 m long screen at the

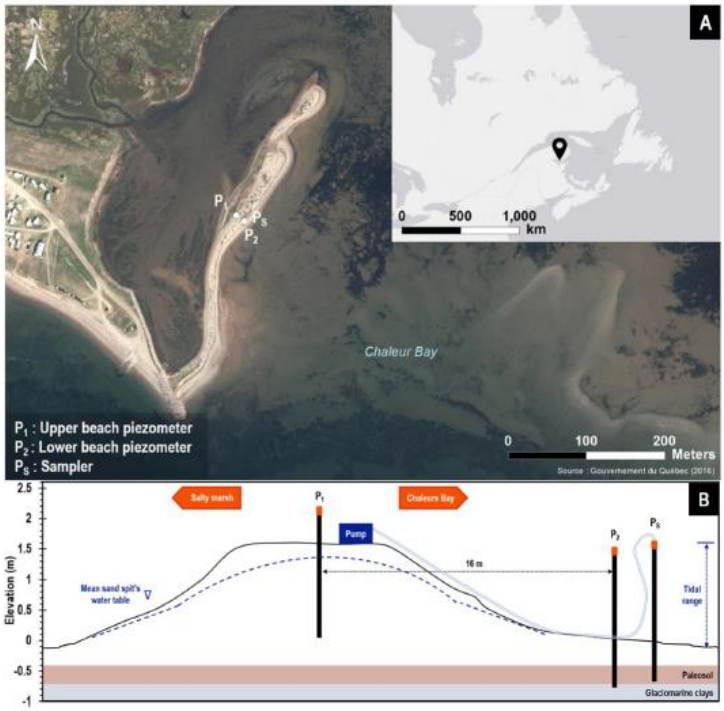

Fig. 1. Aerial photography of the study site (A) and illustrating the sand spit's elevation according to the DGPS profile and experimental sand up (B). P_1, P_2 and Ps refer to the piezometers inserted into the sandy spite to monitor water levels and collect samples. See the text for the details.

bottom. P_S was installed at least 24 h before water collection to allow the system to stabilize. Water in the PVC pipe was continuously pumped at an approximate flow rate varying from 0.2 to 0.8 L min^{-1} through a Teflon tube into an online flow cell where temperature and salinity were monitored with a calibrated multiparametric probe (YSI-600QS). However, the probe malfunctioned in 2018, so we were not able to measure salinity. A 12 h survey was first done on July 19, 2018 when samples for dissolved Fe and radon-222 (^{222}Rn) were collected every 60 min and DOC and CDOM/FDOM were collected every 30 min. Samples were collected during a second survey on 3–4 July 2019 for CDOM, FDOM, DOC, Fe, and ^{222}Rn analysis every 60 min for 24 h. Duplicate DOC samples were collected at the outlet of the Teflon tube using clean 60 mL polypropylene syringes and were directly filtered through pre-combusted 0.7 μm glass fiber filters. The filtered samples were acidified using high-purity HCl (36.5–38.0%) to pH < 2 in borosilicate EPA tubes with PTFE caps and stored in the dark at 4 °C until analysis. Water samples for CDOM/FDOM, and dissolved Fe were pumped through the Teflon tube and directly filtered using a Millipore Opticap® XL4 capsule with a Durapore® membrane (0.22 μm porosity) connected to the outlet of the tube. CDOM/FDOM samples were stored in clean glass tubes in the dark at 4 °C prior to analysis. Dissolved Fe samples were stored in 15 mL Falcon® tubes and the analysis of Fe(III) and Fe(II) was realized on site. If not analyzed immediately, total dissolved Fe samples were acidified to pH < 2 and stored at 4 °C. ^{222}Rn samples were collected into 2 L polyethylene terephthalate bottles that were tightly sealed until analysis. We also systematically sampled DOC, dissolved Fe, ^{222}Rn activities, DOM optical properties, and physicochemical parameters from three adjacent surficial sources: groundwater from the sand spit and surface seawater from the salt marsh and bay. These sources were selected because of their potential contributions to the DOM pool in the discharge zone. Sand spit groundwater samples were collected from P_1 as described for P_S. Seawater samples from the salt marsh and the bay were collected 200–500 m offshore using a submersible pump connected to an online flow cell in the same manner as described for P_S. Finally, sediment and paleosol samples were collected at the flexure of the beach at 0, 10, 30, and 60 cm depth using a hand auger and stored in polypropylene bags. A part was dried, crushed and sealed in vials for further mineral-bound radium activity counts. Other subsamples were frozen at −80 °C and lyophilized prior to their carbon content analysis.

2.4. Chemical analysis

DOC was analyzed using a total organic carbon analyzer (TOC-V_{cpn}, Shimadzu) combined with a total nitrogen measuring unit (TNM-1, Shimadzu). For DOC, the analytical uncertainties were less than 2% and the detection limit was 0.05 mg L^{-1}. Fresh acidified deionized water (blank) and a standard solution (1.1 ± 0.03 mg C L^{-1}) were frequently analyzed during measurements to ensure the stability of the instrument's performance.

Absorbance and fluorescence of chromophoric dissolved organic matter were measured simultaneously. Before optical analysis, samples were gently warm at room temperature (−20 °C) for a few hours during instrument start-up. CDOM absorbance in UV–visible spectra was measured using a Lambda 850 UV-VIS spectrophotometer (PerkinElmer) fitted with two 1-cm pathlength quartz cuvettes, one used for the reference and one for the sample. Measurements were taken from 220 to 800 nm at 1-nm intervals with a scanning speed of 100 nm min^{-1}. Fresh Milli-Q water was used as blanks and references during the analysis. The reference water was refreshed every 30 min. Before each analysis, the quartz cuvette was flushed first with 5% HCl, then with deionized water,

and finally with the sample. Concomitantly, FDOM fluorescence was measured using a Varian Cary Eclipse fluorometer and a 1-cm pathlength quartz cuvette. Emission wavelengths (λ_{Em}) ranged from 230 to 600 nm and excitation wavelengths (λ_{Ex}) from 220 to 450 nm, as previously described by Couturier et al. (2016). When the absorbance was higher than 0.3 at 254 nm, the sample was diluted to avoid saturating the fluorometer (Miller and McKnight, 2010). Fresh deionized water was used as a blank and absorbance measurements of the samples were used to correct the fluorescence data for inner filter effects. All data were corrected for the Raman and Rayleigh effect, using daily fresh deionized water signals, and for the inner filter effect, using absorbance spectra. The collected data were then described as excitation-emission matrices (EEMs).

The presence of substantial amounts of dissolved Fe(III) can interfere with the optical properties of CDOM because Fe(III) absorbs both UV and visible radiation (Xiao et al., 2013; Poulin et al., 2014). Dissolved Fe (II) and Fe(III) were measured using the ferrozine method proposed and modified by Viollier et al. (2000); the method detection limit is 0.3 μM. Measurements were done in the field in 2018 and in the laboratory in 2019 using a Genesis 20 spectrophotometer (Thermo Fisher Scientific) and a quartz cuvette with a path length of 1 cm. Fe(III) concentrations were below the detection limit in all the samples analyzed in 2018 (N = 13). In 2019, only total dissolved Fe was measured.

Radon-222 (^{222}Rn) is a radioactive noble gas produced by the decay of its parent, radium-226 (^{226}Ra). Ultimately, both ^{222}Rn and ^{226}Ra come from the decay of uranium-238 (^{238}U), which is naturally abundant in the Earth's crust. ^{222}Rn activity is nearly null in surface waters due to degassing, while groundwaters often have strong activities because of their extended contact with sediments and limited gas exchanges with the atmosphere. Therefore, ^{222}Rn is often used as a natural groundwater tracer, including in numerous SGD studies (Burnett et al., 2003; Burnett and Dulaiova, 2003; Chen et al., 2018; Webb et al., 2019). Here, we used ^{222}Rn to differentiate the geochemical signature of the hydrological components contributing to the SGD and to calculate SGD fluxes and residence time using the RADH$_2$O Big Bottle technique (DURRIDGE Company Inc.). This technique is based on the laboratory analysis of water samples collected in tightly sealed 2.0-L polyethylene terephthalate bottles. This technique was preferred to direct and continuous ^{222}Rn measurements using the RAD Aqua technique because of the limited amount of water available from Ps. Water was bubbled to allow ^{222}Rn degassing in a 30-mL headspace. The equilibrated air flowed through a drierite desiccant towards two RAD7 alpha spectrometers (DURRIDGE Company Inc.). ^{222}Rn values were then corrected using the air and water volumes used for the analysis, the water temperature, and the radioactive decay associated with the time delay between sampling and analysis, which varied between 2 and 10 h.

The mineral-bound ^{226}Ra activity of sediments was determined using dried samples. These measurements were done as a first attempt at the activity of ^{226}Ra-supported ^{222}Rn in beach groundwater. Sediment samples were sealed in vials fitted for a high-purity Germanium gamma-ray spectrometer (ORTEC® DSPEC jr. 2.0). They were left in sealed vials for at least 23 days prior to the measurement to ensure radioactive re-equilibration between the ^{226}Ra and the short-lived daughters of the ^{238}U series. Counting time was fixed at 3–4 days to provide adequate counts for the peaks of interest. Counts were based on the measurement of ^{214}Pb (using the 295.2 and 352 keV) and 214Bi (609 keV) peaks with a counting error is <10%.

The elemental analysis of total and organic C (fumigation) was done on the organic matter of the paleosol and on intertidal sediments at the GEOTOP facilities (Light stable isotopes geochemistry laboratory, GEOTOP-UQAM, Montreal, QC, Canada) by combustion using an elemental analyzer (Carlo Erba NC2500) combined with a gas chromatograph equipped with a thermal conductivity detector.

2.5. DOM optical indices and EEM-PARAFAC modelling

Different CDOM absorbance metrics were calculated running a routine code on Rstudio. In this study, we only present three of them. The absorption coefficient $a_{CDOM}(\lambda)$ (m^{-1}), where λ is the wavelength (nm), was calculated as 2.303 times the absorbance divided by the pathlength of the cuvette (m). Here, we used the $a_{CDOM}(375)$ value as an estimation of CDOM concentration (Blough and Del Vecchio, 2002). The spectral slope ratio (S_R) was used as an indicator inversely proportional to the average molecular weight of DOM and was calculated using the spectral slopes between the shorter wavelength region (275–295 nm) to that of the longer wavelength region (350–400 nm) using the non-linear regression technique described by Stedmon et al. (2000). This parameter refers to molecules with high molecular weight (HMW) and low molecular weight (LMW) of CDOM (Helms et al., 2008). Furthermore, we estimated the absorbance spectra to calculate specific ultraviolet absorbance at 254 nm by dividing the linear absorbance by DOC concentrations (in mg L^{-1}). $SUVA_{254}$ (in L mg C^{-1} m^{-1}) has been shown to be positively correlated with molecular weight and a good indicator of aromaticity of humic substances: a higher value is associated with greater aromatic content (Weishaar et al., 2003).

EEM and fluorescent metrics were produced using the eemR package proposed by Massicotte (2018) for RStudio software. Briefly, scans were processed as follows: 1) all scans were corrected for Raman and Rayleigh scattering using freshly Milli-Q water signals prior to analysis; 2) the inner filter effect was corrected to account for the quenching of fluorescence by absorbance; 3) a Raman calibration was done to each EEMs to remove the dependency of fluorescence intensities on the measuring equipment, as proposed by Lawaetz and Stedmon (2009); and finally 4) fluorescent DOM metrics were extracted from the EEMs. The biological index (BIX), humification index (HIX) and fluorescence index (FI) were extracted to trace the diagnostic state of the FDOM pool. FI was calculated using the ratio of emission intensity at 450 nm to that at 500 nm, from excitation at 370 nm. It was shown to be a good indicator of the general source and aromaticity of DOM: higher values (>1.7) are mostly associated with microbial-derived DOM while lower values (<1.5) are associated with terrigenous OM (McKnight et al., 2001). HIX corresponds to the peak area under emission of 435–480 nm divided by the peak area under emission of 300–345 nm, at an excitation of 254 nm. It is an indicator of humic substances and the extent of humification of organic matter (Hansen et al., 2016; Ohno, 2002): higher HIX indicates a greater humification of the OM source and HMW compounds. Finally, BIX is the ratio of the fluorescence intensity at an emission wavelength of 380 nm (β peak) to that of the maximum fluorescence intensity at an emission between 420 and 435 nm (α peak), from excitation at 310 nm. The BIX also called the freshness index characterizes the autochthonous production of DOM: higher values (−1.0) are mostly associated with fresh, likely microbial DOM while lower values (−0.6) are associated with more decomposed OM (Huguet et al., 2009).

EEMs spectra of DOM fluorescence were analyzed using a parallel factor analysis model (EEM-PARAFAC), a multi-way data analysis used to decompose the combined fluorescence signal of DOM into distinct modelled components (Bro, 1997; Stedmon et al., 2003; Cory and McKnight, 2005; Lapworth and Kinniburgh, 2009). The PARAFAC model was run on the staRdom package for RStudio (version 4, R Development Core Team, 2019) (Pucher et al., 2019). The staRdom Toolbox was used to explore the data set, validate the PARAFAC modelling and determine the appropriate number of selected modelled components. Furthermore, split-half analysis and core constituency diagnosis were used to confirm the model's validity and 'appropriateness', and external validation was also used through the OpenFluor database to compare the resulting components with the existing literature (Murphy et al., 2013). Here, the four first components were able to satisfactorily model the EEM from the data set (e.g. a reasonable fit above 97% was obtained).

2.6. Data processing

Linear regression was used to identify correlation between optical DOM metrics, DOC concentrations and radon. A correlation matrix was used to evaluate the dependency between the different parameters using a parametric Pearson test (regression coefficient R^2 are significant to $p < 0.05$). Results are presented as a correlogram. When regression coefficients are not significant ($p > 0.05$), R^2 is not reported. Analysis and plots were all performed on RStudio software (v March 1, 1093).

3. Results

3.1. Hydraulic gradients and discharge rates

The hydraulic gradients between P1 and P2, associated with the mean hydraulic conductivity measured using a Guelph permeameter ($K = 1.85 \times 10^{-4}$ m s^{-1}) were used to calculate the SGD velocity (q) according to Darcy's law. To convert these results to volumetric flux (Q in m^3 d^{-1}), the cross-sectional flow area was determined using global positioning system (GPS) measurements of the 425 m long shoreline. These hydrological analyses revealed similar Q values between the two periods, with fluxes varying from 0 to 97 and from 0 to 95 m^3 d^{-1} in 2018 and 2019, respectively, with mean similar values of 53 m^3 d^{-1} in 2018 (Fig. 2A) and 46 m^3 d^{-1} in 2019 (Fig. 2B). Based on the presence of glaciomarine clays under the sand spit permeable sediments, including the organic horizon of the paleosol, we estimated that the depth of the discharge zone at the flexure is limited to an average subsurficial depth of 0.3 m (Fig. 1B). The Q values were shore-normalized by dividing them by the sand spit's length. This leads to shore-normal Q value averaged 0.13 (±0.06) and 0.11 (±0.06) m^3 m^{-1} d^{-1} in 2018 and 2019, respectively.

3.2. Time series of radon

The ^{222}Rn activity observed in the discharge zone was highly variable, ranging from 4 to 715 Bq m^{-3} in 2018 and from 74 to 10,074 Bq m^{-3} in 2019 (Fig. 3). These activities were much higher than those measured in the surface waters of the salt marsh and the adjacent bay (Table 1). These values are however lower than the ^{222}Rn activities likely supported by the mineral-bound ^{226}Ra activities (and assuming secular equilibrium conditions) that varied from 4,900 Bq m^{-3} in surficial sediment to 16,000 Bq m^{-3} in sediment in contact with the glaciomarine clay. This suggests that water masses never spent enough time within the system to reach secular equilibrium, at least during the sampling periods.

The ^{222}Rn activities showed a continuous increase during ebb tide, with the highest values at low tide or a few hours before (Fig. 3). In 2018, we calculated a ^{222}Rn gradient of −150 Bq m^{-3} h^{-1} (Fig. 3A). In contrast, we calculated two similar ^{222}Rn gradients in 2019 of −1,000 and −750 Bq m^{-3} h^{-1} (Fig. 3B), which is 5–6 times higher than the gradient observed in 2018. The gradients likely corresponded to the rapid upward transport of deep ^{222}Rn-rich groundwater to the surface, probably under piston flow, and influenced by vertical seawater infiltration processes as it was already observed in the recirculating seawater cell of a microtidal sandy beach (Chaillou et al., 2018). Using maximal ^{222}Rn activities measured over the sampling period (e.g., 715 and 10,074 Bq m^{-3} in 2018 and 2019, respectively) and assuming a mean (and theoretical) effective porosity of 39% for coarse sand sediment, we

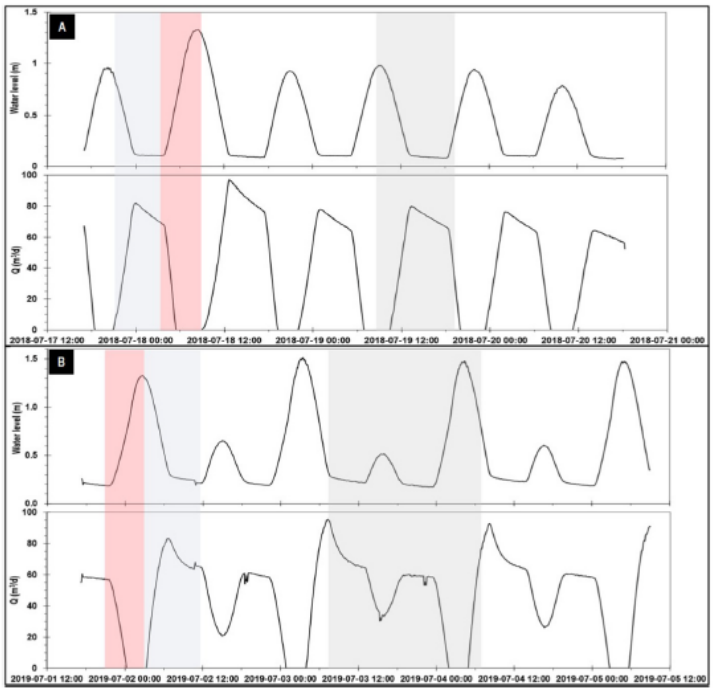

Fig. 2. Groundwater levels recorded at P_2 and associated volumetric SGD (Q in m^3/d) calculated using Darcy's Law in June 2018 (A) and July 2019 (B). Red bands highlight flood and high tide, blue bands highlight ebb and low tide, and grey bands highlight the sampling periods. (For interpretation of the references to colour in this figure legend, the reader is referred to the Web version of this article.)

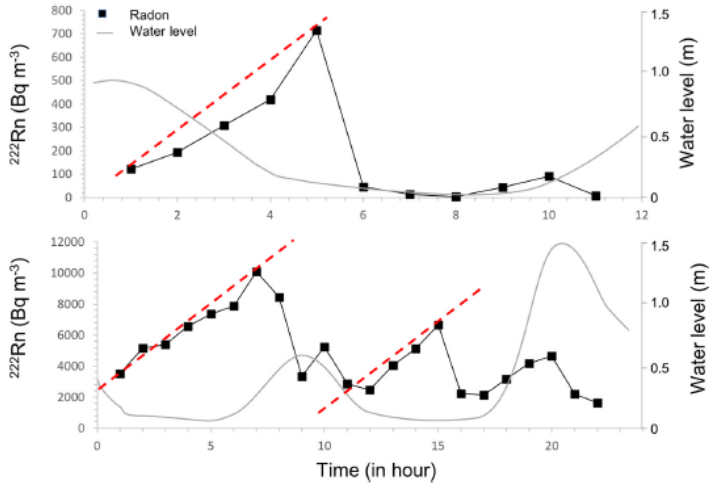

Fig. 3. Tidal variations of ^{222}Rn activities in the discharge zone measured in Ps (black squares) showing water levels at P_2 (grey line) in 2018 (A) and 2019 (B). Red dotted lines highlight the ^{222}Rn activity gradients use to calculate the SGD fluxes. (For interpretation of the references to colour in this figure legend, the reader is referred to the Web version of this article.)

Table 1
Biogeochemical and physical characteristics of waters surrounding the discharge zone. The seawater term included the samples collected in the salt marsh and in the adjacent bay. Sand spit groundwater corresponds to samples collected in P_1.

Parameter	Seawater (N = 7)	Sand spit GW (N = 5)
T (°C)	22.0 (±2.6)	18.7 (±1.9)
^{222}Rn (Bq m^{-3})	47 (±34)	1699 (±1480)
Salinity (g kg^{-1})	32.4 (±1.9)	31.0 (±1.4)
Total dissolved Fe (μM)	1.0 (±0.3)	1.6 (±0.9)
DOC (μM)	169.4 (±14.9)	253.0 (±87.5)
aCDOM$_{375}$ (m^{-1})	2.6 (±1.5)	5.7 (±2.5)

calculated volumetric discharges of 16.8 and 5.9 m^3 d^{-1} in 2018 and 2019, respectively. These discharge rates are lower than total Darcy's flow, representing between 30 and 10% of the Q values.

3.3. Sedimentary organic matter from the paleosol

The particulate analysis of the sedimentary organic matter collected in the paleosol ($N = 8$) showed higher organic carbon content with C_{org} varied from 2.5 to 5.6% compared to low total nitrogen content (N_{tot}) ranging between 0.02 and 0.26%. The mean C_{org}:N_{tot} molar ratio was 26.8 (±8.8), with samples reaching a ratio of 43, which likely corresponds to a pool of sedimentary organic matter of resistant plant material mainly composed of lignified tissues, waxes and polyphenol

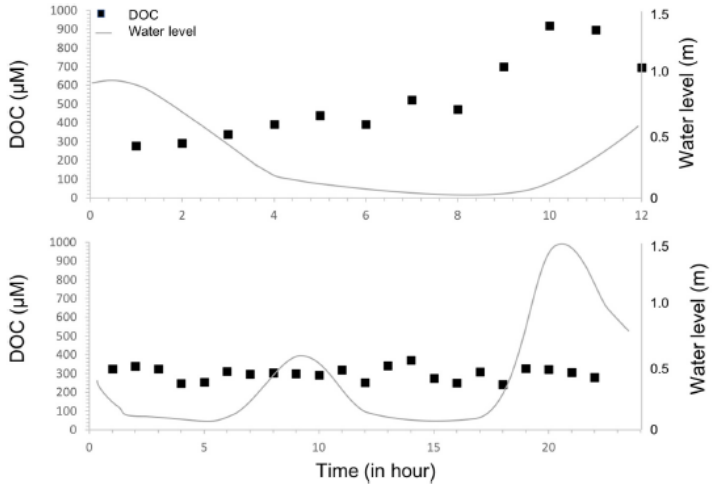

Fig. 4. DOC concentrations (in μM) in the discharge zone (black squares) and water level at P2 (grey line in m) in 2018 (A) and 2019 (B).

compounds (as proposed in the RothC model for the turnover of organic carbon in soil (Coleman and Jenkinson, 1996)). These results agree with the macroscopic observation of needles and pieces of wood as well as with the old and degraded character of the paleosol reported by Barnett et al. (2019).

3.4. Dissolved organic carbon in the discharge zone

High DOC concentrations were observed in the discharge zone, varying from 276.5 to 894.5 µM (Fig. 4), concentrations higher than the concentrations measured in the surrounding waters (Table 1). The increase of DOC concentrations observed at the rising tide in 2018 is absent in 2019 where the DOC remained relatively constant. Based on the hourly averaged Q values, we calculated SGD-derived DOC fluxes varying from 81.8 to 271.6 mmol d^{-1} in 2018, with a mean value of 166.3 mmol d^{-1}, and from 129.7 to 190.7 mmol d^{-1} in 2019, with a mean value of 153.0 mmol d^{-1}. Despite the high DOC concentrations measured in the discharge zone, the SGD-derived DOC fluxes remained low in response to the low volumetric SGD. This led to a mean shore-normal DOC flux of −375 µmol d^{-1} m^{-1}.

3.5. Characterization of the DOM

Mean concentrations of total dissolved Fe are low and varied between 8.0 ± 2.2 µM in 2018 and 7.3 ± 2.5 µM in 2019, resulting in low total Fe:DOC molar ratios, on the order of 10^{-2}. The effect of dissolved Fe on the absorbance and fluorescence of DOM was likely negligible (Poulin et al., 2014). and no correction was applied to the DOM concentration, absorbance, or fluorescence.

3.5.1. Variations in spectral and fluorescent indices

The spectral indices of absorption, the absorption coefficient $a_{CDOM}(375)$, SUVA, and the slope ratio (S_R), and fluorescence indices, the humification index (HIX), fluorescence index (FI) and biological index (BIX) are summarized in Fig. 5. The distribution of $a_{CDOM}(375)$ parallels the DOC distribution in the discharge zone with content ranging from 5.0 to 28.9 m^{-1} and from 7.6 to 11.3 m^{-1} in 2018 and 2019, respectively (Fig. 5A). As for DOC, this DOM content was higher in the discharge zone than in the surrounding waters, including groundwater collected in P_1 and seawater (Table 2). SUVA values were high in the discharge zone with median values around 2.3 L mg C^{-1} m^{-1} (Fig. 5B) with some samples reaching SUVA values higher than 3.5 L mg C^{-1} m^{-1} in 2018. The SUVA values were slightly lower in surrounding waters with values around 1.7 and 1.1 L mg C^{-1} m^{-1}, for groundwater collected in P_1 and seawater, respectively. The S_R median values were higher than 1 in the discharge zone reaching a median value of 1.43 in samples collected in 2018 (Fig. 5C). In surrounding waters, the S_R values were lower, dropping to 0.90 in groundwater samples collected in P_1. The HIX (Fig. 5D), BIX (Fig. 5F) and FI (Fig. 5E) median values were similar for both years, with respective median values of 6.35, 0.55 and 1.34. These values were close to those measured in P_1 and higher than the values calculated in seawater samples.

3.5.2. EEM-PARAFAC modelled DOM

The 4 fluorescing OM peaks (C1-4) identified by the PARAFAC model are presented in Fig. 6 and their theoretical characteristics based on the literature are summarized in Table 2. The two first components were characterized as humic-like components: HMW terrestrial-derived allochthonous components for C1 and microbially produced for C2. Both are correlated with fulvic acids. The two other components (C3-4) were biologically transformed products of LMW with a protein-like character. The fluorescent intensities (F.I.) of components C1, C2 and C3 showed similar distribution, with the highest values in the discharge zone in 2018 and in groundwater samples collected in P1 (Fig. 7). Moreover, C1-3 exhibited relatively homogenous F.I. over the sampling period (Fig. S1 in supplementary material) and over years, as revealed by the low standard deviations of the dataset. The humic-like components of HMW, C1, likely dominated the pool of FDOM in 2018, with an equal contribution of both C2 and C4. While C3 was low in the discharge zone in 2018, the protein-like components of LMW contributed mainly to the FDOM measured in the discharge zone in 2019 and in the seawater samples. They also exhibited large ranges of F.I., from <20 R.U. to more than 80 R.U.

The relationship between DOC, spectral and fluorescence indices, modelled DOM components and radon was explored using linear regressions (Fig. 8). DOC, $a_{CDOM}(375)$, S_R, C4, and to a lesser extent C1, C2 and BIX were positively correlated with each other's. The fluorescent intensity of C3 was strongly negatively correlated with C1, C2 and C4 and to a lesser extent with HIX, BIX, and S_R. However, C3 is positively correlated with radon and FI.

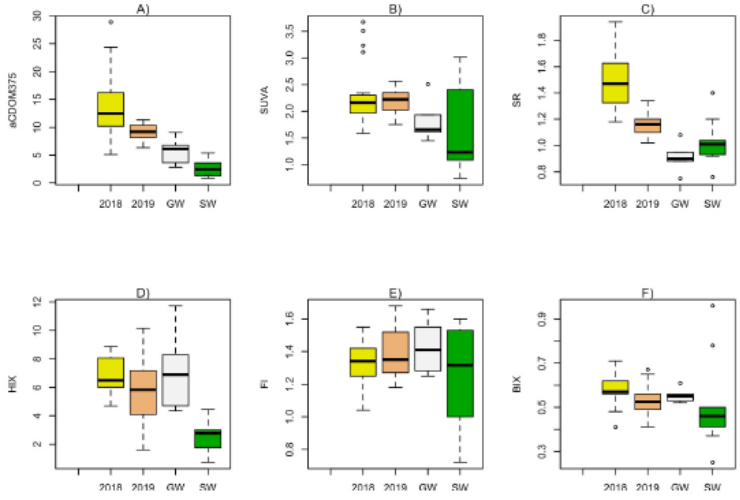

Fig. 5. Box plots of spectral and fluorescent indices: $a_{CDOM}(375)$ (A), SUVA (B), S_R (C), HIX (D), FI (E) and BIX (E). In yellow and orange boxes represent the values measured in the discharge zone in 2018 and 2019, respectively, the grey boxes combined values for both years measured in P_1 (N = 5), and the green boxes represent the values in the surrounding seawater samples (N = 7). Black lines are the median, whiskers are the extent of data, and dots outside the boxes are outliers. (For interpretation of the references to colour in this figure legend, the reader is referred to the Web version of this article.)

Table 2
Description of the EEM-PARAFAC modelled DOM components based on results of literature references.

Component	Peak position (nm)	Coble peak	Probable sources	Reference
1	250-340/468	A (240–260/380–460)	Terrestrial humic substances, widespread	C1: <240 (355)/476, Stedmon and Markager, 2005
		C (320–360/420–480)	Humic-like, terrestrially derived, allochtonous. HMW, aromatic, correlated with lignin phenols and fulvic acids	C3: 260(370)/490, Murphy et al. (2008)
2	250-305/412	M (290–320/380–420)	Marine and terrestrial humic materials	C4: 250–325/416, Stedmon et al. (2003)
			Microbial component	C3:295/398,
			Anthropogenic humic materials, agricultural	Stedmon and Markager (2005a)
			Coupled to fulvic acids	C5 : 325/428, Stedmon and Markager (2005b)
				C2 : 315/418, Murphy et al. (2008)
3	260/294	B(275/310)	Protein-like, tyrosine, biological autochthonous origin (transformed products).	C6: 280/338, Stedmon and Markager, 2005
			LMW phenolic compounds	C1:275/<300, Murphy et al., (2008)
4	270/312	T(275/340)	Protein-like, tryptophan, biological autochthonous origin (transformed products).	C4: 275/306 (338), Stedmon and Markager (2005a)
			LMW phenolic compounds	C6: 280/328, Murphy et al. (2008)

4. Discussion

4.1. Tidal dynamics and discharge rates – inputs from Darcy's law and radon

The absence of connection with the continental aquifer and the hydrostratigraphic context of the sand spit leads to a specific groundwater-seawater interaction where groundwater is mostly saline and the recirculating seawater cell occupies most of the discharge zone, regardless of the tidal level. In this specific context, the maximal Q values (>95 $m^3\ d^{-1}$) were only reached during the strongest low tides. The shore-normal Q estimates were very low compared to other micro and mesotidal STE, such as Martinique Beach (Îles-de-la-Madeleine, Québec, Canada, 1.5–6.1 $m^3\ m^{-1}\ d^{-1}$; Chaillou et al., 2016, 2018), Shelter Island (Long Island, New York, USA, 0.4–17 $m^3\ m^{-1}\ d^{-1}$; Burnett et al., 2006), and Turkey Point (Florida, USA, 0.5–22 $m^3\ m^{-1}\ d^{-1}$; Santos et al., 2009). The small size of the spit and the presence of the glacio-marine clay horizon of low permeability under sandy sediments limited the outflow of groundwater in the discharge zone.

Despite these conditions, the range of ^{222}Rn activities was large in the discharge zone, varying from a few Bq m^{-3} at high tide to −10,000 Bq m^{-3} when the flow was maximal as observed in 2019. The ^{222}Rn activity was not salinity-dependent and two distinct ^{222}Rn activity signatures were observed: surface recirculated saline groundwaters with short residence time in the sand spit and little or no ^{222}Rn activity, and deeper recirculated saline groundwaters with longer residence time and thus high ^{222}Rn activities. The difference in radon activities measured between 2018 and 2019 also indicates different groundwater residence times. The reasons for these differences are not known but could be related to the tidal and meteorological regimes of the days preceding the sampling. A rough estimation of the time spent by these water masses within the system can be determined based on the mineral-bound ^{226}Ra activities as the ^{222}Rn activities at secular equilibrium using the following equation (Eq (2)):

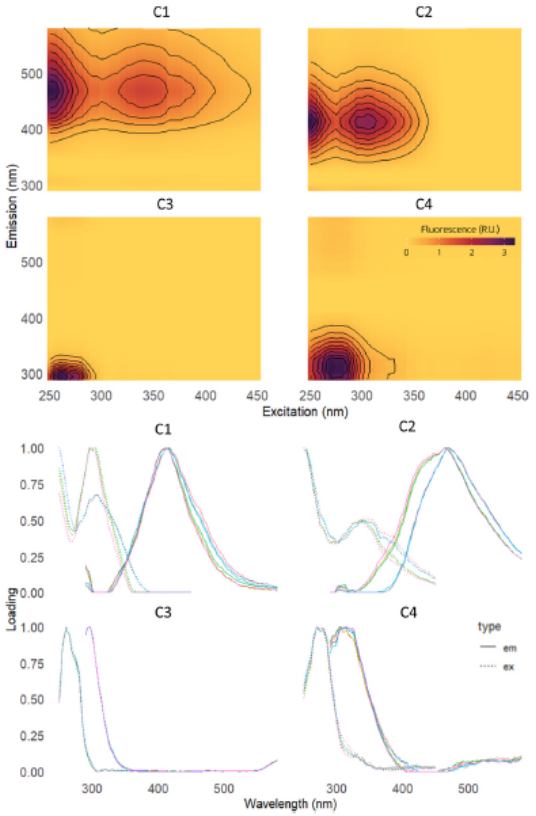

Fig. 6. (A) contour plots of the EEMs and (B) excitation (dotted lines) and emission (solid lines) modelled spectra of the 4 components as identified by the PARAFAC model.

$$At = A0\ e^{-\lambda t} + Asec\ (1 - e^{-\lambda t}) \quad \text{(Eq 2)}$$

where At is the radon activity at the time t, $A0$ is the mean radon activity in seawater samples (e.g. 47 Bq m^{-3}, Table 1), $Asec$ is the radon activity at secular equilibrium (e.g. 16,000 Bq m^{-3}), and λ is the constant decay (e.g. 0.18 d^{-1}). We can roughly estimate the time necessary to reach the maximum radon activities measured in 2018 and 2019 (e.g. −715 and −10,074 Bq m^{-3}). This leads to a residence time of 6 h (one tidal cycle) and 6 days, respectively.

The radon-based SGD yielded deeper groundwater discharge rates of 16.8 and 5.9 $m^3\ d^{-1}$ in 2018 and 2019, respectively. The outflow of these deeper recirculated saline groundwaters contributed between 10 and 30% of the total Q. These results highlight the predominance of the

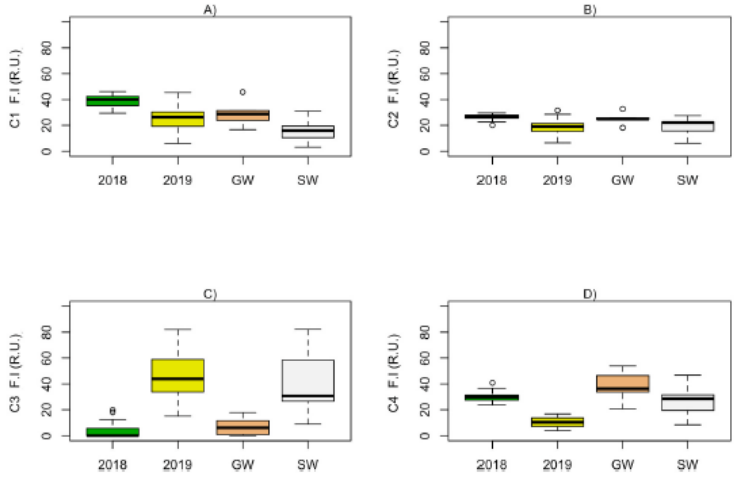

Fig. 7. Box plots of the EEM-PARAFAC modelled OM components: C1 (A), C2 (B), C3 (C) and C4 (D) reported in F.I. (Raman unit). The green and yellow boxes represent the values measured in the discharge zone in 2018 and 2019, respectively, the orange boxes combined values for both years measured in P1 (N = 5), and the grey one presents the values in the surrounding seawater samples (N = 7). Black lines are the median, whiskers are the extent of data, and dots outside the boxes are outliers. (For interpretation of the references to colour in this figure legend, the reader is referred to the Web version of this article.)

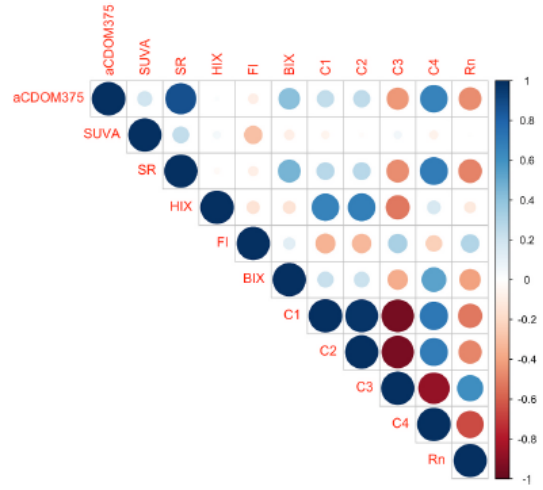

Fig. 8. Correlation matrix of the different parameters used for describing the dynamic of DOM. Positive correlations are displayed in blue and negative correlations in red colour. Colour intensity and the size of the circle are proportional to the correlation coefficients. (For interpretation of the references to colour in this figure legend, the reader is referred to the Web version of this article.)

surficial recirculated saline groundwaters in the discharge zone, which represented >70–90% of the Darcy's flow, as currently observed in other subterranean estuaries (Taniguchi et al., 2002; Mulligan and Charette, 2006; Martin et al., 2007). The predominance of seawater freshly infiltrated as well as the subsurface residence time of the saline groundwater from a few hours to days may control the origin and the transformation of DOM exported from the discharge zone.

4.2. Fluxes and nature of DOM in the discharge zone

4.2.1. Dynamics of the DOC fluxes

DOC concentrations measured in the sand spit's discharge zone were higher than or similar to other beach groundwater characterized by the occurrence of millennia-old paleosol, such as Martinique Beach, where DOC concentrations vary from below the detection limit to 15,000 μM (Chaillou et al., 2016; Couturier et al., 2016). Furthermore, Beck et al. (2008) have measured DOC concentrations varying from 0 to 4,000 μM in pore water from intertidal flats located in the Wadden Sea, highlighting a strong variation of DOC concentrations with depth and through time. In the present study, DOC concentrations were higher in the discharge zone than in the surrounding seawaters suggesting that the system acts as a source of carbon for the adjacent embayment. These results also highlight carbon and DOM production during groundwater flow through the sand spit to coastal water. DOC exports were however considerably lower than those commonly reported in micro and mesotidal systems, with values varying from a few mol to more than 20 mol d^{-1} m^{-1} (see Robinson et al., 2018 and references therein). In Martinique Beach, the strong DOC concentrations supported SGD-derived carbon fluxes around 10 mol d^{-1} m^{-1} (Couturier et al., 2016), for example, a DOG export 4 orders of magnitude larger than those measured here. The low magnitude is mainly explained by the low volumetric SGD rates of the system, which limited the export of DOC to the coastal embayment. Nevertheless, because humic acids and terrigenous organic substances may act as proton acceptors and can affect the buffering capacity (Kuliński et al., 2014) and optical properties (Coble, 2007) of nearshore waters, the determination of the origin of the DOM pool found in the discharge zone remains critical.

4.2.2. Characterization of the organic matter in the discharge zone

The $a_{CDOM}(375)$ is often used as a proxy of DOC concentration in rivers and coastal ocean (Stedmon et al., 2003; Yamashita et al., 2008; Spencer et al., 2012). Nonlinear correlations are observed in many surface systems in response to the preferential degradation of DOC or CDOM through processes such as flocculation, photochemical oxidation, and microbial degradation (Del Vecchio and Blough, 2004). In Martinique Beach, Couturier et al. (2016)Couturier et al. (2016) reported a clear decoupling between DOC and $a_{CDOM}(375)$ along the groundwater flow path. Further, Sirois et al. (2018) suggested that complex interactions involving water-rock interactions as a "rusty" carbon sink and a preferential sink of terrestrial, humic-like components with HMW were responsible for the sequential loss of DOM. Here, we observed a significant positive correlation ($R^2 > 0.9$, $p < 0.05$, Fig. 8) between both parameters suggesting that either the transformation or sequestration of DOM in the subsurface was limited, or that DOC and

DOM were degraded simultaneously. According to the EEM-PARAFAC modelled component, most of the FDOM samples collected in the discharge zone are dominated by terrestrial, humic-like components as C1 and C2 dominated the fluorescent pool over the tidal cycle, particularly in 2018 when the residence time of deep groundwater was short (−6 h) within the sand spit system. The degree of humification of the material is high, likely related to HMW acids (HIX >6) originating from material sources with greater humification. High $a_{CDOM}(375)$ coupled with high SUVA and HIX, and the highest S_R of the data set suggest that, in 2018, there were greater concentrations of CDOM and that this material was more aromatic and had a higher molecular weight than the DOM collected in 2019, in P1 and the surrounding seawater. This is in agreement with the strong positive correlation between C1, C2 and HIX (Fig. 8). The terrestrial character of the FDOM is also supported by low fluorescent indices mostly related to terrestrially derived fulvic acids (McKnightet al., 2001) with a strong aromatic content (Weishaar et al., 2003). The short residence time of the deep groundwater probably limits the production of autochthonous microbially produced components, with lower molecular weights, as observed in P1 and seawater samples where C4 and C3-4 dominated, respectively. The occurrence of degraded and microbially transformed products in these later samples agreed quite well with the decreasing S_R values. As for seawater samples, the FDOM pool in groundwater samples collected in 2019 is dominated by C3 components and exhibited lower values of S_R. The higher residence time (−6 days) and the significant positive correlation between C3 and radon activities suggest however that the material source can be microbially transformed producing protein-like components of LMW as soon as the groundwater residence time is sufficient. All these DOM metrics pointed out a terrestrial material source with a high degree of humification suggesting the sedimentary organic matter of the paleosol may act as a potential source of newly mobilized DOM in the system.

Because of the expected sea-level rise worldwide, future works should focus on SGD-derived radiocarbon dating to better understand the role of old age lignin-rich paleosols as a carbon source in coastal zones. The mechanisms leading to the mobilization of this new DOM in this site are unknown, but it seems contemporaneous to the sampling. The absence of light in the subsurface prevented photochemical degradation. Microbial degradation likely controlled the DOM and DOC behaviour explaining the detection of microbial signature, particularly when the residence time of groundwater increases. The redox conditions in the discharge zone were also suitable for dark oxidation processes by hydroxyl and sulphate radicals (Page et al., 2013; Tong et al., 2016; Fan et al., 2019; Zhang et al., 2019) and these reactions are known to affect the optical properties of DOM by decreasing the molecular weight while showing no or little impact on DOC and DOM concentrations. Both microbial mineralization and dark oxidation of DOM allowed the production of low molecular weight compounds. The molecular weight of DOM is an important factor influencing its bioavailability and its behaviour in surface seawater (Amon and Benner, 1996). This newly formed pool of bioavailable DOM could also be a better source of carbon substrates for bacterial respiration, thus oxidizing DOM into CO_2 (Goldstone et al., 2002; Page et al., 2013).

5. Conclusion

Water levels, ^{222}Rn activities, DOC concentrations and optical properties of CDOM/FDOM were combined to determine the dynamics of groundwater and derived carbon fluxes in a sand spite system characterized by the occurrence of a 2-kyr-old paleosol. At the sampling times, groundwater was saline and ^{222}Rn activities indicated the co-occurrence of two distinct water masses: a surface recirculated saline groundwater cell with no ^{222}Rn activity, and a deeper recirculated saline groundwater with a longer residence time varying between a few hours to a few days and, thus, with higher ^{222}Rn activities. At the falling tide, the upward pulses of ^{222}Rn-rich groundwater contribute to less than 30% of total SGD indicating that recirculated saline seawater dominates. In the discharge zone, DOM and DOC concentrations were high and showed a similar behaviour whatever the flow regime. Spectral and fluorescent metrics as well as EEM-PARAFAC modelled components pointed out the contribution of terrigenous, humic-like and HMW compounds originated from material sources with a high degree of humification. However, when the residence time of deep groundwater was longer, the pool of DOM was dominated by degraded components of protein-like type with lower molecular weights, indicating that microbial processes also occurred within the system. The absence of light and a longer residence time of groundwater enhanced microbial degradation and transformation of humic-type material. Despite the origin of the terrestrial material is not discriminated, the sedimentary lignin-rich paleosol may be the source and thus it may support a new pool of bioavailable DOM for microbial respiration in surface seawater. Because of the specific hydrostratigraphic context of the study area, the fluxes of carbon exported to surrounding seawater were weak. However, the millennia-old sedimentary organic matter buried in paleosol in this transgressive coastal system may act as hot spots for terrigenous DOM transformation and alter the optical and chemical properties of coastal waters. Our findings show the importance of considering marine transgressive systems since their presence may greatly contribute to coastal carbon budgets. Because the sea level rise is exposing many coastal areas around the world to marine submersion, we need to better quantify the impact of transgressive coastal systems on regional and local carbon budgets.

CRediT authorship contribution statement

Anne-Josée Hébert: Writing – original draft, Methodology, Investigation, Formal analysis, Conceptualization. **Aude Flamand:** Writing – review & editing, Formal analysis. **Gwénaëlle Chaillou:** Writing – review & editing, Supervision, Resources, Investigation, Funding acquisition, Conceptualization.

Declaration of competing interest

The authors declare that they have no known competing financial interests or personal relationships that could have appeared to influence the work reported in this paper.

Data availability

Data will be made available on request.

8 Acknowledgments

The authors thank Gwendoline Tommi-Morin, Abigaëlle Dalpé-Castillou, Antoine Biehler and Joannie Cool for their essential help in the field; Sylvio Demers for the DGPS profile of the sand spit; Claude Belzile for DOC samples analysis; Yves Gélinas (Concordia University), Jean-François Lapierre (UdeM) and Huixiang Xie (ISMER-UQAR) for the early corrections of the manuscript; Laure Devine for the English revision. The authors would like to thank the anonymous reviewers for their significant insights over the review process. This project was partially funded by the *Ministère du Développement durable, de l'Environnement et de la Lutte contre les changements climatiques* of the Québec Government as part of the *Projet d'acquisition des connaissances sur les eaux souterraines* (PACES) 2018–2022. This research was also supported by grants from the Natural Sciences and Engineering Research Council of Canada (#402408) by the Canada Research Chair Program to GC. This project also received grants from the Université du Québec à Rimouski to GC and from Québec-Océan network to AJH.

Appendix A. Supplementary data

Supplementary data to this article can be found online at https://doi.

org/10.1016/j.ecss.2022.108137.

References

Amon, R.M.W., Benner, R., 1996. Bacterial utilization of different size classes of dissolved organic matter. Limnol. Oceanogr. 41, 41–51. https://doi.org/10.4319/lo.1996.41.1.0.

Anschutz, P., Smith, T., Mouret, A., Deborde, J., Bujan, S., Poirier, D., et al., 2009. Tidal sands as biogeochemical reactors. Estuar. Coast Shelf Sci. 84, 84–90. https://doi.org/10.1016/j.ecss.2009.06.015.

Barnett, R.L., Bernatchez, P., Garneau, M., Juneau, M.-N., 2017. Reconstructing late Holocene relative sea-level changes at the Magdalen Islands (Gulf of St . Lawrence, Canada) using multi-proxy analyses. J. Quat. Sci. 32, 380–395. https://doi.org/10.1002/jqs.2931.

Barnett, R.L., Bernatchez, P., Garneau, M., Brain, M.J., Charman, D.J., Stephenson, D.B., et al., 2019. Late Holocene sea-level changes in eastern Quebec and potential drivers. Quat. Sci. Rev. 203, 151–169. https://doi.org/10.1016/j.quascirev.2018.10.039.

Beck, A.J., Tsukamoto, Y., Tovar-Sanchez, A., Huerta-Diaz, M., Bokuniewicz, H.J., Sañudo-Wilhelmy, S.A., 2007. Importance of geochemical transformations in determining submarine groundwater discharge-derived trace metal and nutrient fluxes. Appl. Geochem. 22, 477–490. https://doi.org/10.1016/j.apgeochem.2006.10.005.

Beck, M., Dellwig, O., Liebezeit, G., Schnetger, B., Brumsack, H.J., 2008. Spatial and seasonal variations of sulphate, dissolved organic carbon, and nutrients in deep pore waters of intertidal flat sediments. Estuar. Coast Shelf Sci. 79, 307–316. https://doi.org/10.1016/j.ecss.2008.04.007.

Blough, N.V., del Vecchio, R., 2002. Chromophoric DOM in the coastal environment. Biogeochem. Mar. Dissol. Org. Matter 509–546. https://doi.org/10.1016/b978-012323841-2/50012-9.

Bro, R., 1997. PARAFAC. Tutorial and applications. Chemometr. Intell. Lab. Syst. 38, 149–171. https://doi.org/10.1016/s0169-7439(97)00032-4.

Burnett, W.C., Dulaiova, H., 2003. Estimating the dynamics of groundwater input into the coastal zone via continuous radon-222 measurements. J. Environ. Radioact. 69, 21–35. https://doi.org/10.1016/S0265-931X(03)00084-5.

Burnett, W.C., Bokuniewicz, H., Huettel, L., Moore, W.S., Taniguchi, M., 2003. Groundwater and pore water inputs to the coastal zone. Biogeochemistry 66, 3–33. https://doi.org/10.1023/b:biog.0000006066.21240.53.

Burnett, W.C., Aggarwal, P.K., Aureli, A., Bokuniewicz, H., Cable, J.E., Charette, M.A., et al., 2006. Quantifying submarine groundwater discharge in the coastal zone via multiple methods. Sci. Total Environ. 367, 498–543. https://doi.org/10.1016/j.scitotenv.2006.05.009.

Chaillou, G., Couturier, M., Tommi-Morin, G., Rao, A.M., 2014. Total alkalinity and dissolved inorganic carbon production in groundwaters discharging through a sandy beach. Proced. Earth and Planet. Sci. 10, 88–99. https://doi.org/10.1016/j.proeps.2014.08.017.

Chaillou, G., Lemay-Borduas, F., Couturier, M., 2016. Transport and transformations of groundwater-borne carbon discharging through a sandy beach to a coastal ocean. Can. Water Resour. J. 41, 455–468. https://doi.org/10.1080/07011784.2015.1111775.

Chaillou, G., Lemay-Borduas, F., Larocque, M., Couturier, M., Biehler, A., Tommi-Morin, G., 2018. Flow and discharge of groundwater from a snowmelt-affected sandy beach. J. Hydrol. 557, 4–15. https://doi.org/10.1016/j.jhydrol.2017.12.010.

Charbonnier, C., Anschutz, P., Abril, G., Mucci, A., Deirmendjian, L., Poirier, D., Bujan, S., Lecroart, P., 2022. Carbon dynamics drivent by sewater recirculation and groundwater discharge along a forest-dune-beach continuum of a high-energy meso-macro-tidal sandy coast. Geochem. Cosmochim. Acta 137, 18–38.

Charette, M.A., Sholkovitz, E.R., 2002. Oxidative precipitation of groundwater-derived ferrous iron in the subterranean estuary of a coastal bay. Geophys. Res. Lett. 29 https://doi.org/10.1029/2001gl014512, 85-1-85–4.

Charette, M.A., Sholkovitz, E.R., Hansel, C.M., 2005. Trace element cycling in a subterranean estuary: Part 1. Geochemistry of the permeable sediments. Geochem. Cosmochim. Acta 69, 2095–2109. https://doi.org/10.1016/j.gca.2004.10.024.

Chen, X., Zhang, F., Lao, Y., Wang, X., Du, J., Santos, I.R., 2018. Submarine groundwater discharge-derived carbon fluxes in mangroves: an important component of blue carbon budgets? J. Geophys. Res.: Oceans 123, 6962–6979. https://doi.org/10.1029/2018jc014448.

Coble, P.G., 1996. Characterization of marine and terrestrial DOM in seawater using excitation-emission matrix spectroscopy. Mar. Chem. 51, 325–346. https://doi.org/10.1016/0304-4203(95)00062-3.

Coble, P.G., 2007. Marine optical biogeochemistry: the chemistry of ocean color. Chem. Rev. 107, 402–418. https://doi.org/10.1021/cr050350+.

Coleman, K., Jenkinson, D.S., 1996. RothC-26.3 - a Model for the turnover of carbon in soil. Evaluat. Soil Org. Matter. Mod. 38, 237–246. https://doi.org/10.1007/978-3-642-61094-3_17.

Cory, R.M., McKnight, D.M., 2005. Fluorescence spectroscopy reveals ubiquitous presence of oxidized and reduced quinones in dissolved organic matter. Environ. Sci. Tech. 39, 8142–8149. https://doi.org/10.1021/es0506962.

Couturier, M., Nozais, C., Chaillou, G., 2016. Microtidal subterranean estuaries as a source of fresh terrestrial dissolved organic matter to the coastal ocean. Mar. Chem. 186, 46–57. https://doi.org/10.1016/j.marchem.2016.08.001.

Del Vecchio, R., Blough, N., 2004. On the origin of the optical properties of humic substances. Environ. Sci. Tech. 38, 3885–3891. https://doi.org/10.1021/es049912h.

Fan, X., Yu, X., Wang, Y., Xiao, X., Li, F., Xie, Y., et al., 2019. The aging behaviors of chromophoric biomass burning brown carbon during dark aqueous hydroxyl radical oxidation processes in laboratory studies. Atmos. Environ. 205, 9–18. https://doi.org/10.1016/j.atmosenv.2019.02.039.

Gehrels, W.R., Milne, G.A., Kirby, J.R., Patterson, R.T., Belknap, D.F., 2004. Late Holocene sea-level changes and isostatic crustal movements in Atlantic Canada. Quater. Int. 120, 79–89. https://doi.org/10.1016/j.quaint.2004.01.008.

Goldstone, J.V., Pullin, M.J., Bertilsson, S., Voelker, B.M., 2002. Reactions of hydroxyl radical with humic substances: bleaching, mineralization, and production of bioavailable carbon substrates. Environ. Sci. Tech. 36, 364–372. https://doi.org/10.1021/es0109646.

Hansen, A.M., Kraus, T.E.C., Pellerin, B.A., Fleck, J.A., Downing, B.D., Bergamaschi, B.A., 2016. Optical properties of dissolved organic matter (DOM): effects of biological and photolytic degradation. Limnol. Oceanogr. 61, 1015–1032. https://doi.org/10.1002/lno.10270.

Helms, J.R., Stubbins, A., Ritchie, J.D., Minor, E.C., Kieber, D.J., Mopper, K., 2008. Absorption spectral slopes and slope ratios as indicators of molecular weight, source, and photobleaching of chromophoric dissolved organic matter. Limnol. Oceanogr. 53, 955–969. https://doi.org/10.4319/lo.2009.54.3.1023.

Henton, J.A., Craymer, M.R., Ferland, R., Dragert, H., Mazzotti, S., Forbes, D.L., 2006. Crustal motion and deformation monitoring of the Canadian landmass. Geomatica 60, 173–191.

Huguet, A., Vacher, L., Relexans, S., Saubusse, S., Froidefond, J.M., Parlanti, E., 2009. Properties of fluorescent dissolved organic matter in the Gironde Estuary. Org. Geochem. 40, 706–719. https://doi.org/10.1016/j.orggeochem.2009.03.002.

Kim, J., Kim, G., 2017. Inputs of humic fluorescent dissolved organic matter via submarine groundwater discharge to coastal waters off a volcanic island (Jeju, Korea). Sci. Rep. 7, 7921. https://doi.org/10.1038/s41598-017-08518-5.

Kim, T.H., Waska, H., Kwon, E., Suryaputra, I.G.N., Kim, G., 2012. Production, degradation, and flux of dissolved organic matter in the subterranean estuary of a large tidal flat. Mar. Chem. 142 (144), 1–10. https://doi.org/10.1016/j.marchem.2012.08.002.

Kim, T.H., Kwon, E., Kim, I., Lee, S.A., Kim, G., 2013. Dissolved organic matter in the subterranean estuary of a volcanic island, Jeju: importance of dissolved organic nitrogen fluxes to the ocean. J. Sea Res. 78, 18–24. https://doi.org/10.1016/j.seares.2012.12.009.

Kuliński, K., Schneider, B., Hammer, K., Machulik, U., Schulz-Bull, D., 2014. The influence of dissolved organic matter on the acid-base system of the Baltic Sea. J. Mar. Syst. 132, 106–115. https://doi.org/10.1016/j.jmarsys.2014.01.011.

Lapworth, D.J., Kinniburgh, D.G., 2009. An R script for visualising and analysing fluorescence excitation-emission matrices (EEMs). Comput. Geosci. 35, 2160–2163. https://doi.org/10.1016/j.cageo.2008.10.013.

Lawaetz, A.J., Stedmon, C.A., 2009. Fluorescence intensity calibration using the Raman scatter peak of water. Appl. Spectrosc. 63, 936–940. https://doi.org/10.1366/000370209788964548.

Martin, J.B., Cable, J.E., Smith, C., Roy, M., Cherrier, J., 2007. Magnitudes of submarine groundwater discharge from marine and terrestrial sources: Indian River Lagoon, Florida. Water Resour. Res. 43, 1–15. https://doi.org/10.1029/2006wr005266.

Massicotte, P., 2018. eemR: Tools for Pre-Processing Emission-Excitation-Matrix (EEM) Fluorescence Data. R package version 0.1.5.9000. Retrieved from. https://github.com/PMassicotte/eemR.

McCoy, C.A., Corbett, D.R., 2009. Review of submarine groundwater discharge (SGD) in coastal zones of the Southeast and Gulf Coast regions of the United States with management implications. J. Environ. Manag. 90, 644–651. https://doi.org/10.1016/j.jenvman.2008.03.002.

McKnight, D.M., Boyer, E.W., Westerhoff, P.K., Doran, P.T., Kulbe, T., Andersen, D.T., 2001. Spectrofluorometric characterization of dissolved organic matter for indication of precursor organic material and aromaticity. Limnol. Oceanogr. 46, 38–48. https://doi.org/10.4319/lo.2001.46.1.0038.

Miller, M.P., McKnight, D.M., 2010. Comparison of seasonal changes in fluorescent dissolved organic matter among aquatic lake and stream sites in the Green Lakes Valley. J. Geophys. Res. 115, 1–14. https://doi.org/10.1029/2009jg000985.

Moore, W.S., 2010. The Effect of submarine groundwater discharge on the ocean. Ann. Rev. Mar. Sci 2, 59–88. https://doi.org/10.1146/annurev-marine-120308-081019.

Mulligan, A.E., Charette, M.A., 2006. Intercomparison of submarine groundwater discharge estimates from a sandy unconfined aquifer. J. Hydrol. 327, 411–425. https://doi.org/10.1016/j.jhydrol.2005.11.056.

Murphy, K.R., Stedmon, C.A., Waite, T.D., Ruiz, G.M., 2008. Distinguishing between terrestrial and autochthonous organic matter sources in marine environments using fluorescence spectroscopy. Mar. Chem. 108 (1–2), 40–58.

Murphy, K.R., Stedmon, C.A., Graeber, D., Bro, R., 2013. Fluorescence spectroscopy and multi-way techniques. PARAFAC. Anal. Methods 5, 6557–6566. https://doi.org/10.1039/c3ay41160e.

Ohno, T., 2002. Fluorescence inner-filtering correction for determining the humification index of dissolved organic matter. Environ. Sci. Tech. 36, 742–746. https://doi.org/10.1021/es0155276.

Page, S.E., Kling, G.W., Sander, M., Harrold, K.H., Logan, J.R., McNeill, K., et al., 2013. Dark formation of hydroxyl radical supports high rates of dissolved organic matter oxidation in arctic soil and surface waters. Environ. Sci. Tech. 47, 12860–12867. https://doi.org/10.1021/es4033265.

Poulin, B.A., Ryan, J.N., Aiken, G.R., 2014. Effects of iron on optical properties of dissolved organic matter. Environ. Sci. Tech. 48, 10098–10106. https://doi.org/10.1021/es502670r.

Povinec, P.P., Burnett, W.C., Beck, A., Bokuniewicz, H., Charette, M., Gonneea, M.E., et al., 2012. Isotopic, geophysical and biogeochemical investigation of submarine groundwater discharge: IAEA-UNESCO intercomparison exercise at Mauritius Island. J. Environ. Radioact. 104, 24–45. https://doi.org/10.1016/j.jenvrad.2011.09.009.

Pucher, Matthias, Urban, Wünsch, Gabriele Weigelhofer, Murphy, Kathleen, Hein, Thomas, Graeber, Daniel, 2019. staRdom: versatile software for analyzing spectroscopic data of dissolved organic matter in R. Water 11, 2366. https://doi.org/10.3390/w11112366.

Qi, L., Xie, H., Gagné, J.P., Chaillou, G., Massicotte, P., Yang, G.P., 2018. Photoreactivities of two distinct dissolved organic matter pools in groundwater of a subarctic island. Mar. Chem. 202, 97–120. https://doi.org/10.1016/j.marchem.2018.03.003.

Robinson, C.E., Xin, P., Santos, I.R., Charette, M.A., Li, L., Barry, D.A., 2018. Groundwater dynamics in subterranean estuaries of coastal unconfined aquifers: controls on submarine groundwater discharge and chemical inputs to the ocean. Adv. Water Resour. 115, 315–331. https://doi.org/10.1016/j.advwatres.2017.10.041.

Santos, I.R., Burnett, W.C., Dittmar, T., Suryaputra, I.G.N.A., Chanton, J., 2009. Tidal pumping drives nutrient and dissolved organic matter dynamics in a Gulf of Mexico subterranean estuary. Geochem. Cosmochim. Acta 73, 1325–1339. https://doi.org/10.1016/j.gca.2008.11.029.

Shen, Y., Chapelle, F.H., Strom, E.W., Benner, R., 2015. Origins and bioavailability of dissolved organic matter in groundwater. Biogeochemistry 122, 61–78. https://doi.org/10.1007/s10533-014-0029-4.

Sirois, M., Couturier, M., Barber, A., Gélinas, Y., Chaillou, G., 2018. Interactions between iron and organic carbon in a sandy beach subterranean estuary. Mar. Chem. 202, 86–96. https://doi.org/10.1016/j.marchem.2018.02.004.

Spencer, R.G.M., Butler, K.D., Aiken, G.R., 2012. Dissolved organic carbon and chromophoric dissolved organic matter properties of rivers in the USA. J. Geophy. Res. Biogeosci. 117 https://doi.org/10.1029/2011jg001928.

Stedmon, C.A., Markager, S., 2005a. Resolving the variability of dissolved organic matter fluorescence in a temperate estuary and its catchment using PARAFAC analysis. Limnol. Oceanogr. 50, 686–697.

Stedmon, C.A., Markager, S., 2005b. Tracing the production and degradation of autochthonous fractions of dissolved organic matter using fluorescence analysis. Limnol. Oceanogr. 50 (5), 1415–1426.

Stedmon, C.A., Nelson, N.B., 2015. In: Chapter 10 - the Optical Properties of DOM in the Ocean. Biogeochemistry of Marine Dissolved Oranic Matter, second ed., pp. 481–508. https://doi.org/10.1016/b978-0-12-405940-5.00010-8.

Stedmon, C.A., Markager, S., Kaas, H., 2000. Optical properties and signatures of chromophoric dissolved organic matter (CDOM) in Danish coastal waters. Estuar. Coast Shelf Sci. 51, 267–278. https://doi.org/10.1006/ecss.2000.0645.

Stedmon, C.A., Markager, S., Bro, R., 2003. Tracing dissolved organic matter in aquatic environments using a new approach to fluorescence spectroscopy. Mar. Chem. 82, 239–254. https://doi.org/10.1016/S0304-4203(03)00072-0.

Taniguchi, M., Burnett, W.C., Cable, J.E., Turner, J.V., 2002. Investigation of submarine groundwater discharge. Hydrol. Process. 16, 2115–2129. https://doi.org/10.1002/hyp.1145.

Tong, M., Yuan, S., Ma, S., Jin, M., Liu, D., Cheng, D., et al., 2016. Production of abundant hydroxyl radicals from oxygenation of subsurface sediments. Environ. Sci. Tech. 50, 214–221. https://doi.org/10.1021/acs.est.5b04323.

Viollier, E., Inglett, P.W., Hunter, K., Roychoudhury, A.N., Van Cappellen, P., 2000. The ferrozine method revisited: Fe(II)/Fe(III) determination in natural waters. Appl. Geochem. 15, 785–790. https://doi.org/10.1016/s0883-2927(99)00097-9.

Wagner, S., Schubotz, F., Kaiser, K., Hallmann, C., Waska, H., Rossel, P.E., et al., 2020. Soothsaying DOM: a current perspective on the future of oceanic dissolved organic carbon. Front. Mar. Sci. 7, 1–17. https://doi.org/10.3389/fmars.2020.00341.

Ward, N.D., Bianchi, T.S., Medeiros, P.M., Seidel, M., Richey, J.E., Keil, R.G., et al., 2017. Where carbon goes when water flows: carbon cycling across the aquatic continuum. Front. Mar. Sci. 4, 1–27. https://doi.org/10.3389/fmars.2017.00007.

Waska, H., Simon, H., Ahmerkamp, S., Greskowiak, J., Ahrens, J., Seibert, S.L., Schwalfenberg, K., Zielinski, O., Dittmar, T., 2021. Molecular traits of dissolved organic matter in the subterranean estuary of a high-energy beach: indications of sources and sinks. Front. Mar. Sci. 8, 54. https://doi.org/10.3389/fmars.2021.607083.

Webb, J.R., Santos, I.R., Maher, D.T., Tait, D.R., Cyronak, T., Sadat-noori, M., et al., 2019. Groundwater as a source of dissolved organic matter to coastal waters : insights from radon and CDOM observations in 12 shallow coastal systems. Limnol. Oceanogr. 9999, 1–15. https://doi.org/10.1002/lno.11028.

Weishaar, J.L., Aiken, G.R., Bergamaschi, B.A., Fram, M.S., Fujii, R., Mopper, K., 2003. Evaluation of specific ultraviolet absorbance as an indicator of the chemical composition and reactivity of dissolved organic carbon. Environ. Sci. Tech. 37, 4702–4708. https://doi.org/10.1021/es030360x.

Wu, Z., Zhou, H., Zhang, S., Liu, Y., 2013. Using 222 Rn to estimate submarine groundwater discharge (SGD) and the associated nutrient fluxes into Xiangshan Bay, East China Sea. Mar. Pollut. Bull. 73, 183–191. https://doi.org/10.1016/j.marpolbul.2013.05.024.

Xiao, Y.H., Sara-Aho, T., Hartikainen, H., Vähätalo, A.V., 2013. Contribution of ferric iron to light absorption by chromophoric dissolved organic matter. Limnol. Oceanogr. 58, 653–662. https://doi.org/10.4319/lo.2013.58.2.0653.

Yamashita, Y., Jaffé, R., Maie, N., Tanoue, E., 2008. Assessing the dynamics of dissolved organic matter (DOM) in coastal environments by excitation emission matrix fluorescence and parallel factor analysis (EEM-PARAFAC). Limnol. Oceanogr. 53, 1900–1908. https://doi.org/10.4319/lo.2008.53.5.1900.

Zhang, S., Rouge, V., Gutierrez, L., Croue, J.P., 2019. Reactivity of chromophoric dissolved organic matter (CDOM) to sulfate radicals: reaction kinetics and structural transformation. Water Res. 163 https://doi.org/10.1016/j.watres.2019.07.013.

Zhou, Y., Shi, K., Zhang, Y., Jeppesen, E., Liu, X., Zhou, Q., et al., 2017. Fluorescence peak integration ratio IC:IT as a new potential indicator tracing the compositional changes in chromophoric dissolved organic matter. Sci. Total Environ. 574, 1588–1598. https://doi.org/10.1016/j.scitotenv.2016.08.196.

REFERENCES BIBLIOGRAPHIQUES

Abbott, B. W., Larouche, J. R., Jones, J. B., Bowden, W. B., & Balser, A. W. (2014). Elevated dissolved organic carbon biodegradability from thawing and collapsing permafrost. *Journal of Geophysical Research: Biogeosciences*, *119*(10), 2049-2063. https://doi.org/10.1002/2014jg002678

Amon, R. M. W. (2004). The Role of Dissolved Organic Matter for the Organic Carbon Cycle in the Arctic Ocean. *The Organic Carbon Cycle in the Arctic Ocean*, 83-99. https://doi.org/10.1007/978-3-642-18912-8_4

Amon, R. M. W., & Benner, R. (1996). Bacterial utilization of different size classes of dissolved organic matter. *Limnology and Oceanography*, *41*(1), 41-51. https://doi.org/10.4319/LO.1996.41.1.0041

Amon, R. M. W., Rinehart, A. J., Duan, S., Louchouarn, P., Prokushkin, A., Guggenberger, G., Bauch, D., Stedmon, C., Raymond, P. A., Holmes, R. M., McClelland, J. W., Peterson, B. J., Walker, S. A., & Zhulidov, A. V. (2012). Dissolved organic matter sources in large Arctic rivers. *Geochimica et Cosmochimica Acta*, *94*, 217-237. https://doi.org/10.1016/J.GCA.2012.07.015

Anderson, L. G., & Amon, R. M. W. (2015). DOM in the Arctic Ocean. *Biogeochemistry of Marine Dissolved Organic Matter: Second Edition*, 609-633. https://doi.org/10.1016/B978-0-12-405940-5.00014-5

Barber, A., Brandes, J., Leri, A., Lalonde, K., Balind, K., Wirick, S., Wang, J., & Gélinas, Y. (2017). Preservation of organic matter in marine sediments by inner-sphere interactions with reactive iron. *Scientific Reports*, *7*(1). https://doi.org/10.1038/s41598-017-00494-0

Benner, R. (2002). Chemical Composition and Reactivity. *Biogeochemistry of Marine Dissolved Organic Matter*, 59-90. https://doi.org/10.1016/B978-012323841-2/50005-1

Berry, H. B., Whalen, D., & Lim, M. (2021). Long-term ice-rich permafrost coast sensitivity to air temperatures and storm influence: lessons from Pullen Island, Northwest

Territories, Canada. *Arctic Science*, *7*(4), 723-745. https://doi.org/10.1139/as-2020-0003

Bristol, E. M., Connolly, C. T., Lorenson, T. D., Richmond, B. M., Ilgen, A. G., Choens, R. C., Bull, D. L., Kanevskiy, M., Iwahana, G., Jones, B. M., & McClelland, J. W. (2021). Geochemistry of Coastal Permafrost and Erosion-Driven Organic Matter Fluxes to the Beaufort Sea Near Drew Point, Alaska. *Frontiers in Earth Science*, *8*. https://doi.org/10.3389/FEART.2020.598933

Bro, R. (1997). PARAFAC. Tutorial and applications. *Chemometrics and Intelligent Laboratory Systems*, *38*(2), 149-171. https://doi.org/10.1016/S0169-7439(97)00032-4

Brown, R. J. E. (1970). *Permafrost in Canada: its influence on northern development*. University of Toronto Press.

Buchan, A., LeCleir, G. R., Gulvik, C. A., & González, J. M. (2014). Master recyclers: features and functions of bacteria associated with phytoplankton blooms. *Nature reviews. Microbiology*, *12*(10), 686-698. https://doi.org/10.1038/NRMICRO3326

Burn, C. R., & Kokelj, S. V. (2009). The environment and permafrost of the Mackenzie Delta area. *Permafrost and Periglacial Processes*, *20*(2), 83-105. https://doi.org/10.1002/PPP.655

Canfield, D. E. (1997). The geochemistry of river particulates from the continental USA: major elements. *Geochimica et Cosmochimica Acta*, *61*(16), 3349-3365. https://doi.org/10.1016/S0016-7037(97)00172-5

Carlson, C. A. (2002). Production and Removal Processes. *Biogeochemistry of Marine Dissolved Organic Matter*, 91-151. https://doi.org/10.1016/B978-012323841-2/50006-3

Carlson, C. A., & Hansell, D. A. (2015). DOM Sources, Sinks, Reactivity, and Budgets. *Biogeochemistry of Marine Dissolved Organic Matter: Second Edition*, 65-126. https://doi.org/10.1016/B978-0-12-405940-5.00003-0

Chadburn, S. E., Burke, E. J., Cox, P. M., Friedlingstein, P., Hugelius, G., & Westermann, S. (2017). An observation-based constraint on permafrost loss as a function of global warming. *Nature Climate Change 2017 7:5*, *7*(5), 340-344. https://doi.org/10.1038/nclimate3262

Chaillou, G., Lemay-Borduas, F., Larocque, M., Couturier, M., Biehler, A., & Tommi-Morin, G. (2018). Flow and discharge of groundwater from a snowmelt-affected sandy beach. *Journal of Hydrology*, *557*, 4-15. https://doi.org/10.1016/J.JHYDROL.2017.12.010

Charette, M. A., & Sholkovitz, E. R. (2002). Oxidative precipitation of groundwater-derived ferrous iron in the subterranean estuary of a coastal bay. *Geophysical Research Letters*, *29*(10), 85-81. https://doi.org/10.1029/2001GL014512

Chen, H., Yang, Z., Chu, R. K., Tolic, N., Liang, L., Graham, D. E., Wullschleger, S. D., & Gu, B. (2018). Molecular Insights into Arctic Soil Organic Matter Degradation under Warming. *Environ Sci Technol*, *52*(8), 4555-4564. https://doi.org/10.1021/acs.est.7b05469

Coble, P. G. (1996). Characterization of marine and terrestrial DOM in seawater using excitation-emission matrix spectroscopy. *Marine Chemistry*, *51*(4), 325-346. https://doi.org/10.1016/0304-4203(95)00062-3

Connolly, C. T., Cardenas, M. B., Burkart, G. A., Spencer, R. G. M., & McClelland, J. W. (2020). Groundwater as a major source of dissolved organic matter to Arctic coastal waters. *Nat Commun*, *11*(1), 1479. https://doi.org/10.1038/s41467-020-15250-8

Cory, R. M., & McKnight, D. M. (2005). Fluorescence spectroscopy reveals ubiquitous presence of oxidized and reduced quinones in dissolved organic matter. *Environmental Science and Technology*, *39*(21), 8142-8149. https://doi.org/10.1021/ES0506962

Del Vecchio, R., & Blough, N. V. (2004). Spatial and seasonal distribution of chromophoric dissolved organic matter and dissolved organic carbon in the Middle Atlantic Bight. *Marine Chemistry*, *89*(1-4), 169-187. https://doi.org/10.1016/J.MARCHEM.2004.02.027

Drake, T. W., Wickland, K. P., Spencer, R. G., McKnight, D. M., & Striegl, R. G. (2015). Ancient low-molecular-weight organic acids in permafrost fuel rapid carbon dioxide production upon thaw. *Proceedings of the National Academy of Sciences of the United States of America*, *112*(45), 13946-13951. https://doi.org/10.1073/pnas.1511705112

Eckard, R. S., Pellerin, B. A., Bergamaschi, B. A., Bachand, P. A. M., Bachand, S. M., Spencer, R. G. M., & Hernes, P. J. (2017). Dissolved Organic Matter Compositional Change and Biolability During Two Storm Runoff Events in a Small Agricultural

Watershed. *Journal of Geophysical Research: Biogeosciences*, *122*(10), 2634-2650. https://doi.org/10.1002/2017jg003935

Eppley, R. W., Stewart, E., Abbott, M. R., & Owen, R. W. (1987). Estimating ocean production from satellite-derived chlorophyll: Insights from the Eastropac data set. *Oceanologica Acta*, 109-113. https://archimer.ifremer.fr/doc/00267/37854/

Faust, J. C., Tessin, A., Fisher, B. J., Zindorf, M., Papadaki, S., Hendry, K. R., Doyle, K. A., & März, C. (2021). Millennial scale persistence of organic carbon bound to iron in Arctic marine sediments. *Nature Communications*, *12*(1). https://doi.org/10.1038/s41467-020-20550-0

Fellman, J. B., Hood, E., & Spencer, R. G. M. (2010). Fluorescence spectroscopy opens new windows into dissolved organic matter dynamics in freshwater ecosystems: A review. *Limnology and Oceanography*, *55*(6), 2452-2462. https://doi.org/10.4319/LO.2010.55.6.2452

Fichot, C. G., & Benner, R. (2014). The fate of terrigenous dissolved organic carbon in a river-influenced ocean margin. *Global Biogeochemical Cycles*, *28*(3), 300-318. https://doi.org/10.1002/2013GB004670

Fichot, C. G., Kaiser, K., Hooker, S. B., Amon, R. M. W., Babin, M., Bélanger, S., Walker, S. A., & Benner, R. (2013). Pan-Arctic distributions of continental runoff in the Arctic Ocean. *Scientific Reports*, *3*(1), 1053. https://doi.org/10.1038/srep01053

Fouché, J., Christiansen, C. T., Lafrenière, M. J., Grogan, P., & Lamoureux, S. F. (2020). Canadian permafrost stores large pools of ammonium and optically distinct dissolved organic matter. *Nature Communications*, *11*(1), 4500. https://doi.org/10.1038/s41467-020-18331-w

French, H. M., Demitroff, M., Forman, S. L., & Newell, W. L. (2007). A chronology of Late-Pleistocene permafrost events in southern New Jersey, Eastern USA. *Permafrost and Periglacial Processes*, *18*(1), 49-59. https://doi.org/10.1002/PPP.572

Fritz, M., Vonk, J. E., & Lantuit, H. (2017). Collapsing Arctic coastlines. *Nature Climate Change 2017 7:1*, *7*(1), 6-7. https://doi.org/10.1038/nclimate3188

Gabor, R. S., Baker, A., McKnight, D. M., & Miller, M. P. (2014). Fluorescence Indices and Their Interpretation. In *Aquatic Organic Matter Fluorescence* (pp. 303-338). Cambridge University Press. https://doi.org/10.1017/CBO9781139045452.015

GIEC. (2013). *IPCC on Climate Change 2013: The Physical Science Basis. Contribution of Working Group I to the Fifth Assesment Report of the Intergovernmental Panel on climate Change*.

Granskog, M. A., Stedmon, C. A., Dodd, P. A., Amon, R. M. W., Pavlov, A. K., De Steur, L., Hansen, E., Granskog, M. A., Stedmon, C. A., Dodd, P. A., Amon, R. M. W., Pavlov, A. K., De Steur, L., & Hansen, E. (2012). Characteristics of colored dissolved organic matter (CDOM) in the Arctic outflow in the Fram Strait: Assessing the changes and fate of terrigenous CDOM in the Arctic Ocean. *Journal of Geophysical Research: Oceans, 117*(C12), 12021-12021. https://doi.org/10.1029/2012JC008075

Gruber, P., Field, C. B., Valentini, R., Heimann, M., Richey, J. E., Romero Lankao, P., Schulze, E. D., Chen, C.-T. A. N., & Friedlingstein. (2004). *The Global Carbon Cycle: Integrating Humans, Climate, and the Natural World*. Island Press.

Guo, L., Ping, C. L., & Macdonald, R. W. (2007). Mobilization pathways of organic carbon from permafrost to arctic rivers in a changing climate. *Geophysical Research Letters*, *34*(13). https://doi.org/10.1029/2007GL030689

Hansell, D. A., Carlson, C. A., Repeta, D. J., & Schlitzer, R. (2009). Dissolved Organic Matter in the Ocean: A Controversy Stimulates New Insights. *Oceanography*, *22*, 202-211. https://doi.org/10.5670/OCEANOG.2009.109

Harvey, G. R., Boran, D. A., Chesal, L. A., & Tokar, J. M. (1983). The structure of marine fulvic and humic acids. *Marine Chemistry*, *12*(2), 119-132. https://doi.org/https://doi.org/10.1016/0304-4203(83)90075-0

He, W., Chen, M., Schlautman, M. A., & Hur, J. (2016). Dynamic exchanges between DOM and POM pools in coastal and inland aquatic ecosystems: A review. *Science of the Total Environment*, *551-552*, 415-428. https://doi.org/10.1016/j.scitotenv.2016.02.031

Hébert, A.-J., Flamand, A., & Chaillou, G. (2022). Origins and transformations of terrigenous dissolved organic matter in a transgressive coastal system. *Estuarine, Coastal and Shelf Science*, *279*, 108137-108137. https://doi.org/10.1016/J.ECSS.2022.108137

Hedges, J. I., Clark, W. A., Quay, P. D., Richey, J. E., Devol, A. H., & Santos, M. (1986). Compositions and fluxes of particulate organic material in the Amazon River1. *Limnology and Oceanography*, *31*(4), 717-738. https://doi.org/10.4319/LO.1986.31.4.0717

Hedges, J. I., Cowie, G. L., Richey, J. E., Quay, P. D., Benner, R., Strom, M., & Forsberg, B. R. (1994). Origins and processing of organic matter in the Amazon River as indicated by carbohydrates and amino acids. *Limnology and Oceanography*, *39*(4), 743-761. https://doi.org/10.4319/LO.1994.39.4.0743

Hedges, J. I., & Ertel, J. R. (1982). Characterization of lignin by gas capillary chromatography of cupric oxide oxidation products. *Analytical chemistry*, *54*(2), 174.

Hedges, J. I., & Keil, R. G. (1995). Sedimentary organic matter preservation: an assessment and speculative synthesis. *Marine Chemistry*, *49*(2-3), 81-115. https://doi.org/10.1016/0304-4203(95)00008-F

Hedges, J. I., Keil, R. G., & Benner, R. (1997). What happens to terrestrial organic matter in the ocean? *Organic Geochemistry*, *27*(5-6), 195-212. https://doi.org/10.1016/S0146-6380(97)00066-1

Helms, J. R., Stubbins, A., Ritchie, J. D., Minor, E. C., Kieber, D. J., & Mopper, K. (2008). Absorption spectral slopes and slope ratios as indicators of molecular weight, source, and photobleaching of chromophoric dissolved organic matter. *Limnology and Oceanography*, *53*(3), 955-969. https://doi.org/10.4319/lo.2008.53.3.0955

Holmes, R. M., McClelland, J. W., Peterson, B. J., Tank, S. E., Bulygina, E., Eglinton, T. I., Gordeev, V. V., Gurtovaya, T. Y., Raymond, P. A., Repeta, D. J., Staples, R., Striegl, R. G., Zhulidov, A. V., & Zimov, S. A. (2012). Seasonal and Annual Fluxes of Nutrients and Organic Matter from Large Rivers to the Arctic Ocean and Surrounding Seas. *Estuaries and Coasts*, *35*(2), 369-382. https://doi.org/10.1007/S12237-011-9386-6/TABLES/3

Holmes, R. M., McClelland, J. W., Raymond, P. A., Frazer, B. B., Peterson, B. J., Stieglitz, M., McClelland, W., Raymond, P. A., Frazer, B. B., Peterson, B. J., & Stieglitz, M. (2008). Lability of DOC transported by Alaskan rivers to the Arctic Ocean. *Geophysical Research Letters*, *35*(3). https://doi.org/10.1029/2007GL032837

Hugelius, G., Strauss, J., Zubrzycki, S., Harden, J. W., Schuur, E. A. G., Ping, C. L., Schirrmeister, L., Grosse, G., Michaelson, G. J., Koven, C. D., O'Donnell, J. A., Mishra, U., Camill, P., Yu, Z., Palmtag, J., & Kuhry, P. (2014). Estimated stocks of circumpolar permafrost carbon with quantified uncertainty ranges and identified data gaps. *Biogeosciences*, *11*, 6573-6593. https://doi.org/10.5194/bg-11-6573-2014

Huguet, A., Vacher, L., Relexans, S., Saubusse, S., Froidefond, J. M., & Parlanti, E. (2009). Properties of fluorescent dissolved organic matter in the Gironde Estuary. *Organic Geochemistry*, *40*(6), 706-719. https://doi.org/10.1016/j.orggeochem.2009.03.002

Johnson, K. S., Michael Gordon, R., & Coale, K. H. (1997). What controls dissolved iron concentrations in the world ocean? *Marine Chemistry*, *57*(3-4), 137-161. https://doi.org/10.1016/S0304-4203(97)00043-1

Jones, B. M., Irrgang, A. M., Farquharson, L. M., Lantuit, H., Whalen, D., Ogorodov, S., Grigoriev, M., Tweedie, C., Gibbs, A. E., Strzelecki, M. C., Baranskaya, A., Belova, N., Sinitsyn, A., Kroon, A., Maslakov, A., Vieira, G., Grosse, G., Overduin, P., Nitze, I., . . . Romanovsky, V. E. (2020). *Arctic Report Card 2020: Coastal Permafrost Erosion* (Arctic Report Card, Issue. NOAA. http://pubs.er.usgs.gov/publication/70217611

Jones, D. L., & Edwards, A. C. (1998). Influence of sorption on the biological utilization of two simple carbon substrates. *Soil Biology and Biochemistry*, *30*(14), 1895-1902. https://doi.org/10.1016/S0038-0717(98)00060-1

Judge, A. S. (1986). *Permafrost distribution and the Quaternary history of the Mackenzie–Beaufort region: a geothermal perspective* (Correlation of Quaterny Deposits and Events Around the Margin of the Beaufort Sea, Issue.

Kaiser, K., Benner, R., & Amon, R. M. W. (2017a). The fate of terrigenous dissolved organic carbon on the Eurasian shelves and export to the North Atlantic. *Journal of Geophysical Research: Oceans*, *122*(1), 4-22. https://doi.org/10.1002/2016jc012380

Kaiser, K., Canedo-Oropeza, M., McMahon, R., & Amon, R. M. W. (2017b). Origins and transformations of dissolved organic matter in large Arctic rivers. *Scientific Reports*, *7*(1). https://doi.org/10.1038/s41598-017-12729-1

Kaiser, K., & Guggenberger, G. (2000). The role of DOM sorption to mineral surfaces in the preservation of organic matter in soils. *Organic Geochemistry*, *31*(7-8), 711-725. https://doi.org/10.1016/S0146-6380(00)00046-2

Kaiser, K., & Guggenberger, G. (2003). Mineral surfaces and soil organic matter. *European Journal of Soil Science*, *54*(2), 219-236. https://doi.org/10.1046/j.1365-2389.2003.00544.x

Keil, R. G., Montluçon, D. B., Prahl, F. G., & Hedges, J. I. (1994). Sorptive preservation of labile organic matter in marine sediments. *Nature*, *370*, 549-552. https://doi.org/10.1038/370549A0

Khvorostyanov, D. V., Ciais, P., Krinner, G., Zimov, S. A., Corradi, C., & Guggenberger, G. (2008). Vulnerability of permafrost carbon to global warming. Part II: sensitivity of permafrost carbon stock to global warming. *Tellus B*, *60*(2), 265-275. https://doi.org/10.1111/J.1600-0889.2007.00336.X

Kipp, L. E., Charette, M. A., Moore, W. S., Henderson, P. B., & Rigor, I. G. (2018). Increased fluxes of shelf-derived materials to the central arctic ocean. *Science Advances*, *4*(1). https://doi.org/10.1126/SCIADV.AAO1302

Köhler, H., Meon, B., Gordeev, V. v., Spitzy, A., & Amon, R. M. W. (2003). Dissolved organic matter (DOM) in the estuaries of Ob and Yenisei and the adjacent. *Journal of Geophysical Research Atmospheres*, *108*.

Kwasigroch, U., Bełdowska, M., Jędruch, A., & Saniewska, D. (2018). Coastal erosion—a "new" land-based source of labile mercury to the marine environment. *Environmental Science and Pollution Research*, *25*(28), 28682-28694. https://doi.org/10.1007/S11356-018-2856-7/FIGURES/4

Lalonde, K., Mucci, A., Ouellet, A., & Gelinas, Y. (2012). Preservation of organic matter in sediments promoted by iron. *Nature*, *483*, 198-200. https://doi.org/10.1038/nature10855

Lantuit, H., Overduin, P. P., Couture, N., Wetterich, S., Aré, F., Atkinson, D., Brown, J., Cherkashov, G., Drozdov, D., Donald Forbes, L., Graves-Gaylord, A., Grigoriev, M., Hubberten, H. W., Jordan, J., Jorgenson, T., Ødegård, R. S., Ogorodov, S., Pollard, W. H., Rachold, V., . . . Vasiliev, A. (2012). The Arctic Coastal Dynamics Database: A New Classification Scheme and Statistics on Arctic Permafrost Coastlines. *Estuaries and Coasts*, *35*(2), 383-400. https://doi.org/10.1007/S12237-010-9362-6

Letscher, R. T., Hansell, D. A., & Kadko, D. (2011). Rapid removal of terrigenous dissolved organic carbon over the Eurasian shelves of the Arctic Ocean. *Marine Chemistry*, *123*(1-4), 78-87. https://doi.org/10.1016/J.MARCHEM.2010.10.002

Li, G., Liu, J., Ma, Y., Zhao, R., Hu, S., Li, Y., Wei, H., & Xie, H. (2014). Distribution and spectral characteristics of chromophoric dissolved organic matter in a coastal bay in northern China. *Journal of Environmental Sciences*, *26*(8), 1585-1595. https://doi.org/10.1016/J.JES.2014.05.025

Lilleøren, K. S., Etzelmüller, B., Schuler, T. V., Gisnås, K., & Humlum, O. (2012). The relative age of mountain permafrost — estimation of Holocene permafrost limits in Norway. *Global and Planetary Change*, *92-93*, 209-223. https://doi.org/10.1016/J.GLOPLACHA.2012.05.016

Linkhorst, A., Dittmar, T., & Waska, H. (2017). Molecular Fractionation of Dissolved Organic Matter in a Shallow Subterranean Estuary: The Role of the Iron Curtain. *Environ Sci Technol*, *51*(3), 1312-1320. https://doi.org/10.1021/acs.est.6b03608

Lipczynska-Kochany, E. (2018). Effect of climate change on humic substances and associated impacts on the quality of surface water and groundwater: A review. *The Science of the total environment*, *640-641*, 1548-1565. https://doi.org/10.1016/J.SCITOTENV.2018.05.376

Lizotte, M., Juhls, B., Matsuoka, A., Massicotte, P., Mével, G., Anikina, D. O. J., Antonova, S., Bécu, G., Béguin, M., Bélanger, S., Bossé-Demers, T., Bröder, L., Bruyant, F., Chaillou, G., Comte, J., Couture, R.-M., Devred, E., Deslongchamps, G., Dezutter, T., . . . Babin, M. (2022). *Nunataryuk field campaigns: Understanding the origin and fate of terrestrial organic matter in the coastal waters of the Mackenzie Delta region*. Copernicus GmbH. https://dx.doi.org/10.5194/essd-2022-163

Lønborg, C., Carreira, C., Jickells, T., & Álvarez-Salgado, X. A. (2020). Impacts of Global Change on Ocean Dissolved Organic Carbon (DOC) Cycling. *Frontiers in Marine Science*, *7*, 1-24. https://doi.org/10.3389/fmars.2020.00466

Ma, X., Liu, G., Wu, X., Smoak, J. M., Ye, L., Xu, H., Zhao, L., & Ding, Y. (2018). Influence of land cover on riverine dissolved organic carbon concentrations and export in the Three Rivers Headwater Region of the Qinghai-Tibetan Plateau. *Science of the Total Environment*, *630*, 314-322. https://doi.org/10.1016/J.SCITOTENV.2018.02.152

Macdonald, R. W., Solomon, S. M., Cranston, R. E., Welch, H. E., Yunker, M. B., & Gobeil, C. (1998). A sediment and organic carbon budget for the Canadian Beaufort Shelf. *Marine Geology*, *144*(4), 255-273.

Mackay, J. R. (1971). The Origin of Massive Icy Beds in Permafrost, Western Arctic Coast, Canada. *Canadian Journal of Earth Sciences*, *8*(4), 397-422. https://doi.org/10.1139/E71-043

Mann, P. J., Eglinton, T. I., McIntyre, C. P., Zimov, N., Davydova, A., Vonk, J. E., Holmes, R. M., & Spencer, R. G. M. (2015). Utilization of ancient permafrost carbon in

headwaters of Arctic fluvial networks. *Nature Communications*, *6*(1), 7856. https://doi.org/10.1038/ncomms8856

Mathis, J. T., Grebmeier, J. M., Hansell, D. A., Hopcroft, R. R., Kirchman, D. L., Lee, S. H., Moran, S. B., Bates, N. R., Van Laningham, S., Cross, J. N., & Cai, W. J. (2014). Carbon biogeochemistry of the western arctic: Primary production, carbon export and the controls on ocean acidifi cation. *The Pacific Arctic Region: Ecosystem Status and Trends in a Rapidly Changing Environment*, 223-268. https://doi.org/10.1007/978-94-017-8863-2_9/FIGURES/12

Matsuoka, A., Bricaud, A., Benner, R., Para, J., Sempéré, R., Prieur, L., Bélanger, S., & Babin, M. (2012). Tracing the transport of colored dissolved organic matter in water masses of the Southern Beaufort Sea: relationship with hydrographic characteristics. *Biogeosciences*, *9*(3), 925-940. https://doi.org/10.5194/bg-9-925-2012

McGuire, A. D., Lawrence, D. M., Koven, C., Clein, J. S., Burke, E., Chen, G., Jafarov, E., MacDougall, A. H., Marchenko, S., Nicolsky, D., Peng, S., Rinke, A., Ciais, P., Gouttevin, I., Hayes, D. J., Ji, D., Krinner, G., Moore, J. C., Romanovsky, V., . . . Zhuang, Q. (2018). Dependence of the evolution of carbon dynamics in the northern permafrost region on the trajectory of climate change. *Proceedings of the National Academy of Sciences of the United States of America*, *115*(15), 3882-3887. https://doi.org/10.1073/PNAS.1719903115

McKnight, D. M., Boyer, E. W., Westerhoff, P. K., Doran, P. T., Kulbe, T., & Andersen, D. T. (2001). Spectrofluorometric characterization of dissolved organic matter for indication of precursor organic material and aromaticity. *Limnology and Oceanography*, *46*, 38-48. https://doi.org/https://doi.org/10.4319/lo.2001.46.1.0038

McMeans, B. C., McCann, K. S., Humphries, M., Rooney, N., & Fisk, A. T. (2015). Food Web Structure in Temporally-Forced Ecosystems. *Trends in Ecology & Evolution*, *30*(11), 662-672. https://doi.org/10.1016/J.TREE.2015.09.001

Meilleur, C., Kamula, M., Kuzyk, Z. A., & Guéguen, C. (2023). Insights into surface circulation and mixing in James Bay and Hudson Bay from dissolved organic matter optical properties. *Journal of Marine Systems*, *238*, 103841-103841. https://doi.org/10.1016/J.JMARSYS.2022.103841

Menard, H. W., & Smith, S. M. (1966). Hypsometry of ocean basin provinces. *Journal of Geophysical Research*, *71*(18), 4305-4325. https://doi.org/10.1029/JZ071I018P04305

Meredith, M., Sommerkorn, M., Cassotta, S., Derksen, C., Ekaykin, A., Hollowed, A., Kofinas, G., Mackintosh, A., Melbourne-Thomas, J., Muelbert, M. M. C., Ottersen, G., Pritchard, H., & Schuur, E. A. G. (2019). Polar Regions. In *IPCC Special Report on the Ocean and Cryosphere in a Changing Climate* (pp. 203-320). Cambridge University Press. https://doi.org/10.1017/9781009157964.005

Moody, C. S., & Worrall, F. (2017). Modeling rates of DOC degradation using DOM composition and hydroclimatic variables. *Journal of Geophysical Research: Biogeosciences*, *122*(5), 1175-1191. https://doi.org/10.1002/2016JG003493

Mopper, K., Kieber, D. J., & Stubbins, A. (2015). Chapter 8 - Marine Photochemistry of Organic Matter: Processes and Impacts. In D. A. Hansell & C. A. Carlson (Eds.), *Biogeochemistry of Marine Dissolved Organic Matter (Second Edition)* (pp. 389-450). Academic Press. https://doi.org/https://doi.org/10.1016/B978-0-12-405940-5.00008-X

Müller, S., Vähätalo, A. V., Granskog, M. A., Autio, R., & Kaartokallio, H. (2011). Behaviour of dissolved organic matter during formation of natural and artificially grown Baltic Sea ice. *Annals of Glaciology*, *52*(57), 233-241. https://doi.org/10.3189/172756411795931886

Murphy, K. R., Stedmon, C. A., Graeber, D., & Bro, R. (2013). Fluorescence spectroscopy and multi-way techniques. PARAFAC. *Analytical Methods*, *5*(23). https://doi.org/10.1039/c3ay41160e

Murtagh, F., & Legendre, P. (2014). Ward's Hierarchical Agglomerative Clustering Method: Which Algorithms Implement Ward's Criterion? *Journal of Classification*, *31*(3), 274-295. https://doi.org/10.1007/s00357-014-9161-z

Murton, J. B., Opel, T., Toms, P., Blinov, A., Fuchs, M., Wood, J., Gärtner, A., Merchel, S., Rugel, G., Savvinov, G., & Wetterich, S. (2022). A multimethod dating study of ancient permafrost, Batagay megaslump, east Siberia. *Quaternary Research*, *105*, 1-22. https://doi.org/10.1017/QUA.2021.27

Mustaffa, N. I. H., Kallajoki, L., Biederbick, J., Binder, F. I., Schlenker, A., & Striebel, M. (2020). Coastal Ocean Darkening Effects via Terrigenous DOM Addition on Plankton: An Indoor Mesocosm Experiment. *Frontiers in Marine Science*, *7*, 841-841. https://doi.org/10.3389/FMARS.2020.547829/BIBTEX

Obu, J., Westermann, S., Bartsch, A., Berdnikov, N., Christiansen, H. H., Dashtseren, A., Delaloye, R., Elberling, B., Etzelmüller, B., Kholodov, A., Khomutov, A., Kääb, A.,

Leibman, M. O., Lewkowicz, A. G., Panda, S. K., Romanovsky, V., Way, R. G., Westergaard-Nielsen, A., Wu, T., . . . Zou, D. (2019). Northern Hemisphere permafrost map based on TTOP modelling for 2000–2016 at 1 km2 scale. *Earth-Science Reviews*, *193*, 299-316. https://doi.org/10.1016/j.earscirev.2019.04.023

Ohno, T. (2002). Fluorescence Inner-Filtering Correction for Determining the Humification Index of Dissolved Organic Matter. *Environmental Science and Technology*, *36*(4), 742-746. https://doi.org/10.1021/ES0155276

Olefeldt, D., Persson, A., & Turetsky, M. R. (2014). Influence of the permafrost boundary on dissolved organic matter characteristics in rivers within the Boreal and Taiga plains of western Canada. *Environmental Research Letters*, *9*(3), 035005. https://doi.org/10.1088/1748-9326/9/3/035005

Opsahl, S., Benner, R., & Amon, R. M. W. (1999). Major flux of terrigenous dissolved organic matter through the Arctic Ocean. *Limnology and Oceanography*, *44*(8), 2017-2023. https://doi.org/10.4319/LO.1999.44.8.2017

Orem, W. H., & Gaudette, H. E. (1984). Organic matter in anoxic marine pore water: oxidation effects. *Organic Geochemistry*, *5*(4), 175-181. https://doi.org/10.1016/0146-6380(84)90003-2

Ouellette, D. S. (2021). *Thermal and Mechanical Modeling of Coastal Erosion Processes on Tuktoyaktuk Island, Northwest Territories* University of Calgary]. Calgary. https://prism.ucalgary.ca/handle/1880/113949

Page, S. E., Kling, G. W., Sander, M., Harrold, K. H., Logan, J. R., McNeill, K., & Cory, R. M. (2013). Dark Formation of Hydroxyl Radical in Arctic Soil and Surface Waters. *Environmental Science & Technology*, *47*(22), 12860-12867. https://doi.org/10.1021/es4033265

Page, S. E., Sander, M., Arnold, W. A., & McNeill, K. (2012). Hydroxyl radical formation upon oxidation of reduced humic acids by oxygen in the dark. *Environmental Science and Technology*, *46*(3), 1590-1597. https://doi.org/10.1021/ES203836F

Palangi, S., & Zare-Abyaneh, H. (2017). Impacts of Climate Change on PERMAFROST as a threat to the future of the Earth International Conference of Climate Change.

Patzner, M. S., Kainz, N., Lundin, E., Barczok, M., Smith, C., Herndon, E., Kinsman-Costello, L., Fischer, S., Straub, D., Kleindienst, S., Kappler, A., & Bryce, C. (2021).

Seasonal fluctuations of the rusty carbon sink in thawing permafrost peatlands. *Earth ArXiv*. https://doi.org/https://doi.org/10.31223/X5P35J

Pavia, D. L., Lampman, G. M., Kriz, G. S., & Vyvyan, J. A. (2008). *Introduction to Spectroscopy* (4 ed.). Cengage Learning.

Poulin, B. A., Ryan, J. N., & Aiken, G. R. (2014). Effects of iron on optical properties of dissolved organic matter. *Environ Sci Technol*, *48*(17), 10098-10106. https://doi.org/10.1021/es502670r

Pucher, M., Wünsch, U., Weigelhofer, G., Murphy, K., Hein, T., & Graeber, D. (2019). staRdom: Versatile Software for Analyzing Spectroscopic Data of Dissolved Organic Matter in R. *Water*, *11*(11). https://doi.org/10.3390/w11112366

Rampton, V. N. (1988). *Quaternary Geology of the Tuktoyaktuk Coastlands, Northwest Territories* (Geological Suvey of Canada, Issue. M. a. R. C. Energy.

Raymond, P. A., McClelland, J. W., Holmes, R. M., Zhulidov, A. V., Mull, K., Peterson, B. J., Striegl, R. G., Aiken, G. R., & Gurtovaya, T. Y. (2007). Flux and age of dissolved organic carbon exported to the Arctic Ocean: A carbon isotopic study of the five largest arctic rivers. *Global Biogeochemical Cycles*, *21*(4). https://doi.org/10.1029/2007GB002934

Repeta, D. J. (2015). Chemical Characterization and Cycling of Dissolved Organic Matter. In *Biogeochemistry of Marine Dissolved Organic Matter: Second Edition* (pp. 21-63). Academic Press. https://doi.org/10.1016/B978-0-12-405940-5.00002-9

Riedel, T., Biester, H., & Dittmar, T. (2012). Molecular fractionation of dissolved organic matter with metal salts. *Environmental Science and Technology*, *46*(8), 4419-4426. https://doi.org/10.1021/ES203901U

Riedel, T., Zak, D., Biester, H., & Dittmar, T. (2013). Iron traps terrestrially derived dissolved organic matter at redox interfaces. *Proceedings of the National Academy of Sciences*, *110*(25), 10101-10105. https://doi.org/10.1073/pnas.1221487110

Romanovsky, V., Isaken, K., Drozdov, D., Anisimov, O., Instanes, A., Leibman, M., McGuire, A. D., Shiklomanov, N., Smith, S., & Walker, D. (2017). Changing Permafrost and its Impacts. In *Snow, Water, Ice and Permafrost in the Arctic (SWIPA)* (pp. 65-136). Arctic Monitoring and Assessment Programme (AMAP).

Schaefer, K., Lantuit, H., Romanovsky, V. E., Schuur, E. A. G., & Witt, R. (2014). The impact of the permafrost carbon feedback on global climate. *Environmental Research Letters*, *9*, 085003. https://doi.org/10.1088/1748-9326/9/8/085003

Schaefer, K., Zhang, T., Bruhwiler, L., & Barrett, A. P. (2011). Amount and timing of permafrost carbon release in response to climate warming. *Tellus B: Chemical and Physical Meteorology*, *63*(2), 165-180. https://doi.org/10.1111/J.1600-0889.2011.00527.X

Schindler, D. W., & Curtis, P. J. (1997). The role of DOC in protecting freshwaters subjected to climatic warming and acidification from UV exposure. *Biogeochemistry*, *36*(1), 1-8. https://doi.org/10.1023/A:1005768527751

Schuur, E. A. G., Abbott, B. W., Bowden, W. B., Brovkin, V., Camill, P., Canadell, J. G., Chanton, J. P., Chapin, F. S., Christensen, T. R., Ciais, P., Crosby, B. T., Czimczik, C. I., Grosse, G., Harden, J., Hayes, D. J., Hugelius, G., Jastrow, J. D., Jones, J. B., Kleinen, T., . . . Zimov, S. A. (2013). Expert assessment of vulnerability of permafrost carbon to climate change. *Climatic Change*, *119*(2), 359-374. https://doi.org/10.1007/S10584-013-0730-7/FIGURES/2

Schuur, E. A. G., Bockheim, J., Canadell, J. G., Euskirchen, E., Field, C. B., Goryachkin, S. V., Hagemann, S., Kuhry, P., Lafleur, P. M., Lee, H., Mazhitova, G., Nelson, F. E., Rinke, A., Romanovsky, V. E., Shiklomanov, N., Tarnocai, C., Venevsky, S., Vogel, J. G., & Zimov, S. A. (2008). Vulnerability of Permafrost Carbon to Climate Change: Implications for the Global Carbon Cycle. *BioScience*, *58*(8), 701-714. https://doi.org/10.1641/B580807

Schuur, E. A. G., McGuire, A. D., Schädel, C., Grosse, G., Harden, J. W., Hayes, D. J., Hugelius, G., Koven, C. D., Kuhry, P., Lawrence, D. M., Natali, S. M., Olefeldt, D., Romanovsky, V. E., Schaefer, K., Turetsky, M. R., Treat, C. C., & Vonk, J. E. (2015). Climate change and the permafrost carbon feedback. *Nature*, *520*(7546), 171-179. https://doi.org/10.1038/nature14338

Schuur, T., McGuire, A. D., Romanovsky, V., Schädel, C., & Mack, M. (2018). Chapter 11: Arctic and Boreal Carbon (Second State of the Carbon Cycle Report (SOCCR2): A Sustained Assessment Report, Issue. Shields, M. R., Bianchi, T. S., Gélinas, Y., Allison, M. A., & Twilley, R. R. (2016). Enhanced terrestrial carbon preservation promoted by reactive iron in deltaic sediments. *Geophysical Research Letters*, *43*(3), 1149-1157. https://doi.org/10.1002/2015GL067388

Shen, Y., Chapelle, F. H., Strom, E. W., & Benner, R. (2014). Origins and bioavailability of dissolved organic matter in groundwater. undefined, 122(1), 61-78. https://doi.org/10.1007/S10533-014-0029-4

Shields, M. R., Bianchi, T. S., Gélinas, Y., Allison, M. A., & Twilley, R. R. (2016). Enhanced terrestrial carbon preservation promoted by reactive iron in deltaic sediments. Geophysical Research Letters, 43(3), 1149-1157. https://doi.org/10.1002/2015GL067388

Sholkovitz, E. R. (1976). Flocculation of dissolved organic and inorganic matter during the mixing of river water and seawater. *Geochimica et Cosmochimica Acta*, *40*(7), 831-845. https://doi.org/10.1016/0016-7037(76)90035-1

Simoneit, B. R. T. (2005). Atmospheric Transport of Terrestrial Organic Matter to the Sea. *2*, 165-208. https://doi.org/10.1007/698_2_006

Sirois, M., Couturier, M., Barber, A., Gélinas, Y., & Chaillou, G. (2018). Interactions between iron and organic carbon in a sandy beach subterranean estuary. *Marine Chemistry*, *202*, 86-96. https://doi.org/10.1016/j.marchem.2018.02.004

Solomon, S. M. (2005). Spatial and temporal variability of shoreline change in the Beaufort-Mackenzie region, northwest territories, Canada. *Geo-Marine Letters*, *25*(2-3), 127-137. https://doi.org/10.1007/S00367-004-0194-X

Spencer, R. G. M., Mann, P. J., Dittmar, T., Eglinton, T. I., McIntyre, C., Holmes, R. M., Zimov, N., & Stubbins, A. (2015). Detecting the signature of permafrost thaw in Arctic rivers. *Geophysical Research Letters*, *42*(8), 2830-2835. https://doi.org/10.1002/2015GL063498

Stedmon, C. A., Amon, R. M. W., Rinehart, A. J., & Walker, S. A. (2011a). The supply and characteristics of colored dissolved organic matter (CDOM) in the Arctic Ocean: Pan Arctic trends and differences. *Marine Chemistry*, *124*(1-4), 108-118.

Stedmon, C. A., Thomas, D. N., Papadimitriou, S., Granskog, M. A., & Dieckmann, G. S. (2011b). Using fluorescence to characterize dissolved organic matter in Antarctic sea ice brines. *Journal of Geophysical Research: Biogeosciences*, *116*. https://doi.org/10.1029/2011jg001716

Stedmon, C. A., Markager, S., & Bro, R. (2003). Tracing dissolved organic matter in aquatic environments using a new approach to fluorescence spectroscopy. *Marine Chemistry*, *82*(3-4), 239-254. https://doi.org/10.1016/s0304-4203(03)00072-0

Stedmon, C. A., & Nelson, N. B. (2015). The Optical Properties of DOM in the Ocean. In *Biogeochemistry of Marine Dissolved Organic Matter* (pp. 481-508). https://doi.org/10.1016/b978-0-12-405940-5.00010-8

Stookey, L. L. (1970). Ferrozine-A New Spectrophotometric Reagent for Iron. Analytical chemistry, 42(7), 779-781. https://doi.org/https://doi.org/10.1021/AC60289A016

Stubbins, A., Mann, P. J., Powers, L., Bittar, T. B., Dittmar, T., McIntyre, C. P., Eglinton, T. I., Zimov, N., & Spencer, R. G. M. (2017). Low photolability of yedoma permafrost dissolved organic carbon. *Journal of Geophysical Research: Biogeosciences*, *122*(1), 200-211. https://doi.org/10.1002/2016JG003688

Tanguy, R., Whalen, D., Prates, G., & Vieira, G. (2023). Shoreline change rates and land to sea sediment and soil organic carbon transfer in eastern Parry Peninsula from 1965 to 2020 (Amundsen Gulf, Canada). *Arctic Science*, 1-20. https://doi.org/10.1139/as-2022-0028

Tanski, G., Wagner, D., Knoblauch, C., Fritz, M., Sachs, T., & Lantuit, H. (2019). Rapid CO2 Release From Eroding Permafrost in Seawater. *Geophysical Research Letters*, *46*(20), 11244-11252. https://doi.org/10.1029/2019gl084303

Tesi, T., Muschitiello, F., Smittenberg, R. H., Jakobsson, M., Vonk, J. E., Hill, P., Andersson, A., Kirchner, N., Noormets, R., Dudarev, O., Semiletov, I., & Gustafsson, Ö. (2016). Massive remobilization of permafrost carbon during post-glacial warming. *Nature Communications*, *7*(1), 13653. https://doi.org/10.1038/ncomms13653

Thingstad, T. F., Bellerby, R. G. J., Bratbak, G., Børsheim, K. Y., Egge, J. K., Heldal, M., Larsen, A., Neill, C., Nejstgaard, J., Norland, S., Sandaa, R. A., Skjoldal, E. F., Tanaka, T., Thyrhaug, R., & Töpper, B. (2008). Counterintuitive carbon-to-nutrient coupling in an Arctic pelagic ecosystem. *Nature 2008 455:7211*, *455*(7211), 387-390. https://doi.org/10.1038/nature07235

Thomas, D. N., Lara, R. J., Eicken, H., Kattner, G., & Skoog, A. (1995). Dissolved organic matter in Arctic multi-year sea ice during winter: major components and relationship to ice characteristics. *Polar Biology 1995*, *15*(7), 477-483. https://doi.org/10.1007/BF00237461

Turetsky, M. R., Abbott, B. W., Jones, M. C., Anthony, K. W., Olefeldt, D., Schuur, E. A. G., Grosse, G., Kuhry, P., Hugelius, G., Koven, C., Lawrence, D. M., Gibson, C., Sannel, A. B. K., & McGuire, A. D. (2020). Carbon release through abrupt permafrost

thaw. *Nature Geoscience*, *13*(2), 138-143. https://doi.org/10.1038/s41561-019-0526-0

Viollier, E., Inglett, P. W., Hunter, K., Roychoudhury, A. N., & Van Cappellen, P. (2000). The ferrozine method revisited: Fe(II)/Fe(III) determination in natural waters. Applied Geochemistry, 15(6), 785-790. https://doi.org/10.1016/S0883-2927(99)00097-9

Vonk, J. E., & Gustafsson, Ö. (2013). Permafrost-carbon complexities. *Nature Geoscience*, *6*(9), 675-676. https://doi.org/10.1038/ngeo1937

Vonk, J. E., Semiletov, I. P., Dudarev, O. V., Eglinton, T. I., Andersson, A., Shakhova, N., Charkin, A., Heim, B., & Gustafsson, Ö. (2014). Preferential burial of permafrost-derived organic carbon in Siberian-Arctic shelf waters. *Journal of Geophysical Research: Oceans*, *119*(12), 8410-8421. https://doi.org/10.1002/2014JC010261

Vonk, J. E., Tank, S. E., Bowden, W. B., Laurion, I., Vincent, W. F., Alekseychik, P., Amyot, M., Billet, M. F., Canário, J., Cory, R. M., Deshpande, B. N., Helbig, M., Jammet, M., Karlsson, J., Larouche, J., Macmillan, G., Rautio, M., Walter Anthony, K. M., & Wickland, K. P. (2015). Reviews and syntheses: Effects of permafrost thaw on Arctic aquatic ecosystems. *Biogeosciences*, *12*, 7129-7167. https://doi.org/10.5194/bg-12-7129-2015

Vonk, J. E., Van Dongen, B. E., & Gustafsson, Ö. (2010). Selective preservation of old organic carbon fluvially released from sub-Arctic soils. *Geophysical Research Letters*, *37*(11). https://doi.org/10.1029/2010GL042909

Wagai, R., & Mayer, L. M. (2007). Sorptive stabilization of organic matter in soils by hydrous iron oxides. *Geochimica et Cosmochimica Acta*, *71*(1), 25-35. https://doi.org/10.1016/J.GCA.2006.08.047

Walvoord, M. A., & Striegl, R. G. (2007). Increased groundwater to stream discharge from permafrost thawing in the Yukon River basin: Potential impacts on lateral export of carbon and nitrogen. *Geophysical Research Letters*, *34*(12). https://doi.org/10.1029/2007gl030216

Ward, C. P., & Cory, R. M. (2015). Chemical composition of dissolved organic matter draining permafrost soils. *Geochimica et Cosmochimica Acta*, *167*, 63-79. https://doi.org/10.1016/J.GCA.2015.07.001

Waska, H., Simon, H., Ahmerkamp, S., Greskowiak, J., Ahrens, J., Seibert, S. L., Schwalfenberg, K., Zielinski, O., & Dittmar, T. (2021). Molecular Traits of Dissolved Organic Matter in the Subterranean Estuary of a High-Energy Beach: Indications of Sources and Sinks. *Frontiers in Marine Science*, *8*, 54-54. https://doi.org/10.3389/FMARS.2021.607083/BIBTEX

Wauthy, M., Rautio, M., Christoffersen, K. S., Forsström, L., Laurion, I., Mariash, H. L., Peura, S., & Vincent, W. F. (2018). Increasing dominance of terrigenous organic matter in circumpolar freshwaters due to permafrost thaw. Limnology and Oceanography Letters(3), 186-198. https://doi.org/10.1002/lol2.10063

Weishaar, J. L., Aiken, G. R., Bergamaschi, B. A., Fram, M. S., Fujii, R., & Mopper, K. (2003). Evaluation of Specific Ultraviolet Absorbance as an Indicator of the Chemical Composition and Reactivity of Dissolved Organic Carbon. *Environmental Science & Technology*, *37*(20), 4702-4708. https://doi.org/10.1021/es030360x

Whalen, D., Forbes, D. L., Kostylev, V., Lim, M., Fraser, P., Nedimović, M. R., & Stuckey, S. (2022). Mechanisms, volumetric assessment, and prognosis for rapid coastal erosion of Tuktoyaktuk Island, an important natural barrier for the harbour and community. *Canadian Journal of Earth Sciences*, *59*(11), 945-960. https://doi.org/10.1139/cjes-2021-0101

Williams, P. J., & Smith, M. W. (1989). The Frozen Earth: Fundamentals of Geocryology. *The Frozen Earth*. https://doi.org/10.1017/CBO9780511564437

Zak, D., Gelbrecht, J., & Steinberg, C. E. W. (2004). Phosphorus Retention at the Redox Interface of Peatlands Adjacent to Surface Waters in Northeast Germany. *Biogeochemistry 2004*, *70*(3), 357-368. https://doi.org/10.1007/S10533-003-0895-7

Zimov, S. A., Davydov, S. P., Zimova, G. M., Davydova, A. I., Schuur, E. A. G., Dutta, K., & Chapin, I. S. (2006). Permafrost carbon: Stock and decomposability of a globally significant carbon pool. *Geophysical Research Letters*, *33*(20). https://doi.org/10.1029/2006GL027484

Zsolnay, A., Baigar, E., Jimenez, M., Steinweg, B., & Saccomandi, F. (1999). Differentiating with fluorescence spectroscopy the sources of dissolved organic matter in soils subjected to drying. *Chemosphere*, *38*(1), 45-50. https://doi.org/10.1016/S0045-6535(98)00166-0